A&A 573, A26 (2015)
DOI: 10.1051/0004-6361/201424110

Astronomy & Astrophysics

The elemental composition of the Sun

II. The iron group elements Sc to Ni⋆

Pat Scott[1], Martin Asplund[2], Nicolas Grevesse[3,4], Maria Bergemann[5], and A. Jacques Sauval[6]

[1] Department of Physics, Imperial College London, Blackett Laboratory, Prince Consort Road, London SW7 2AZ, UK
e-mail: p.scott@imperial.ac.uk
[2] Research School of Astronomy and Astrophysics, Australian National University, Cotter Rd., Weston Creek, ACT 2611, Australia
e-mail: martin.asplund@anu.edu.au
[3] Centre Spatial de Liège, Université de Liège, avenue Pré Aily, 4031 Angleur-Liège, Belgium
[4] Institut d'Astrophysique et de Géophysique, Université de Liège, Allée du 6 août, 17, B5C, 4000 Liège, Belgium
e-mail: nicolas.grevesse@ulg.ac.be
[5] Institute of Astronomy, University of Cambridge, Madingley Road, CB3 0HA, Cambridge, UK
e-mail: mbergema@ast.cam.ac.uk
[6] Observatoire Royal de Belgique, avenue circulaire, 3, 1180 Bruxelles, Belgium
e-mail: jacques.sauval@oma.be

Received 1 May 2014 / Accepted 1 September 2014

ABSTRACT

We redetermine the abundances of all iron group nuclei in the Sun, based on neutral and singly-ionised lines of Sc, Ti, V, Mn, Fe, Co and Ni in the solar spectrum. We employ a realistic 3D hydrodynamic model solar atmosphere, corrections for departures from local thermodynamic equilibrium (NLTE), stringent line selection procedures and high quality observational data. We have scoured the literature for the best quality oscillator strengths, hyperfine constants and isotopic separations available for our chosen lines. We find $\log \epsilon_{\rm Sc} = 3.16 \pm 0.04$, $\log \epsilon_{\rm Ti} = 4.93 \pm 0.04$, $\log \epsilon_{\rm V} = 3.89 \pm 0.08$, $\log \epsilon_{\rm Cr} = 5.62 \pm 0.04$, $\log \epsilon_{\rm Mn} = 5.42 \pm 0.04$, $\log \epsilon_{\rm Fe} = 7.47 \pm 0.04$, $\log \epsilon_{\rm Co} = 4.93 \pm 0.05$ and $\log \epsilon_{\rm Ni} = 6.20 \pm 0.04$. Our uncertainties factor in both statistical and systematic errors (the latter estimated for possible errors in the model atmospheres and NLTE line formation). The new abundances are generally in good agreement with the CI meteoritic abundances but with some notable exceptions. This analysis constitutes both a full exposition and a slight update of the preliminary results we presented in Asplund et al. (2009, ARA&A, 47, 481), including full line lists and details of all input data we employed.

Key words. Sun: abundances – Sun: photosphere – Sun: granulation – line: formation – line: profiles – convection

1. Introduction

Cosmic abundances of the transition metals Sc – Ni ($21 \leq Z \leq 28$) tend to form a "peak" around iron. This behaviour approximately tracks the variation in average binding energy per nucleon with Z, and reflects the predominantly common origin of iron peak nuclei in core-collapse and thermonuclear supernovae (e.g. Pagel 1997). Variations of abundances within the group provide information on nuclear physics and the physical environments in which the elements were processed. To compare such analyses with theories of stellar structure and evolution, galactic chemical evolution, supernova nucleosynthesis and the formation history of the solar system, accurate solar abundances of the iron group elements are required. In this paper, we present a reanalysis of the solar composition of the iron peak elements Sc, Ti, V, Cr, Mn, Fe, Co and Ni, using a realistic 3D hydrodynamic solar model atmosphere.

This paper is part of a series detailing, and updating, the chemical composition of the Sun presented in Asplund et al. (2009, hereafter AGSS09). This paper covers the iron group nuclei Sc – Ni. Scott et al. (2014, hereafter Paper I) deals with the intermediate-mass elements Na – Ca, whereas Grevesse et al. (2014, hereafter Paper III) is devoted to the heavy elements Cu – Th. Later studies will describe the analysis of the light elements C, N and O, as well as summarise and compare the solar photospheric abundances with the meteoritic evidence, indications from helioseismology and the solar neighbourhood. In an earlier series of papers (Asplund et al. 2000a,b; Asplund 2000; Allende Prieto et al. 2001b, 2002; Asplund et al. 2004, 2005b,a; Asplund 2004; Scott et al. 2006, hereafter AGS05; Meléndez & Asplund 2008; Scott et al. 2009), we examined the abundances of all elements up to Ca, as well as Fe and Ni, using a predecessor of the current 3D solar model atmosphere. The only 3D solar analyses of any iron group elements to date have been of nickel (Scott et al. 2009) and iron itself (Atroshchenko & Gadun 1994; Asplund et al. 2000a,b; Caffau et al. 2011; also the 1D calculations of Bergemann et al. 2012 based on an averaged 3D model).

In Sect. 2 we summarise the current state of knowledge about the solar abundances of the iron peak elements. We describe the observational data we employ in Sect. 3, then give brief recapitulations of our solar model atmosphere, line synthesis code (Sect. 4) and abundance calculations (Sect. 5). In Sect. 6 we justify our selection of atomic data, spectral lines and non-LTE (NLTE) corrections. Our results are presented in

⋆ Tables 1–3 are available in electronic form at http://www.aanda.org

Sect. 7, discussed in Sect. 8, compared to previous compilations in Sect. 9 and summarised in Sect. 10.

2. Previous solar analyses of the iron group

Scandium: earlier reference compilations of the solar composition (Grevesse & Sauval 1998, hereafter GS98; AGS05) included the scandium abundance $\log \epsilon_{Sc} = 3.05 \pm 0.08$ from Youssef & Amer (1989), derived using spectrum synthesis of Sc II lines and the Holweger & Müller (1974, hereafter HM) model atmosphere. A more recent study, adopted as the standard in Grevesse et al. (2007), was that of Neuforge (1993), who used the HM model with both Sc I and Sc II lines. Despite using accurate oscillator strengths (the same values as we use in this paper in fact), abundance scatter was high ($\log \epsilon_{Sc} = 3.14 \pm 0.12$ for Sc I, 3.20 ± 0.07 for Sc II). The dominant ionisation stage of scandium is Sc II, so one expects Sc II lines to return the most reliable abundances. However, the Sc II results could not be reconciled with the meteoritic value, nor could close agreement between ionisation stages be claimed. Zhang et al. (2008) performed a detailed analysis of NLTE effects on Sc I and Sc II lines in the Sun, finding large NLTE corrections to abundances from Sc I lines. This finally reconciled abundances from the neutral and once-ionised species: with the MAFAGS-ODF 1D model atmosphere (based on opacity distribution functions: ODF; Fuhrmann et al. 1997), Zhang et al. found $\log \epsilon_{Sc} = 3.07$–$3.13$, depending upon the oscillator strengths adopted.

Titanium: Blackwell et al. (1987) presented a thorough study of the solar abundance of Ti using a large number of Ti I lines with both the HM and MARCS (Gustafsson et al. 1975) solar photospheric models (see Sect. 4). These results were corrected by Grevesse et al. (1989) for a systematic shift in Ti I oscillator strengths of 0.056 dex (see Sect. 6.2.1), resulting in $\log \epsilon_{Ti} = 4.99 \pm 0.04$ with the HM model. With the MARCS model, the result would have been 0.10 dex smaller. Using Ti II (the dominant species) instead, along with the HM model, Bizzarri et al. (1993) found $\log \epsilon_{Ti} = 5.04 \pm 0.04$, in very good agreement with the Ti I result. The first NLTE analysis of the solar Ti abundance was performed by Bergemann (2011), who found strong NLTE effects in Ti I line formation, and a severe dependence upon the adopted solar model atmosphere and rates of inelastic collisions with H I and e^-. From Ti II lines, Bergemann (2011) found a mean abundance of $\log \epsilon_{Ti} = 4.93$–$4.98$, depending mostly on the adopted oscillator strengths. The most recent results are from Lawler et al. (2013) and Wood et al. (2013), who found $\log \epsilon_{Ti} = 4.97 \pm 0.04$ and $\log \epsilon_{Ti} = 4.98 \pm 0.03$ from Ti I and Ti II lines respectively, using spectrum synthesis with the HM model and new laboratory oscillator strengths.

Vanadium: the most recent derivations of the solar abundance of vanadium are due to Whaling et al. (1985, with V I and the HM model: $\log \epsilon_V = 3.99 \pm 0.01$) and Biémont et al. (1989, with V I, V II and the HM model: $\log \epsilon_V = 4.00 \pm 0.02$). The latter is the previously-adopted reference abundance (GS98; AGS05; Grevesse et al. 2007), giving more weight to the V I data, which is derived from a much larger number of lines than the V II result. The error estimate given is probably unrealistically low however, as we describe in Sect. 6.3.1. Both these studies assumed that V lines form in LTE. During the refereeing phase of our paper, we became aware of a recent determination of the solar V abundance using newly determined experimental transition probabilities for V II (Wood et al. 2014a). Using spectrum synthesis with the HM model for a set of 15 often heavily blended V II lines, they estimated $\log \epsilon_V = 3.95 \pm 0.01$ ($\sigma = 0.05$ dex).

Chromium: recent compilations (AGS05; Grevesse et al. 2007) recommended a Cr abundance of $\log \epsilon_{Cr} = 5.64 \pm 0.10$, derived from two papers. Using various gf-values available at the time, Biémont et al. (1978) found $\log \epsilon_{Cr} = 5.67 \pm 0.03$ with Cr I lines and the HM model, and $\log \epsilon_{Cr} = 5.64 \pm 0.03$ using the VAL (Vernazza et al. 1976) model. Blackwell et al. (1987), using the accurate gf-values measured at Oxford and different solar spectra, found $\log \epsilon_{Cr} = 5.68 \pm 0.06$ with the HM model. As for Ti I, with the MARCS model this would have been 0.10 dex smaller. Sobeck et al. (2007) measured new gf-values for Cr I lines (see Sect. 6.4.1) and used them to revise the solar abundance assuming LTE. When two highly discrepant outlying lines are removed, the results are $\log \epsilon_{Cr} = 5.64 \pm 0.05$ with the HM model and $\log \epsilon_{Cr} = 5.53 \pm 0.05$ with MARCS. Sobeck et al. also used a small number of Cr II lines with gf-values from Nilsson et al. (2006). These lines lead to higher abundances and much larger dispersions: $\log \epsilon_{Cr} = 5.77 \pm 0.13$ (HM) and $\log \epsilon_{Cr} = 5.67 \pm 0.13$ (MARCS). Bergemann & Cescutti (2010) investigated NLTE effects in solar Cr line formation for the first time, finding corrections of order +0.05–0.10 dex to abundances from Cr I with the 1D MAFAGS-ODF model. Using Cr II lines and gf-values from Nilsson et al. (2006), Bergemann & Cescutti confirmed the high abundance and large scatter seen by Sobeck et al. (2007). With the complete exclusion of inelastic collisions with hydrogen, chosen so as to satisfy Cr ionisation balance for the Sun and a number of late-type stars, they also found a high abundance from Cr I: $\log \epsilon_{Cr} = 5.74 \pm 0.05$.

Manganese: previous reference solar manganese abundances (GS98; AGS05; Grevesse et al. 2007) came from Booth et al. (1984b), who found $\log \epsilon_{Mn} = 5.39 \pm 0.03$ using the HM model and Mn I lines. The derived abundance is almost 3σ below the meteoritic value (Lodders et al. 2009), quite a striking discrepancy when one considers that agreement between photospheric and meteoritic values is typically quite good (cf. Anders & Grevesse 1989, hereafter AG89; AGSS09; Lodders et al. 2009). The errors on the photospheric value have probably been underestimated however, as revealed by a detailed investigation of Mn I oscillator strengths and line selection (Sect. 6.5.1). Bergemann & Gehren (2007) made a detailed NLTE analysis of a large number of Mn I lines in the solar flux spectrum, showing that NLTE abundance corrections are of order +0.08 dex for solar lines. Their analysis with the MAFAGS-ODF model produced an abundance of $\log \epsilon_{Mn} = 5.36 \pm 0.10$. This work was subsequently revised with improved oscillator strengths by Blackwell-Whitehead & Bergemann (2007), giving $\log \epsilon_{Mn} = 5.37 \pm 0.05$ with the same model. Using the HM model, the result was $\log \epsilon_{Mn} = 5.46 \pm 0.08$, in reasonable agreement with the meteoritic value but exhibiting an uncomfortably high scatter.

Iron: Grevesse & Sauval (1999) and Asplund et al. (2000b) summarised the long and well-known debate as to whether the solar abundance of Fe is equal to or higher than seen in meteorites. Discrepant results in older studies of the solar Fe abundance using 1D solar models appeared to be due to differences in the adopted gf-values, equivalent widths, microturbulent velocities and collisional damping parameters, as well as differences in computer codes. Grevesse & Sauval (1999) succeeded in reconciling LTE abundances from Fe I and Fe II lines by modifying the temperature structure of the HM model, so as to remove the observed trend with excitation potential in abundances from Fe I lines.

The first pioneering work aimed at determining the solar Fe abundance using a 3D solar model that we are aware of was by Atroshchenko & Gadun (1994), who used two different 3D models (with what nowadays is obviously very modest

numerical resolution and simplified radiative transfer). Perhaps not surprisingly, their derived Fe abundance showed a large difference between Fe I ($\log \epsilon_{\rm Fe} \approx 7.0$) and Fe II ($\log \epsilon_{\rm Fe} \approx 7.6$) lines when using either equivalent widths or line depths. Asplund et al. (2000b) analysed Fe I and Fe II lines with a more realistic 3D model, albeit still in LTE. They found abundances from weak Fe I lines to be independent of the excitation energy, and in very good agreement with both Fe II results and the meteoritic abundance: $\log \epsilon_{\rm Fe} = 7.45 \pm 0.05$. Both Grevesse & Sauval (1999) and Asplund et al. (2000b) found that abundances derived from Fe II lines, using gf-values available at the time, showed a very large scatter, 0.10 dex. Caffau et al. (2011) analysed a set of Fe II lines using a 3D solar model computed with the CO^{5}BOLD code Freytag et al. (2002) and improved gf-values from Meléndez & Barbuy (2009), finding $\log \epsilon_{\rm Fe} = 7.52 \pm 0.06$.

Mashonkina et al. (2011) and Bergemann et al. (2012) carried out NLTE calculations of Fe line formation, using the most up-to-date theoretical and experimental atomic data to construct their model atoms. Mashonkina et al. (2011), using the MAFAGS-OS[1] models, obtained $\log \epsilon_{\rm Fe} = 7.56 \pm 0.09$ from Fe I lines, and rather discrepant results from Fe II lines (7.41–7.56 dex depending on the adopted gf-values). Bergemann et al. (2012) also investigated NLTE Fe line formation with the MARCS and ⟨3D⟩ (Sect. 4) model atmospheres, finding values fully consistent with the meteoritic abundance, and, in view of the small NLTE effects for the Sun, with the result of Asplund et al. (2000b). With the ⟨3D⟩ model, they found a mean abundance of $\log \epsilon_{\rm Fe} = 7.46 \pm 0.02$ dex.

Cobalt: the Co content of the Sun was derived by Cardon et al. (1982) under the assumption of LTE using Co I lines, giving $\log \epsilon_{\rm Co} = 4.92 \pm 0.08$ with the HM model atmosphere. This was the reference value adopted by AG89, GS98, AGS05, Grevesse et al. (2007) and Lodders et al. (2009), although it only overlaps the meteoritic value because of the rather large errors. Recently, Bergemann et al. (2010) re-analysed a series of Co lines in flux, taking into account departures from NLTE. They found large NLTE corrections, of order +0.15 dex. Using a MAFAGS-ODF solar photospheric model, they derived an NLTE Co abundance of $\log \epsilon_{\rm Co} = 4.95 \pm 0.04$.

Nickel: we recently provided a revised solar nickel abundance in the context of the Ni-blended forbidden oxygen line at 630 nm (Scott et al. 2009). Using the 3D model of Asplund et al. (2000a), that analysis gave $\log \epsilon_{\rm Ni} = 6.17 \pm 0.05$. Here we update those results using an improved 3D solar model atmosphere (AGSS09; Paper I). Wood et al. (2014b) found $\log \epsilon_{\rm Ni} = 6.28 \pm 0.06$ by employing spectrum synthesis of Ni I lines, the HM model and new laboratory oscillator strengths. The previous reference solar Ni abundance (Grevesse & Sauval 1998; Asplund et al. 2005a; Grevesse et al. 2007) was $\log \epsilon_{\rm Ni} = 6.25 \pm 0.09$, from an HM-based analysis of Ni I by Biémont et al. (1980).

3. Observations

We compared theoretical line profiles to the Fourier Transform Spectrograph (FTS) spectral intensity atlas of Brault & Neckel (1987, see also Neckel 1999) at solar disc-centre ($\mu = 1$). We removed the solar gravitational redshift of 633 m s^{-1} from the observed spectrum, and convolved simulated profiles with an instrumental sinc function of width $\Delta\sigma = \frac{c}{R} = 0.857$ km s^{-1}, reflecting the FTS resolving power $R = 350\,000$ (Neckel 1999).

Our adopted equivalent widths are the integrated values we previously obtained in full χ^2-based profile fits, using the earlier version of the 3D model (Asplund et al. 2000a) and the observed FTS spectrum of Brault & Neckel (1987). We masked sections of profiles perturbed by nearby lines from the fitting procedure. We fitted local continua independently using nearby clear sections of the spectrum. We were sure to use the same spectral regions to integrate both the observed and theoretical profiles. As a cross-check, we also directly measured the equivalent widths of all lines on two different disc-centre solar atlases: the FTS atlas mentioned above (Brault & Neckel 1987), and the atlas of Delbouille et al. (1973) recorded with a classical double-pass spectrometer at the Jungfraujoch high-altitude station. We noted excellent agreement between these two sets of measurements, and with the equivalent widths derived from the fitted 3D profiles (i.e. to within 1–2%). In order to ensure that our 1D and 3D abundances were derived consistently, for the 1D analyses we used the same equivalent widths as in the 3D analysis (i.e. those arising from the earlier 3D line profile fits).

4. Solar model atmospheres and spectral line formation

We use the improved 3D model atmosphere introduced in AGSS09 and described in more detail in Paper I. We carried out comparative calculations with four 1D models: HM, MARCS (Gustafsson et al. 1975; Asplund et al. 1997; Gustafsson et al. 2008), MISS (Allende Prieto et al. 2001a) and ⟨3D⟩. The ⟨3D⟩ model is a temporal average of the 3D model, contracted into the vertical dimension with horizontal averages taken over surfaces of common optical depth. The reader is directed to Paper I for further details of these model atmospheres.

We obtain NLTE abundances by applying NLTE corrections to the values we obtained in LTE[2]. This is not strictly correct unless full 3D NLTE calculations are carried out; for computational reasons, this is not the case for any of the elements we investigate here. 3D NLTE line formation is still very challenging, and only very few such studies have been undertaken to date (e.g. Asplund et al. 2004; Pereira et al. 2009; Lind et al. 2013). Instead, we apply NLTE abundance corrections computed using 1D model atmospheres. For most elements (Ti, Cr, Mn, Fe, Co), we computed NLTE corrections for solar disc-centre intensity profiles of the selected lines, using the HM, MARCS, and ⟨3D⟩ models. For calculating 3D+NLTE abundances we adopt offsets computed with the ⟨3D⟩ model, which we expect to be a close approximation to the full 3D NLTE problem, given that radiative transfer proceeds primarily vertically. For MISS we adopt the offsets computed with the HM model. We performed statistical equilibrium calculations with the DETAIL code (Giddings 1981; Butler & Giddings 1985). For Sc, we rely on NLTE corrections from the literature, while V and Ni have not been exposed to a NLTE study. Our NLTE calculations are described in detail in Sect. 6.

We do not discuss the NLTE line formation in detail in this work, as this aspect has been extensively discussed previously (e.g. Bruls 1993; Bergemann & Gehren 2007; Zhang et al. 2008; Bergemann et al. 2010; Bergemann & Cescutti 2010; Bergemann 2011; Bergemann et al. 2012), along with descriptions of the adopted atomic models. In short, the Fe-group elements are predominantly singly-ionised in the solar atmosphere, and departures from LTE are significant only for the

[1] MAFAGS-OS models are successors to MAFAGS-ODF models by Fuhrmann et al. (1997), relying on opacity sampling instead of ODFs.

[2] An NLTE abundance correction is defined as a difference in abundance required to equalise NLTE and LTE equivalent widths.

neutral species, which are overionised. NLTE effects on the lines of singly-ionised atoms are typically negligible. One remaining uncertainty in NLTE calculations is the unknown cross-sections for inelastic collisions between hydrogen and the element in question. In the absence of quantum mechanical calculations that still only exist for lighter elements, most NLTE studies rely on the classical and therefore uncertain formula of Drawin (1969), which at best should be considered an order-of-magnitude estimate. Therefore, a scaling factor $S_{\rm H}$ for the Drawin cross-sections is used. At least with iron lines and averaged 3D models, the unscaled Drawin formula ($S_{\rm H} = 1$) leads to ionisation balance and consistent inferred effective temperatures and surface gravities across a substantial sample of metal-poor stars (Bergemann et al. 2012). Wherever possible, we therefore prefer to use $S_{\rm H} = 1$ for iron-group elements; we do this for all elements where we calculate our own NLTE abundance corrections (Ti, Cr, Mn, Fe and Co). For Sc, not having a model atom of our own to draw on, we must rely on results from the literature assuming $S_{\rm H} = 0.1$ (Zhang et al. 2008). Indeed, this parameter remains quite uncertain, and will likely differ across lines, elements and stars. In the absence of detailed quantum mechanical calculations to rely on, or better, solar observations to guide our choices, our selection is by necessity somewhat arbitrary. However, we argue that it is a reasonable approach to adopt the same scaling factor $S_{\rm H}$ for all Fe-peak elements as empirically estimated for Fe. Reliable atomic physics computations are urgently needed for inelastic H collisions, not only for these but also other elements.

5. Abundance calculations

We derived abundances as per Paper I: by matching equivalent widths of simulated and observed line profiles, and including isotopic and hyperfine components in our calculations as blends.

As in Paper I, the final uncertainties of our 3D+NLTE abundance results are the sum in quadrature of a systematic term and a statistical one. We take the statistical term to be the standard error of the mean abundance. We calculate the systematic term as the sum in quadrature of uncertainties due to the mean temperature structure (half the mean difference between the ⟨3D⟩ and HM results), atmospheric inhomogeneities (half the mean difference between the 3D and ⟨3D⟩ results), and departures from LTE (the greater of 0.03 dex and half the mean NLTE correction).

6. Atomic data and line selection

For each element and ionisation stage, we performed an extensive search of the atomic literature for the most reliable oscillator strengths, hyperfine splitting constants, isotopic separations, wavelengths, excitation potentials, transition designations and partition functions. We preferred to make our own independent critical selection rather than relying on any existing compilation, though the NIST Atomic Transition Probability Bibliographical Database (Fuhr et al. 2007) proved invaluable for this task. We used the compilations of Martin et al. (1988), Fuhr et al. (1988), Doidge (1995) and especially Morton (2003) as guides and secondary comparators.

We extracted radiative broadening parameters from the Vienna Atomic Line Database (VALD, Kupka et al. 1999). We treated collisional broadening of neutral lines via the Anstee-Barklem-O'Mara technique (Anstee & O'Mara 1995; Barklem & O'Mara 1997; Barklem et al. 1998). The broadening parameters σ and α we used were previously calculated for many individual lines (Barklem et al. 2000). For others we interpolated within the tables of Anstee & O'Mara (1995) or Barklem & O'Mara (1997). No such data exist for ionised iron-peak elements except iron itself (Barklem & Aspelund-Johansson 2005), so we employed the classical Unsöld (1955) broadening recipe for such lines, with an enhancement factor of 2.0. The same is true for the small number of neutral lines that lie outside the Anstee-Barklem-O'Mara tables. This scaling factor reflects the approximate proportionality typically seen between accurate modern broadening calculations and the Unsöld (1955) treatment, as observed over a large range of lines for which modern data are available. We note that most of the lines for which we have to resort to using scaled Unsöld (1955) broadening are weak and thus insensitive to the adopted damping.

We typically only used a line if it had a gf-value available from the source that we deemed most reliable. Each candidate line was checked for blends, by inspection of the solar spectra (Brault & Neckel 1987; Delbouille et al. 1973) and the tables of Moore et al. (1966). Line strengths were also checked in Moore et al. (1966), and only lines weaker than ∼60 mÅ were generally allowed; in some circumstances, these requirements were relaxed slightly[3]. The selected lines were assigned a relative ranking from 1 to 3 based upon their appearance in the observed spectrum, with rankings sometimes also adjusted to reflect differences in uncertainties in atomic data. These rankings were used to weight the contribution of each line to mean abundances. Note that the rankings are only indications of relative merit within a line list, so the same rank for lines of different species does not necessarily imply the same line quality.

Our adopted lines, oscillator strengths, NLTE corrections, equivalent widths, excitation potentials and derived abundances for all elements are given in Table 1. We provide isotopic and hyperfine splitting data separately in Table 2. The isotopic ratios given for individual elements are taken from AGSS09, but the original data are the terrestrial ratios recommended by Rosman & Taylor (1998). Our chosen partition functions are from Barklem & Collet (in prep.), and our ionisation energies from NIST data tables. These data are given in Table 3.

6.1. Scandium

Wavelengths, excitation potentials and transition identifications come from Kaufman & Sugar (1988) for Sc I, and from Johansson & Litzén (1980) for Sc II. Scandium exhibits hyperfine but not isotopic structure, as it has just one stable isotope (Rosman & Taylor 1998): ^{45}Sc, with spin $I = \frac{7}{2}$.

6.1.1. Oscillator strengths

For both Sc I and Sc II, we prefer the gf-values of Lawler & Dakin (1989). These authors obtained emission FTS branching fractions (BFs), which they set to an absolute scale using the time-resolved laser-induced fluorescence (TRLIF) lifetimes of Marsden et al. (1988). These techniques are currently the most accurate means available for determining relative spectral intensities and radiative lifetimes respectively, and their combination is the most reliable way of determining absolute atomic gf-values. For Sc II, accurate lifetimes are also available from

[3] Even with the 3D model, weaker lines are to be preferred because they lie on the linear section of the curve of growth and are less sensitive to errors in the treatment of broadening or the atmospheric temperature structure, which is less certain in the higher parts of the atmosphere where stronger lines are formed.

Vogel et al. (1985), where results are in excellent agreement with those of Marsden et al. (1988); using the former or the latter data would result in gf-values differing by less than 0.01 dex.

Three very good solar lines (624.56, 630.07 and 632.08 nm) were not measured by Lawler & Dakin (1989). We derived gf-values for these lines from existing experimental (Corliss & Bozman 1962, CB) and theoretical (Kurucz 2011) data, using the lifetimes of Vogel et al. (1985) for normalisation. However, the resulting scatter in the abundances from these lines (with all models) left us ultimately unconvinced as to the accuracy of the oscillator strengths, so we chose to discard these lines.

6.1.2. Hyperfine structure

The HFS of Sc I has been studied extensively. The atomic-beam magnetic-resonance technique (ABMR; also known as laser-rf double resonance or ABMR-LIRF when detected using laser-induced resonance fluorescence) was employed by Childs (1971) to give highly accurate data for the 3d4s^2 ^{2}D$_{3/2,5/2}$ levels. For the 3d4s4p levels, the data with lowest uncertainties are the FTS results of Aboussaïd et al. (1996). In some cases Aboussaïd et al. (1996) provide more than one measurement for a given level; we take the average of these measurements, weighted according to their uncertainties. For the (^{3}F)4s ^{2}F$_{5/2,7/2}$ levels, theoretical results presented by Başar et al. (2004) are the only data available. Ertmer & Hofer (1976) also presented ABMR data for the (^{3}F)4s ^{4}F$_{3/2,9/2}$ levels. We note that optogalvanic spectroscopy (OGS) data presented by Singh et al. (1991) for the (^{1}D)4s ^{2}D$_{3/2,5/2}$ levels are not reliable, due to errors in their relative intensity formula pointed out by Aboussaïd et al. (1996), and confirmed by Bieron et al. (2002) and Başar et al. (2004). Singh et al. also measured the (^{3}F)4p ^{4}G levels, though these were not affected by this error; for these levels we thus adopt either the data of Singh et al. (for ^{4}G$_{5/2,11/2}$) or Ertmer & Hofer (1976, for ^{4}G$_{7/2,9/2}$), based upon the size of the quoted uncertainties in each case.

Work on the HFS of Sc II is rather less common. The most recent and accurate data that we could find come from Villemoes et al. (1992) and Mansour et al. (1989), the latter of whom employed the ultra-high-resolution ABMR technique. We use the results of both these studies where available, adopting an average weighted according to the stated uncertainties; in practice this means that the results of Mansour et al. (1989) dominate due to their smaller error bars. Where data are not available from both Villemoes et al. (1992) and Mansour et al. (1989), we turn to each of these studies individually, followed by the experiments of Young et al. (1988) and then Arnesen et al. (1982). Apart from the recent work by Zhang et al. (2008), previous determinations of the solar Sc abundance have not considered the effects of HFS in Sc I, and only incompletely considered the effects in Sc II.

6.1.3. NLTE corrections

NLTE formation of solar Sc I and Sc II lines has been thoroughly investigated by Zhang et al. (2008), using the MAFAGS-ODF model. As might be expected from the minority status of neutral Sc in the Sun and its quite low ionisation potential (6.56 eV), Zhang et al. (2008) found very large NLTE corrections to Sc I abundances: about +0.15 dex for flux profiles of the lines of interest in our analysis, when employing the standard Drawin (1969) recipe for treating collisions with hydrogen rescaled by a factor $S_{\rm H} = 0.1$. Corrections to Sc II abundances were less severe (about −0.01 dex for lines of interest to us). In the absence of any calculations for intensity profiles and/or in 3D, we simply adopt these results for disc centre in Table 1, noting that this way the NLTE corrections may be slightly overestimated. For lines not studied by Zhang et al. (2008), given the size of corrections and the error likely induced by neglecting NLTE, we use the typical correction observed with similar lines. Although we have NLTE corrections available in both flux and disc-centre intensity for most other iron-group elements, we choose not to rescale the NLTE flux corrections for Sc by the mean ratio of those corrections in order to estimate intensity corrections. This is because the ratio of intensity to flux corrections, although sometimes substantially less than 1, is quite line specific; the line-to-line scatter in this ratio, across other elements, is actually comparable to the offset of the mean ratio from 1. Dedicated calculations of Sc NLTE intensity abundance offsets, for the lines and model atmospheres that we employ here, would be most welcome.

6.1.4. Line selection

We applied our line selection criteria (see the beginning of this Section) to all Sc I and Sc II lines in the solar spectrum measured by Lawler & Dakin (1989). We also compared with the previous work of Biémont (1974), Neuforge (1993), Youssef & Amer (1989) and Reddy et al. (2003), retaining the five Sc I and nine Sc II lines given in Table 1. We note that the gf-value of the very good Sc II line at 660.5 nm has a large uncertainty (>40%; Lawler & Dakin 1989). Rather than exclude this line, we reduced its weight (as indicated by the asterisk beside its weight in Table 1).

6.2. Titanium

Our adopted wavelengths, transition designations and excitation potentials for Ti I come from Forsberg (1991). For Ti II, we took wavelengths from Pickering et al. (2001, with erratum: Pickering et al. 2002) where possible, based upon unpublished work of Zapadlik et al. in Lund. Otherwise, wavelengths came from Huldt et al. (1982), as did all excitation potentials and transition identifications. Ti has five stable isotopes (Rosman & Taylor 1998): ^{46}Ti (8.2% by number on Earth), ^{47}Ti (7.4%), ^{48}Ti (73.7%), ^{49}Ti (5.4%) and ^{50}Ti (5.2%). ^{47}Ti has a nuclear spin of $I = \frac{5}{2}$ and ^{49}Ti has $I = \frac{7}{2}$.

6.2.1. Oscillator strengths

Nitz et al. (1998) and Blackwell-Whitehead et al. (2006) produced Ti I oscillator strengths by combining their own FTS BFs with accurate TRLIF lifetimes from Salih & Lawler (1990) and Lawler (1991), respectively.

Lawler et al. (2013) have recently expanded and improved the work of Nitz et al. (1998), providing accurate oscillator strengths for nearly a thousand lines by combining their FTS and eschelle BFs with the lifetimes of Salih & Lawler (1990) and Lawler (1991).

Grevesse et al. (1989) earlier produced accurate gf values by renormalising the relative oscillator strengths of Blackwell et al. (1982a,b, 1983, 1986c), which had been obtained by absorption spectroscopy in the Oxford furnace. As opposed to the original Oxford works, in which relative oscillator strengths were set to an absolute scale using less accurate beam-foil lifetimes from Roberts et al. (1973) and the absolute data of Bell et al. (1975),

Grevesse et al. (1989) set their new values to an absolute scale using the accurate TRLIF lifetimes of Rudolph & Helbig (1982).

We prefer the data of Lawler et al. (2013) where possible, but we also performed some preliminary calculations of abundances arising from lines in common between Nitz et al. (1998), Blackwell-Whitehead et al. (2006) and the revised Oxford gf-values, in order to establish which set of data was the next most reliable. Based upon the internal scatter and relative agreement between different lists, we concluded that the Nitz et al. values are to be preferred very slightly over the revised Oxford values, while the Blackwell-Whitehead et al. gf-values are surprisingly discrepant.

High-quality Ti II oscillator strengths are available from the FTS BFs and TRLIF lifetimes of Bizzarri et al. (1993), and the extensive FTS and eschelle work by Wood et al. (2013). The FTS study of Pickering et al. (2001) also produced gf-values for many lines, where fractions for some branches were completed using theoretical oscillator strengths of weak lines from Kurucz (2011). Pickering et al. set different BFs to an absolute scale using either the Bizzarri et al. lifetimes or lifetimes derived from the theoretical Kurucz gf-values. Our preliminary investigations with lines common to the lists of Bizzarri et al. (1993) and Pickering et al. (2001) revealed a much larger abundance scatter with the Pickering et al. data; we thus prefer the Wood et al. (2013) and Bizzarri et al. oscillator strengths to those from Pickering et al. (2001).

6.2.2. Isotopic and hyperfine structure

Much complimentary data exist on the isotopic splitting of Ti I lines, though unfortunately only for two of the lines we use here. The data we use come from laser fluorescence spectroscopy (LFS, also known simply as laser-induced fluorescence, LIF; Gangrsky et al. 1995). We prefer the data of Gangrsky et al. over the less accurate work of Cruz et al. (1994) and previous results from the same group (Anastassov et al. 1994). Isotopic separations can be estimated for many of our our chosen Ti II lines using the LFS measurements of Nouri et al. (2010).

It has been consistently found that the hyperfine A constants for ^{47}Ti and ^{49}Ti are essentially equal, and $B(47)/B(49) \approx 1.22$, for all levels (Channappa & Pendlebury 1965; Aydin et al. 1990; Stachowska et al. 1994; Gangrsky et al. 1995). We therefore use the experimental values for the relevant isotope where available, but use rescaled experimental data from the other where it does not exist for both isotopes. Data on hyperfine structure for the Ti I lines for which we have isotopic information are best obtained from Gangrsky et al. (1995) and Aydin et al. (1990). In cases of overlap, the ABMR data of Aydin et al. have smaller uncertainties than those of Johann et al. (1981), whereas the LFS data of Gangrsky et al. is preferable to Aydin et al.'s LFS. LFS data from Jin et al. (2009) is of similar quality to, and agrees well with, that of Gangrsky et al. (1995). The only HFS data on Ti II are the experimental ABMR and corresponding theoretical values produced by Berrah-Mansour et al. (1992), and the LFS data of Nouri et al. (2010).

6.2.3. NLTE corrections

The NLTE line formation of Ti lines has been extensively discussed by Bergemann (2011). Our NLTE calculations rely on the same model atom, although we adopt a different scaling factor to the Drawin (1969) formula for inelastic H I collision cross-sections ($S_{\rm H} = 1$ rather than $S_{\rm H} = 3$; cf. Sect. 4). We computed Ti I NLTE abundance corrections for disc-centre intensity with the ⟨3D⟩, MARCS and HM 1D model atmospheres; we adopt the ⟨3D⟩ results as an approximation to the real 3D NLTE corrections. It is interesting that even with the relatively large value $S_{\rm H} = 1$, the resulting NLTE corrections for the Ti I lines are significant. For the ⟨3D⟩ model, they range from 0.04 to 0.09 dex, whereas the use of the HM model reduces them by a factor of two, mainly because its reduced temperature gradient makes over-ionisation less pronounced. Bergemann (2011) found minimal NLTE effects on the relatively weak Ti II lines we consider, so we simply adopt the LTE results for this species.

6.2.4. Line selection

We applied our selection criteria to numerous solar lines, including those used in previous works by Blackwell et al. (1987), Reddy et al. (2003) and Bizzarri et al. (1993). We ultimately retained 34 lines of Ti I and 14 of Ti II (Table 1). Twenty-four of our Ti I lines we included by Lawler et al. (2013).

6.3. Vanadium

For V I we sourced wavelengths and excitation potentials from Davis & Andrew (1978), calculating wavelengths of missing lines from the stated energy levels. We adopted transition identifications from Whaling et al. (1985), with corrections to V I 573.1 nm and V I 609.0 nm following consultation with Davis & Andrew and Martin et al. (1988). V II wavelengths and transition identifications came from Biémont et al. (1989), with excitation potentials from Sugar & Corliss (1985).

Vanadium has two stable isotopes: ^{51}V ($I = 7/2$) and ^{50}V ($I = 6$). The isotopes are present in the ratio ^{51}V/^{50}V $\approx$ 400 on Earth (Rosman & Taylor 1998); because of this large ratio, isotopic structure is of no importance for vanadium lines. V I and V II lines are given in Table 1 with corresponding atomic data.

6.3.1. Oscillator strengths

The best V I oscillator strengths available are those of Whaling et al. (1985), who measured both TRLIF lifetimes and FTS BFs. In some cases we correct this data for arithmetic errors in converting from BFs to transition probabilities, as per Martin et al. (1988). There are also a few accurate gf-values from Doerr et al. (1985), who combined TRLIF lifetimes with BFs from hook absorption and hollow cathode emission. We prefer the data of Whaling et al. (1985), as their lifetime uncertainties are lower than Doerr et al.'s, and obtaining BFs by FTS is generally considered the most reliable method available.

For V II, until very recently the most accurate gf-values come from the FTS BFs and TRLIF lifetimes of Biémont et al. (1989). In addition to their own, these authors drew on a large number of accurate TRLIF lifetimes measured by Karamatskos et al. (1986) to arrive at their final oscillator strengths. Karamatskos et al. (1986) had also obtained FTS BFs, and also produced mostly accurate gf values, but their results disagree with those of Biémont et al. (1989) below around 350 nm. Biémont et al. suggest that this is likely due to an FTS calibration error by Karamatskos et al. (1986), so we prefer Biémont et al.'s results in general. However, we do choose the gf value of Karamatskos et al. over that of Biémont et al. for the V II 395.2 nm line, as in this case the uncertainty of Biémont et al.'s measurement is 50%, whereas that of Karamatskos et al.'s

is 8%. Schade et al. (1987) also produced TRILF lifetimes, which agree nearly perfectly with those of Karamatskos et al. (1986), and exhibit similar errors. Biémont et al. (1989) preferred the lifetimes of Karamatskos et al. (1986) because they were more extensive, but also because in the one case of disagreement, the errors of Karamatskos et al. are smaller.

During the final stages of refereeing of our article, we became aware of new experimental FTS+LIF measurements of V II transition probabilities for a large number of UV/optical lines by the Wisconsin group (Wood et al. 2014a). Without a doubt, these should be the most accurate V II data available now. Although it was too late to adopt these new gf-values, below we discuss how our results would have changed had we done so.

By comparing the claimed uncertainties of the vanadium abundances stated by Biémont et al. (1989) with the internal uncertainties of the sets of gf-values used to derive the abundances, we note that the uncertainty of their vanadium abundance is almost certainly underestimated.

6.3.2. Hyperfine structure

Quite a lot of good data exists on the HFS of V I, with little overlap between the levels investigated by different authors. Based on the uncertainties assigned to levels common to different studies, we placed the data into a preferential tier system. In this system, no tier contained more than one value for any given level. In the top tier were the ABMR and LFS data of Childs et al. (1979), the ABMR results of El-Kashef & Ludwig (1992), Unkel et al. (1989), Johann et al. (1981) and Childs & Goodman (1967), and the FTS data of Palmeri et al. (1997). The second tier consisted of an earlier FTS study by Palmeri et al. (1995) and the crossed-beam results of Cochrane et al. (1998). On the third tier were additional results from Unkel et al. (1989) using LFS, FTS data of Lefèbvre et al. (2002) and Doppler-free LFS results from Gough et al. (1985). Whaling et al. (1985) and Biémont et al. (1989) included the effects of HFS in their analysis of V I, though we are now able to draw upon better HFS data.

Until the recent fast-ion-beam LFS work of Armstrong et al. (2011), no HFS data existed in the literature for ionised vanadium. Biémont et al. (1989) estimated hyperfine broadening of V II lines empirically, adding multiple line components by eye to approximately reproduce line shapes and sufficiently desaturate modelled solar lines. We have done something similar for the one line (399.7 nm) where HFS data are not available from Armstrong et al. (2011), iteratively altering the hyperfine A constants of the two levels involved until we achieved a synthetic spectral line that looked qualitatively similar to the observed line. To account for the effects of convective velocities upon line shapes, it was necessary to use a 3D model for this exercise. Due to the computational demands of recalculating the radiative transfer every time however, we performed these calculations on a single snapshot of the earlier 3D model (Asplund et al. 2000a) only[4]. The results of this estimation procedure, along with all other data pertaining to our chosen V I and V II lines, are given in Table 1.

[4] Interestingly, the resulting hyperfine constants for this line are in reasonable agreement with the experimental measurements of Wood et al. (2014a), which appeared only at the end of the refereeing stage of this paper.

6.3.3. NLTE corrections

NLTE formation of solar vanadium lines has not yet been investigated. Like Sc, Ti and Cr, the rather low ionisation energy of V means that it is predominantly singly-ionised in the solar atmosphere. As the minority species, V I is expected to exhibit significant NLTE effects. In the absence of any better guidance, we adopt a blanket NLTE correction of +0.1 dex for all V I lines; this is of a similar order as the mean NLTE offsets observed in Sc I (+0.15 dex), Ti I (+0.06 dex) and Cr I (+0.03 dex). A dedicated NLTE study of V is sorely needed.

6.3.4. Line selection

We retained 32 V I lines (Table 1) from previous analyses by Biémont (1978), Whaling et al. (1985), Reddy et al. (2003) and McWilliam & Rich (1994). The solar V II lines are very poor quality, because of severe blending, and are ultimately only really useful as weak supporting indicators of the solar vanadium abundance. After careful analysis of various lines used by Youssef & Amer (1989), Biémont et al. (1989) and McWilliam et al. (1995), we choose to keep only the five lines in Table 1.

6.4. Chromium

We sourced Cr I and Cr II excitation potentials from Sugar & Corliss (1985), and used them to calculate wavelengths. Where possible, we took transition identifications from Sobeck et al. (2007) for Cr I and Nilsson et al. (2006) for Cr II. Otherwise, we sourced transitions from VALD and checked them against the NIST database (Yalchenko et al. 2007). Chromium has four stable isotopes (Rosman & Taylor 1998): ^{50}Cr (4.3%), ^{52}Cr (83.8%), ^{53}Cr (9.5%) and ^{54}Cr (2.4%). Only ^{53}Cr has non-zero nuclear spin ($I = \frac{3}{2}$).

6.4.1. Oscillator strengths

Highly accurate Cr I oscillator strengths have been produced by Sobeck et al. (2007), who measured FTS BFs and normalised them with the extensive, very accurate TRLIF lifetimes of Cooper et al. (1997). Other accurate lifetimes have been measured by TRLIF (Hannaford & Lowe 1981; Kwiatkowski et al. 1981; Kwong & Measures 1980; Measures et al. 1977) and level-crossing (Becker et al. 1977); these data all agree well with Cooper et al.'s, and have comparable uncertainties. Other accurate gf-values were produced by Tozzi et al. (1985), also based upon FTS BFs but normalised to Kwiatkowski et al.'s lifetimes, and Blackwell et al. (1984, 1986b), who measured relative gf-values using absorption spectroscopy and set them to an absolute scale with the lifetimes of Hannaford & Lowe (1981), Kwiatkowski et al. (1981) and Becker et al. (1977). To complete their systems of lines, Blackwell et al. also drew upon some of the relative oscillator strengths carefully measured by Huber & Sandeman (1977) using the hook method. Because they are all of high quality, we use gf-values from Sobeck et al. (2007), Blackwell et al. (1984, 1986b) and Tozzi et al. (1985) without any preference for data from one source or another; where data overlap, we take the mean of the $\log gf$-values available from each of these sources.

Oscillator strengths for Cr II were recently produced by Gurell et al. (2010) and Nilsson et al. (2006), who each combined their own FTS BFs with accurate TRLIF lifetimes; Gurell et al. (2010) used their own lifetimes, whereas Nilsson et al. utilised a mixture of TRLIF lifetimes from Schade et al. (1990),

Bergeson & Lawler (1993a) and their own work. Unfortunately, Gurell et al. (2010) measured no useful solar lines, and Nilsson et al. only very few of them. The small number of gf-values available from Nilsson et al. for good solar lines also return abundances that are highly inconsistent with each other. In the absence of any good gf-values for the unblended Cr II lines in the solar spectrum, we default to using the theoretical Kurucz (2011) oscillator strengths. Given that the Kurucz gf-values are known to often be inaccurate, especially for weak transitions, this is not a satisfactory situation; high-quality atomic data is urgently needed for Cr II.

6.4.2. Isotopic and hyperfine structure

The only data on the isotopic splitting of Cr I lines come from the recent LFS work of Furmann et al. (2005) and the much older Fabry-Perot spectroscopy of Heilig & Wendlandt (1967); we use the former. HFS of ^{53}Cr I has been measured very accurately with ABMR by Jarosz et al. (2007). No data exist on the isotopic splitting of Cr II lines, nor HFS of ^{53}Cr II.

6.4.3. NLTE corrections

We computed Cr I NLTE abundance corrections in intensity at disc-centre, for the ⟨3D⟩, MARCS and HM 1D model atmospheres, using the Cr model atom of Bergemann & Cescutti (2010). For the majority of our Cr I lines, the corrections are in the range +0.02 to +0.04 dex for the ⟨3D⟩ model, and typically a factor of two lower for the HM semi-empirical model. As for the other iron-peak elements except Sc (cf. Sect. 4), we used a scaling factor of $S_{\rm H} = 1$ to the Drawin (1969) recipe for inelastic collisions with H. Bergemann & Cescutti (2010) excluded inelastic H I collisions from their model atom ($S_{\rm H} = 0$), in order to obtain ionisation balance with MAFAGS-ODF model atmospheres in a larger sample of late-type stars. This, together with the fact that they considered flux spectra, explains the rather large differences (of order ∼0.1 dex) between our NLTE abundance corrections and theirs for solar Cr I lines.

For Cr II, Bergemann & Cescutti (2010) found that LTE is an excellent approximation even without inelastic hydrogen collisions; we therefore do not apply any NLTE corrections for Cr II.

6.4.4. Line selection

Based on the solar analyses by Sobeck et al. (2007) and Biémont et al. (1978), we selected the 29 best Cr I and 10 best Cr II lines in the solar spectrum. These are given in Table 1.

6.5. Manganese

We took Mn I wavelengths and transition designations from Adelman et al. (1989), and excitation potentials from Corliss & Sugar (1977). Mn has just a single stable isotope (Rosman & Taylor 1998): ^{55}Mn, with $I = \frac{5}{2}$. Mn I lines and atomic data used in the current study are given in Table 1. None of the Mn II lines that we investigated were ultimately of sufficient quality for abundance determination.

6.5.1. Oscillator strengths

FTS Mn I BFs have been most recently measured by Den Hartog et al. (2011), Blackwell-Whitehead & Bergemann (2007) and Blackwell-Whitehead et al. (2005b). Blackwell-Whitehead & Bergemann (2007) used highly accurate TRLIF lifetimes from Schnabel et al. (1995), along with one other lifetime from the laser-excited delayed coincidence of Marek (1975) to produce accurate oscillator strengths. Blackwell-Whitehead et al. (2005b) used their own TRLIF lifetimes to also convert their BFs into accurate oscillator strengths, though for some levels slightly more accurate TRLIF lifetimes are also available from Schnabel et al. (1995). Den Hartog et al. (2011) also measured TRLIF lifetimes with which to convert their BFs into very accurate gf-values, and averaged their data with previous accurate measurements in order to produce a set of recommended values.

Until these three recent studies, the most commonly used Mn oscillator strengths were those of Booth et al. (1984a). These data were measured as a set of relative gf-values in the Oxford furnace and set to an absolute scale using the laser-excited delayed coincidence lifetimes of Becker et al. (1980) and Marek (1975), as well as the phase-shift results of Marek & Richter (1973). Booth et al. (1984a) measured three different systems of lines. The first system consisted of eight lines with excitation potentials of around 0 eV, and was set to an absolute scale using a single averaged lifetime from Marek (1975) and Marek & Richter (1973). The second system (24 lines with excitation potential ∼2 eV) was normalised using an average of the absolute scales implied by lifetimes of six different levels, taken from Becker et al. (1980). The 27 lines of the third system (with excitations ∼3 eV) were normalised using a pyrometry link to the second system, setting the two systems to the same absolute scale.

One concern with the gf-values of Booth et al. (1984a) were some odd discrepancies with the BFs derived earlier by Greenlee & Whaling (1979, GW). There is no immediate reason for the BFs by GW to be unreliable. However, if one compares gf-values given for the 3 eV lines by Booth et al. with gf-values for the same lines derived using GW BFs and either Becker et al. (1980) or Schnabel et al. (1995) lifetimes, an odd dichotomy appears. Whilst we expect both sets to be reliable, the gf-values of Booth et al. (1984a) are consistently ∼0.15–0.20 dex higher than the GW-Becker et al. or GW-Schnabel et al. values. This is confirmed when the gf-values of Blackwell-Whitehead & Bergemann (2007) are compared with the data of Booth et al. (1984a): the values of Booth et al. are systematically larger, by 0.13 dex (±0.02). This is however not the case for the 2 eV system, where the two sets agree very well. These discrepancies have often been ignored in the literature.

The obvious question is whether the pyrometry link utilised by Booth et al. was indeed accurate, seeing as the discrepancy only exists for the 3 eV lines. It seems that poor pyrometry is an unlikely explanation for a ∼40% difference. Clearly something is amiss, but we cannot explain the discrepancy with any confidence. The confusion in the 3 eV oscillator strengths is our main reason for concluding that the stated uncertainty in the solar manganese abundance of Booth et al. (1984b, $\log \epsilon_{\rm Mn} = 5.39 \pm 0.03$) probably substantially underestimated the true error. In the end, two of our adopted Mn I lines are affected by the uncertainties in the Booth et al. gf-values, as we explain below.

Wherever possible, we use the oscillator strengths of Blackwell-Whitehead & Bergemann (2007) or those recommended by Den Hartog et al. (2011). In cases of overlap, we use the recommended Den Hartog et al. (2011) values wherever the uncertainty of Den Hartog et al.'s own measured value is smaller than the error given by Blackwell-Whitehead & Bergemann (2007); the differences are however tiny (∼0.01 dex or less). For the 408.3 nm line, where the value recommended by Den Hartog et al. is the average of their own very accurate value and

the slightly less accurate result of Blackwell-Whitehead et al. (2005b), we adopt Den Hartog et al.'s own raw result rather than the recommended value.

For lines without gf-values available from either Den Hartog et al. (2011) or Blackwell-Whitehead & Bergemann (2007), we derive new oscillator strengths from the BFs of GW and the lifetimes of Schnabel et al. (1995). For the two good 3 eV lines (426.59 and 445.70 nm) measured only by Booth et al., we use the gf-values of Booth et al. but renormalise them to the absolute scale of Blackwell-Whitehead & Bergemann, i.e. decrease them by 0.13 dex. Consummate with this rather approximate gf derivation, we only give these lines a weighting of 1 in the final mean abundance. These lines are marked with asterisks in Table 1. For the remaining line in the 2 eV system (542.0 nm), we continue to use the original oscillator strength of Booth et al. (1984a).

6.5.2. Hyperfine structure

A wealth of data exists on HFS in Mn I, which we have classified into a similar tier system as for other elements. The best original data come from the extremely accurate spin-exchange results of Davis et al. (1971), the ABMR of Johann et al. (1981), ABMR by Dembczyński et al. (1979), interference spectroscopy by Brodzinski et al. (1987) and laser-atomic-beam spectroscopy by Kronfeldt et al. (1985). The second and third tiers consist of FTS and OGS data obtained by Blackwell-Whitehead et al. (2005a) and Başar et al. (2003) respectively. We do not use the B values of Başar et al. for the odd levels however, because in our opinion their accuracy is insufficient to clearly distinguish them from zero. The next most accurate data come from Lefèbvre et al. (2003), followed by Luc & Gerstenkorn (1972), Handrich et al. (1969) and Walther (1962). The solar abundance determinations of Blackwell-Whitehead & Bergemann (2007) and Bergemann & Gehren (2007) include extensive HFS data from many of the sources listed above.

6.5.3. NLTE corrections

The NLTE formation of solar Mn I lines was considered by Bergemann & Gehren (2007), using the 1D theoretical MAFAGS-ODF model atmosphere. Differences between the LTE and NLTE abundances determined using the solar flux spectrum were typically found to be around +0.07 dex for the lines of interest to us. We performed NLTE calculations with the same model atom, but adopted a scaling factor $S_{\rm H} = 1$ to the Drawin (1969) formula (cf. Sect. 4), instead of Bergemann & Gehren's default of $S_{\rm H} = 0.05$. We calculated corrections in disc-centre intensity with the ⟨3D⟩, MARCS and HM 1D model atmospheres; as for other elements we adopt the ⟨3D⟩ results as proxies for the 3D case. The NLTE abundance corrections depend on the line properties, i.e. upper and lower excitation potentials, equivalent width and HFS. For example, the saturated 408.2 nm line ($E_{\rm exc} = 2.2$ eV) has an NLTE correction of only +0.016 dex. In contrast, the 542.0 nm line, with roughly the same equivalent width but different upper level, has an NLTE correction of +0.07 dex. NLTE effects in the solar Mn I lines are not very sensitive to the adopted efficiency of inelastic hydrogen collisions. Reducing $S_{\rm H}$ to 0.05 increases the NLTE corrections for all investigated lines by a maximum of ∼0.02 dex. Our adopted NLTE corrections are given in Table 1.

6.5.4. Line selection

The 3 eV system yields better lines for solar abundance determination than the 0 eV or 2 eV systems, as the 3 eV lines are formed lower in the photosphere, and are therefore less prone to uncertainties associated with the temperature structure of the model atmosphere. Even amongst the 3 eV lines however, most usable Mn I lines are not particularly weak, so we were forced to consider mostly lines of intermediate strength. The large HFS of many of these lines should at least mitigate the effects of line strength, by desaturating profiles and lowering formation heights. Unfortunately, apart from Mn I 408.3 nm, all the lines with BFs available from Blackwell-Whitehead et al. (2005b) are too weak or blended to be useful in the Sun, so most of our chosen lines came from Blackwell-Whitehead & Bergemann (2007). After considering previous solar abundance analyses (e.g. Blackwell et al. 1972; Biémont 1975; Booth et al. 1984b; Blackwell-Whitehead & Bergemann 2007; Bergemann & Gehren 2007), we retained the 14 lines given in Table 1.

6.6. Iron

We used wavelengths from Nave et al. (1994) for Fe I, and from Nave & Johansson (2013) for Fe II. Excitation potentials and transition designations for both species were taken from VALD. Iron has four stable isotopes (Rosman & Taylor 1998): ^{54}Fe (5.8%), ^{56}Fe (91.8%), ^{57}Fe (2.1%) and ^{58}Fe (0.3%). The only one of these with non-zero nuclear spin is ^{57}Fe, with $I = \frac{1}{2}$. Iron lines therefore exhibit virtually no isotopic or hyperfine structure.

6.6.1. Oscillator strengths

The best gf-values for Fe I have been obtained by quite different techniques. The Oxford dataset (see Blackwell et al. 1995, and references therein) is based on absorption spectroscopy: very precise relative gf-values were measured in the Oxford furnace, and then normalised to an absolute scale using one line for which the absolute gf-value is known with high precision (±0.02 dex). Two other groups at Hannover (Bard et al. 1991; Bard & Kock 1994) and at Madison (O'Brian et al. 1991) used emission spectroscopy, measuring lifetimes and BFs. These three sources provide our adopted gf-values. When gf-values were available from more than one of these sets for any given line, we adopted an unweighted mean of the values from the different sets. The exception to this rule was a group of three lines where we gave less weight to the O'Brian et al. (1991) data, because of their larger uncertainties for these specific lines. For one line (Fe I 829.4 nm) where the error on the gf-value remains large, we degrade the weight of the line in our analysis by one unit, as indicated by the asterisk in Table 1; the uncertainty of the other Fe I gf-values given in Table 1 is probably of order 5–10%. Newer oscillator strengths are also available from Ruffoni et al. (in prep.), but for the only line in our list to have been remeasured (Fe I 578.4 nm), the newer oscillator strength results in a clearly discrepant abundance (by ≈0.1 dex).

Fe II oscillator strengths increased in accuracy over the past 20 years as progressively more accurate TRLIF lifetimes were measured by Hannaford et al. (1992), Schnabel et al. (1999) and Schnabel et al. (2004), and used to normalise earlier FTS and grating spectrometer emission BFs from Heise & Kock (1990) and Kroll & Kock (1987). Probably the most accurate gf-values now come from the compilation of Meléndez & Barbuy (2009), who used these and other experimental lifetimes to recalibrate

and average a raft of theoretical and experimental BFs; we adopt these data for all our Fe II lines. All of our Fe II lines have laboratory-based rather than astrophysical gf-values from Meléndez & Barbuy (2009).

6.6.2. NLTE corrections

We computed NLTE corrections for Fe I lines using the Fe model atom of Bergemann et al. (2012), which was constructed from the most up-to-date theoretical and experimental atomic data available for Fe I and Fe II. We computed the disc-centre intensity spectrum using a scaling factor $S_{\rm H} = 1$ to the Drawin (1969) recipe for inelastic H collisions, as preferred by the analysis of Bergemann et al. (cf. Sect. 4). We did the calculations with the ⟨3D⟩, MARCS and HM 1D model atmospheres, resulting in mean NLTE corrections of +0.01 dex. Larger Fe I NLTE effects were advocated by Mashonkina et al. (2011), who also used an extended Fe model atom, but a lower efficiency for hydrogen collisions ($S_{\rm H} = 0.1$). This choice, together with the fact that Mashonkina et al. (2011) considered flux spectra, mostly explains the difference with our results. Mashonkina et al.'s NLTE corrections were +0.04 dex for lines with excitation energies up to 1 eV, and about +0.03 dex for higher-excitation lines. NTLE corrections are negligible for Fe II (Bergemann et al. 2012), so we adopt LTE results for the ionised lines.

6.6.3. Line selection

We selected the 22 best Fe I and 9 best Fe II lines, i.e. those lines for which equivalent widths are easily measured, that do not show any intractable trace of blending, and are not too strong. Our selected lines and atomic data are given in Table 1. For Fe I, we made sure to have a sample of lines that covers a large range of excitation potentials (0–4.6 eV) to probe the performance of the different atmospheric models over a range of heights.

6.7. Cobalt

We took excitation potentials of Co I from Pickering & Thorne (1996), as well as wavelengths and transition designations where available; otherwise, we sourced wavelengths and transitions from Cardon et al. (1982). The only stable isotope of cobalt is ^{59}Co (Rosman & Taylor 1998), which has nuclear spin $I = \frac{7}{2}$. Our chosen Co I lines and atomic data are given in Table 1. None of the Co II lines in the solar spectrum are suitable for abundance analyses.

6.7.1. Oscillator strengths

The most reliable Co I oscillator strengths currently available come from Nitz et al. (1999), who measured FTS BFs and set them to an absolute scale using their own TRLIF lifetimes (Nitz et al. 1995). The next most accurate data are those of Cardon et al. (1982), who measured BFs that they set to an absolute scale using the TRLIF lifetimes of Marek & Vogt (1977) and Figger et al. (1975). For some lines, the gf-values of Cardon et al. (1982) are accurate to better than 10%, which is comparable to the accuracy obtained by Nitz et al. (1999); for other lines the uncertainties are much larger, of order 20–30%. BFs contemporary with those of Cardon et al. (1982) are also available from Guern & Lotrian (1982), but we prefer the data of Cardon et al. as they are based upon FTS recordings and include a more complete set of branches.

6.7.2. Hyperfine structure

We used stated uncertainties to classify the wealth of data available on Co I HFS into a similar tier system as for other elements. Our first choice of HFS data were the ABMR results of Childs & Goodman (1968), and the combined Doppler-free and Doppler-limited LFS/OGS results of Guthöhrlein & Keller (1990). The next most accurate data come from the FTS of Pickering (1996). Also available are unpublished data obtained by J. Ibrahim-Rüd and R. Wenzel, reproduced in the paper of Guthöhrlein & Keller (1990). We fit these data into the hierarchy on a level-by-level basis around Guthöhrlein & Keller (1990), Pickering (1996) and Childs & Goodman (1968). Bergemann et al. (2010) included extensive HFS data in their calculation of the solar Co abundance, showing that neglect or inaccurate treatment of HFS can lead to severe errors in derived abundances.

6.7.3. NLTE corrections

Non-LTE formation of solar Co I and Co II lines has been investigated by Bergemann et al. (2010) using the MAFAGS-ODF models. The results indicate large departures from LTE in Co I, leading to NLTE abundance corrections of +0.1–0.2 dex at $S_{\rm H} = 0.05$ (Bergemann et al. 2010, cf. their Table 4), resembling the situation with Sc I lines (Zhang et al. 2008). We use the same Co model atom, but adopt $S_{\rm H} = 1$ (cf. Sect. 4) and disc-centre intensity spectra for the ⟨3D⟩, MARCS and HM 1D model atmospheres. This leads to somewhat smaller NLTE abundance corrections, of order +0.09 dex for ⟨3D⟩ and +0.07 dex for the HM model.

6.7.4. Line selection

Unfortunately, there are rather few good lines in the solar spectrum with oscillator strengths available from Nitz et al. (1999), so the bulk of our lines have gf values drawn from Cardon et al. (1982). For some of the cleanest weak lines, the Cardon et al. gf-values have rather large uncertainties (over 20% in some cases). We include such lines because of their excellent profiles, but downgrade their weightings; affected lines are marked with an asterisk in Table 1. From the lines considered in the abundance analyses of Cardon et al. (1982), Biémont (1978), Kerola & Aller (1976) and Holweger & Oertel (1971), we retained the 13 transitions given in Table 1.

6.8. Nickel

We obtained Ni I wavelengths and excitation potentials from Litzen et al. (1993). Transition identities came from Wickliffe & Lawler (1997), except for Ni I 481.2 nm, where the transition designation is from VALD (Kupka et al. 1999). Our selected Ni I lines are given in Table 1. We also considered Ni II, but it ultimately played a very minimal role in our analysis; we omit it from Table 1, give a truncated discussion of its atomic data and line selection in this section, and discuss only briefly the mean implied Ni abundance in Sect. 7.8.

Nickel has five stable isotopes, so exhibits significant isotopic structure (as seen by e.g. Brault & Holweger 1981; Meléndez & Barbuy 1999). These are ^{58}Ni, ^{60}Ni, ^{61}Ni, ^{62}Ni and ^{64}Ni, present in the approximate ratios 68:26:1:4:1 (Rosman & Taylor 1998). In practice, the isotopic structure of nickel lines is dominated by ^{58}Ni and ^{60}Ni due to their much greater natural abundances. As an even-Z element, all the even-A nuclei of nickel have $I = 0$, so nickel lines do not exhibit any HFS apart

from ^{61}Ni. The contribution of ^{61}Ni to the HFS of nickel is minimal, given its very low abundance relative to ^{58}Ni and ^{60}Ni. For spectroscopic purposes, one can thus effectively regard nickel as consisting of four isotopes, and devoid of HFS.

6.8.1. Oscillator strengths

High-quality Ni I oscillator strengths are available from the FTS BFs of Wickliffe & Lawler (1997), which the authors placed on an absolute scale using the TRLIF lifetimes of Bergeson & Lawler (1993b). These have recently been updated and greatly extended by Wood et al. (2014b). A small number of high-quality gf-values are also available from Johansson et al. (2003), based upon FTS BFs and a single TRLIF lifetime. Bergeson & Lawler (1993b) used their new lifetimes to produce other accurate gf-values from the BFs of Blackwell et al. (1989), but these lines are all in the UV, so of little use to us because the ultraviolet solar spectrum is so crowded. Accurate oscillator strengths for optical lines of Ni II do not exist, so we turned to the extensive theoretical transition probabilities of Fritzsche et al. (2000).

6.8.2. Isotopic structure

Wherever available, we employ isotopic separations from Wood et al. (2014b), who fitted the isotopic shifts of a large number of Ni I energy levels to earlier spectroscopic data. Much of the power of that analysis can be attributed to the accurate FTS wavelengths of ^{58}Ni and ^{60}Ni line components recorded by Litzen et al. (1993). As in Wood et al.'s analysis, we model ^{58}Ni and ^{60}Ni components explicitly, and estimate the contribution of the remaining isotopes by placing them in a single line component, which we offset from ^{60}Ni by the same amount as ^{60}Ni is offset from ^{58}Ni. These data are included in Table 2.

6.8.3. NLTE corrections

The only explicit investigation of non-LTE effects on solar nickel line formation so far has been that of Bruls (1993), who looked at the Ni I 676.8 nm line often used for helioseismology. Although Bruls did not give any explicit NLTE abundance correction for this line, his Fig. 4 would imply a correction of about +0.06 dex. This line corresponds to a transition between low-lying atomic levels and is thus formed higher than those we employ here. It may therefore be expected to show stronger NLTE effects than our weaker high-excitation lines. Because Bruls (1993) completely neglected inelastic H collisions, his results can probably be taken as an upper limit for possible NLTE effects. We therefore do not expect significant departures from NLTE for our own weak, high-excitation lines, and simply adopt LTE results for Ni I. Further investigation of NLTE Ni line formation (e.g. Vieytes & Fontenla 2013) would be welcome however, as this expectation bears additional verification.

6.8.4. Line selection

From the most accurate gf-values available for Ni I, we have retained the 16 weak, unblended lines of Table 1. We also included the slightly stronger Ni I 617.7 nm line, because of its pristine appearance in the solar spectrum and the quality of its atomic data.

Although the situation with Ni II is better than for Mn II or Co II, most of the Ni II lines in the IR are too weak to be useful for abundance purposes, and those in the optical are generally at very short wavelengths and severely blended. We attempted to use the lines at 340.2, 342.1, 345.4 and 376.9 nm; all are perturbed to some degree, so the scatter in resultant abundances probably reflects both large intrinsic errors in the theoretical gf-values and the crowding in this spectral region.

7. Derived solar elemental abundances

We have derived the solar abundances of Sc, Ti, V, Cr, Mn, Fe, Co and Ni from each of the lines given in Table 1. The interpolated theoretical 3D line profiles show good agreement with the observed solar spectrum, as can be seen in the sample of lines shown in Figs. 1 and 2. This agreement is a result of the inhomogeneous, three-dimensional temperature and velocity structure of the 3D model atmosphere, and the inclusion of HFS and isotopic structure wherever necessary. A small systematic deviation of the theoretical profiles from the observed spectrum can be seen in the cores and wings of some lines: the lines are slightly too deep in the core and too shallow in the wings, which may signal NLTE effects (note that full 3D line formation calculations have not been attempted). These small discrepancies may also indicate that the photospheric velocity structure of the 3D model, whilst certainly highly realistic, is not quite perfect.

The 3D abundance results are given for each line in Table 1, including NLTE corrections where possible. In Table 1 we also give the LTE abundances derived from each line with the ⟨3D⟩, HM, MARCS and MISS 1D models. In Figs. 3–10 we plot the 3D abundances as a function of line strength and excitation potential. We also show in these figures the difference between the abundances derived using the 3D and HM models, and between those derived from the 3D and ⟨3D⟩ models, as a function of line strength and excitation potential.

In the following sections we discuss the results for each element in detail, comparing with previous determinations of the solar abundance and with the meteoritic values. The latter we take from the recent careful compilation and analysis of Lodders et al. (2009), renormalised to the photospheric abundance of silicon determined in Paper I ($\log \epsilon_{\rm Si} = 7.51$, as already done in AGSS09). We also describe the updates we have made for specific elements since AGSS09. In addition to those updates, before reiterating on all abundance calculations a final time, we updated all partition functions and ionisation potentials (Table 3), and updated our equation-of-state tables and base atmospheric composition to the published AGSS09 mixture. We summarise our full results in Table 4, including our final recommended abundances. We compare these results to previous solar abundance compilations in Table 5. We remind the reader that the error treatment used in the following sections is summarised in Sect. 5.

7.1. Scandium

For Sc I lines, the 3D+NLTE result is $\log \epsilon_{\rm Sc} = 3.14 \pm 0.09$ (± 0.01 stat, ± 0.09 sys). The corresponding result from Sc II lines is $\log \epsilon_{\rm Sc} = 3.17 \pm 0.04$ (± 0.02 stat, ± 0.04 sys), in good agreement with the Sc I result. Taking all Sc I and Sc II lines together, our final recommended Sc abundance becomes

$$\log \epsilon_{\rm Sc} = 3.16 \pm 0.04 \ (\pm 0.01 \ \text{stat}, \ \pm 0.04 \ \text{sys}).$$

Intriguingly, this value is 0.11 dex, or more than two standard deviations, larger than the meteoritic value (3.05 ± 0.02; Lodders et al. 2009). We leave speculation as to the importance of this and other photospheric-meteoritic differences for future work.

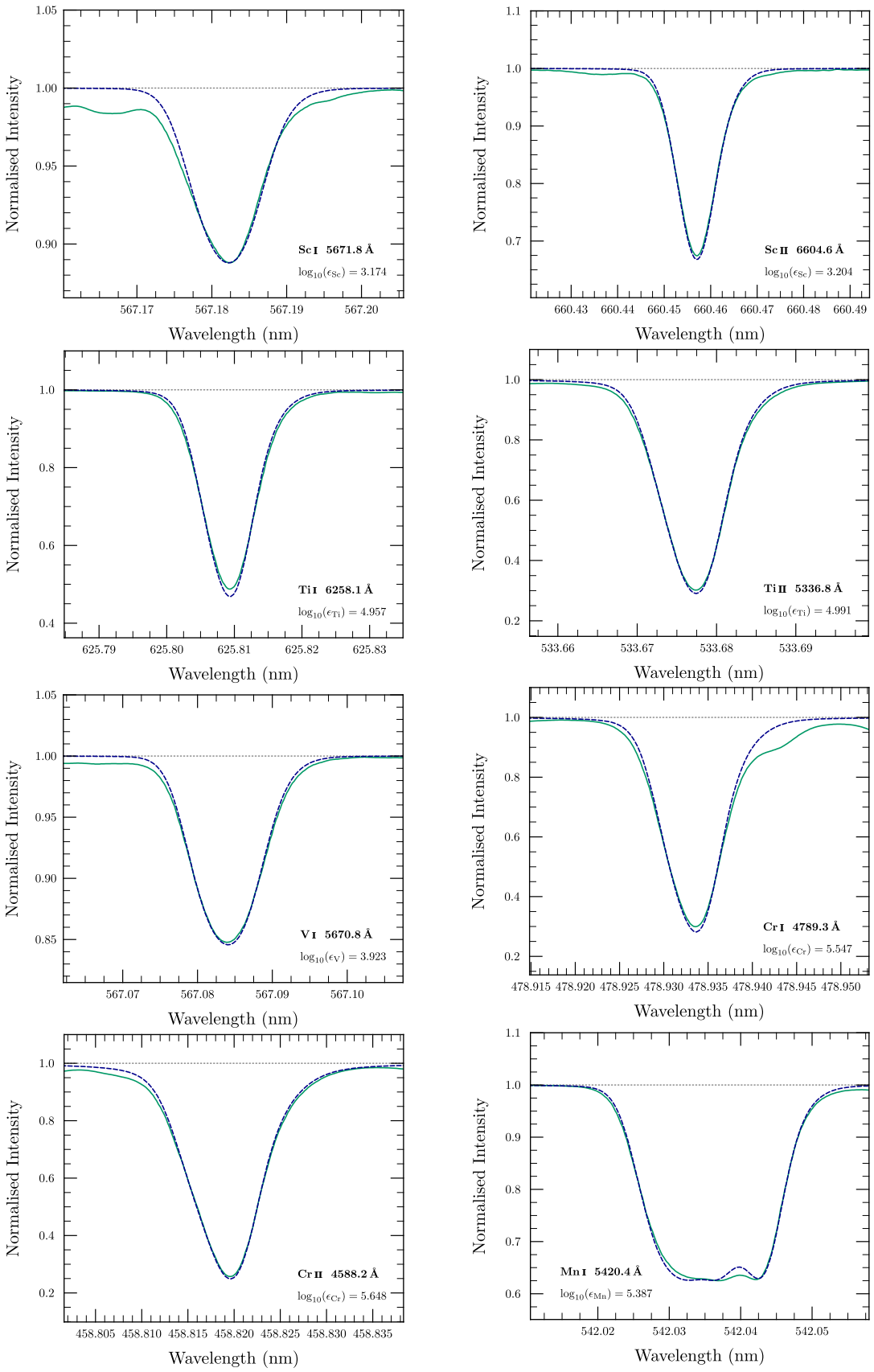

Fig. 1. Example spatially and temporally averaged, disc-centre synthesised Sc I, Sc II, Ti I, Ti II, V I, Cr I, Cr II and Mn I line profiles (blue dashed), shown in comparison to the observed FTS profile (solid green). We removed the solar gravitational redshift from the FTS spectrum, convolved the synthesised profile with an instrumental sinc function and fitted it in abundance. Wavelengths and continuum placements have been adjusted for display purposes. Plotted profiles are computed in LTE, but quoted abundances in each panel include NLTE corrections computed in 1D (wherever available).

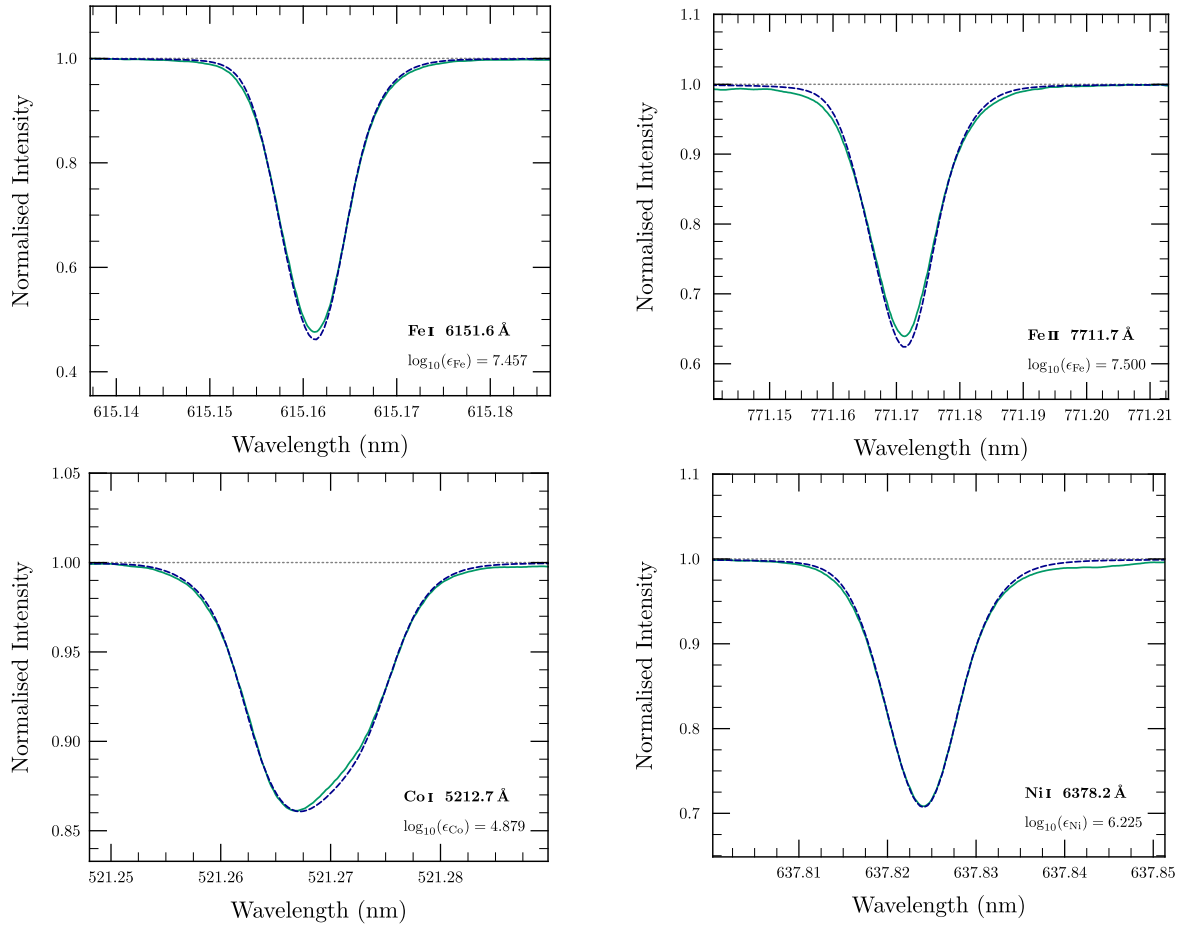

Fig. 2. As per Fig. 1, but for Fe I, Fe II, Co I and Ni I.

We see from Table 4 and the right-hand panels of Fig. 3 that the model atmosphere plays only a minor role for Sc II lines, as is generally true for the dominant ionisation stage. On the other hand, abundances derived from Sc I are extremely sensitive to the choice of model, as expected for a low ionisation neutral species. We also see in Fig. 3 that 3D Sc abundances do not show any significant trend with excitation potential or line strength. Abundance scatter is generally higher with Sc II than Sc I lines, reflecting the greater uncertainty in the Sc II gf-values.

Our results are in good agreement with the Sc abundance of Zhang et al. (2008). Their value of $\log \epsilon_{\rm Sc} = 3.13 \pm 0.05$ was essentially based on Sc II lines, and derived using the same experimental gf-values as we do here, along with a theoretical 1D photospheric model. Compared to the result we presented in AGSS09 ($\log \epsilon_{\rm Sc} = 3.16 \pm 0.04$), in this analysis we have discarded the three lines discussed in Sect. 6.1.1 as having excellent profiles but unsatisfactory oscillator strengths.

7.2. Titanium

Titanium is in principle an ideal case: a large number of good solar lines with accurate transition probabilities, very minor HFS and isotopic broadening, and extensive NLTE calculations available for the minority species (Ti I).

Nonetheless, the derived 3D+NLTE Ti abundances from Ti I ($\log \epsilon_{\rm Ti} = 4.88 \pm 0.05$; ± 0.01 stat, ± 0.05 sys), and Ti II ($\log \epsilon_{\rm Ti} = 4.97 \pm 0.04$; ± 0.01 stat, ± 0.03 sys) show a 0.09 dex discrepancy. Even more puzzlingly, this discrepancy is not present in either the mean HM or ⟨3D⟩ results. Referring to Fig. 4, 3D+NLTE abundances from Ti I and Ti II show no perceptible trend with line strength or excitation potential, whereas the HM and ⟨3D⟩ results show a clear trend with line strength for both ionisation stages. Given the rather large 3D corrections for Ti I, and the fact that we always *assume* the NLTE corrections for the 3D model to be equal to those calculated for the ⟨3D⟩ model, we suspect that the NLTE corrections are somewhat underestimated in ⟨3D⟩ compared to full 3D. Alternatively, our chosen efficiency of inelastic collisions with hydrogen ($S_{\rm H} = 1$) may be somewhat too high in this case; had we instead adopted $S_{\rm H} = 0.05$, the 3D+NLTE abundance from Ti I would have been $\log \epsilon_{\rm Ti} = 4.93$.

Considering the sensitivity of the Ti I NTLE corrections to $S_{\rm H}$, for our final recommended Ti abundance we take a weighted mean of the Ti I and Ti II results, with the weightings determined by the respective uncertainties of the two results. This favours Ti II due to its smaller systematic uncertainty, resulting in

$$\log \epsilon_{\rm Ti} = 4.93 \pm 0.04 \ (\pm 0.01 \ \text{stat}, \ \pm 0.04 \ \text{sys}).$$

Here we have estimated the errors by considering all Ti I and Ti II lines equally in a single list, rather than by using the same statitistical weighting procedure as for the mean. Had we instead used the latter procedure, the final uncertainty would be just 0.03 dex; owing to the tension between Ti I and Ti II , and for consistency with other elements where we include both ionisation stages in a single list, we think it more appropriate to adopt the larger estimate. The final Ti abundance is in excellent agreement with the meteoritic value (4.91 ± 0.03; Lodders et al. 2009), but the difference between the results returned by the two ionisation stages remains troubling.

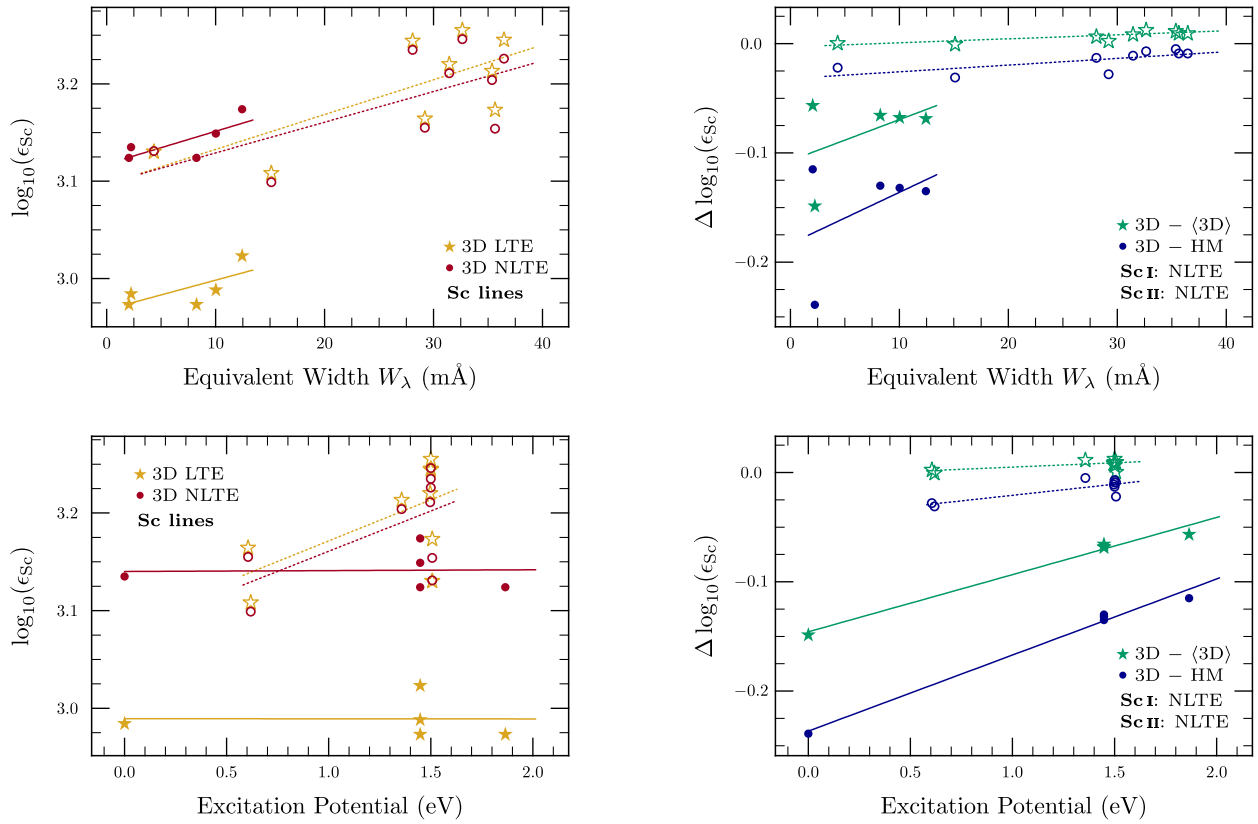

Fig. 3. *Left*: Sc abundances derived from Sc I and Sc II lines with the 3D model, shown as a function of equivalent width and lower excitation potential. *Right*: line-by-line differences between Sc abundances obtained with the 3D and ⟨3D⟩ models, and between those obtained with the 3D and HM models. Filled symbols and solid trendlines indicate lines of the neutral species (Sc I), whereas open symbols and dotted lines indicate singly-ionised (Sc II) lines. Trendlines give equal weight to each line (unlike our mean abundances, where we give larger weights to better lines).

Bergemann (2011) found that Ti ionisation balance would be best satisfied with the MAFAGS-OS model if one were to adopt the Blackwell-Whitehead et al. (2006) and Pickering et al. (2001) gf-values, giving $\log \epsilon_{\rm Ti} = 4.94 \pm 0.05$ from Ti I lines and $\log \epsilon_{\rm Ti} = 4.95 \pm 0.06$ for Ti II lines. Using more accurate gf-values (Bizzarri et al. 1993) would lead to a larger discrepancy between Ti I and Ti II: $\log \epsilon_{\rm Ti} = 4.93 \pm 0.04$ from Ti I lines and $\log \epsilon_{\rm Ti} = 4.98 \pm 0.04$ for Ti II lines. As in this paper, Bergemann (2011) observed a strong dependence of Ti I abundances upon the chosen model atmosphere and collisional efficiency parameters.

Compared to the result we adopted in AGSS09 ($\log \epsilon_{\rm Ti} = 4.95 \pm 0.05$), we now have dedicated NLTE calculations available in intensity for Ti I based on the work of Bergemann (2011). We have also now dropped the Ti I line at 522.4 nm from our line list due to blending, adopted isotopic splitting and HFS data for Ti II, and employed accurate new oscillator strengths for both ionisation stages (Lawler et al. 2013; Wood et al. 2013).

7.3. Vanadium

Quality atomic data exists for both ionisation stages of V, but the only clear solar lines are of V I. Unfortunately, only V II lines are expected to form in LTE; the magnitude of NLTE corrections for V I is unknown, so we apply an ad hoc correction of +0.1 dex, as discussed in Sect. 6.3.1.

The minority species, V I, is more strongly affected by the temperature structure of the model atmosphere than V II. The 3D LTE abundance from V I lines is $\log \epsilon_{\rm V} = 3.79 \pm 0.04$ (1σ dispersion), whereas with the HM model we obtain $\log \epsilon_{\rm V} = 3.97 \pm 0.03$ (1σ). For V II, the 3D and HM LTE results agree well: $\log \epsilon_{\rm V} = 4.00 \pm 0.05$ (1σ) in 3D, $\log \epsilon_{\rm V} = 4.01 \pm 0.05$ (1σ) with HM.

These numbers are not a complete surprise: we know that HM "includes" NLTE effects to some degree by way of its empirical temperature construction, as effects of departures from LTE can be partially mimicked by adjusting the spatially-averaged temperature structure of the model atmosphere, a phenomenon dubbed "NLTE masking" by Rutten & Kostik (1982). Similarly, the 3D V I results exhibit a strong dependence upon excitation potential, whereas the results from HM do not (Fig. 5). Because we applied the same NLTE correction to all V I lines, the trend also remains in NLTE. In reality we expect more pronounced NLTE effects for lower-excitation lines, as these are sensitive to higher atmospheric layers, where lower densities and temperatures make LTE an increasingly poor approximation.

Although low-excitation lines are most sensitive to the temperature structure, and therefore less reliable as abundance indicators, we have no way to know whether our universal NLTE correction of +0.1 dex is more accurate at high or low excitation potential. To avoid introducing any further systematic bias into our result, we therefore retain both the high- and low-excitation lines in our sample of V I lines. A dedicated NLTE study of V line formation in the Sun would clarify matters substantially.

Given the abysmal nature of the V II lines in the solar spectrum, abundances from these lines are dominated by systematic and statistical errors in the determination of equivalent widths. We therefore trust the absolute values of the V II results even less than our ad hoc V I NLTE correction, and adopt the

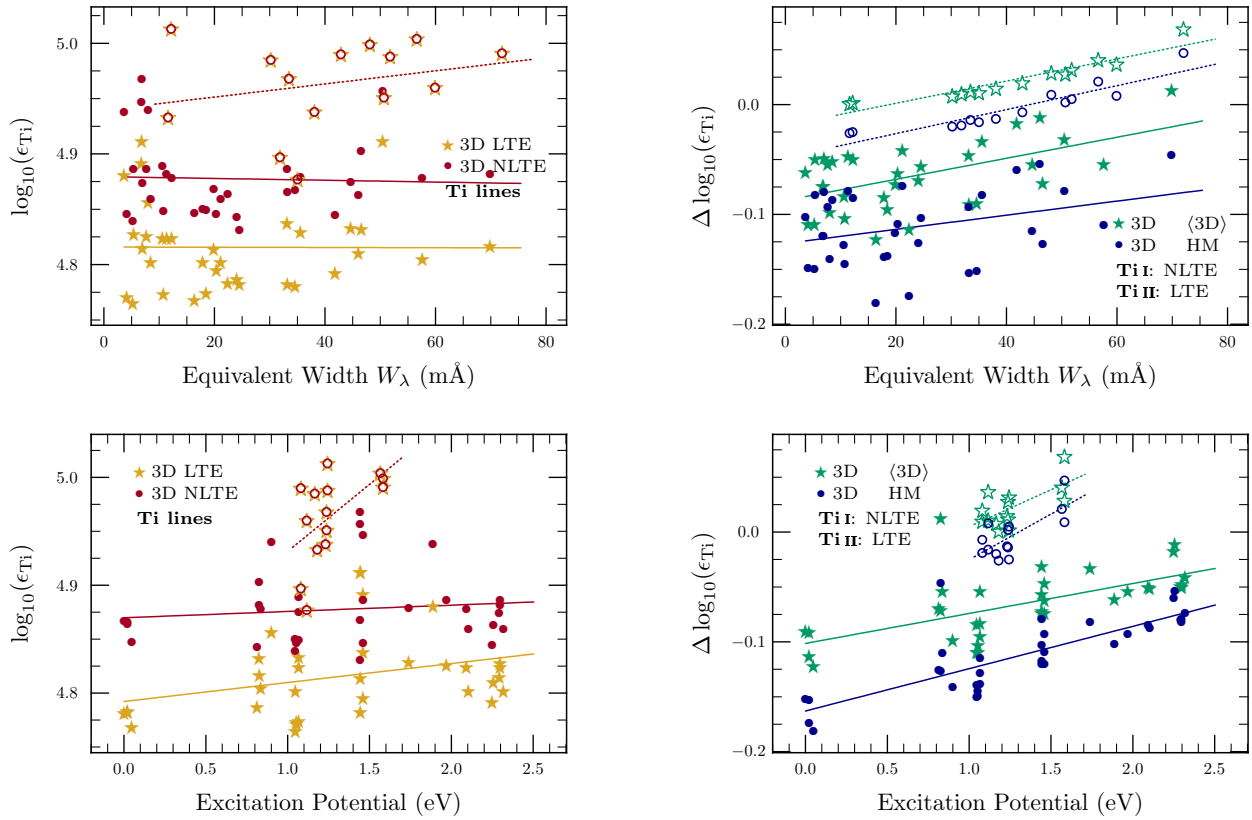

Fig. 4. *Left*: 3D Ti abundances from Ti I and Ti II lines, as a function of equivalent width and lower excitation potential. *Right*: line-by-line differences between abundances obtained with the 3D and ⟨3D⟩ models, and between those obtained with the 3D and HM models. Filled symbols and solid trendlines indicate neutral lines, open symbols and dotted lines indicate singly-ionised lines.

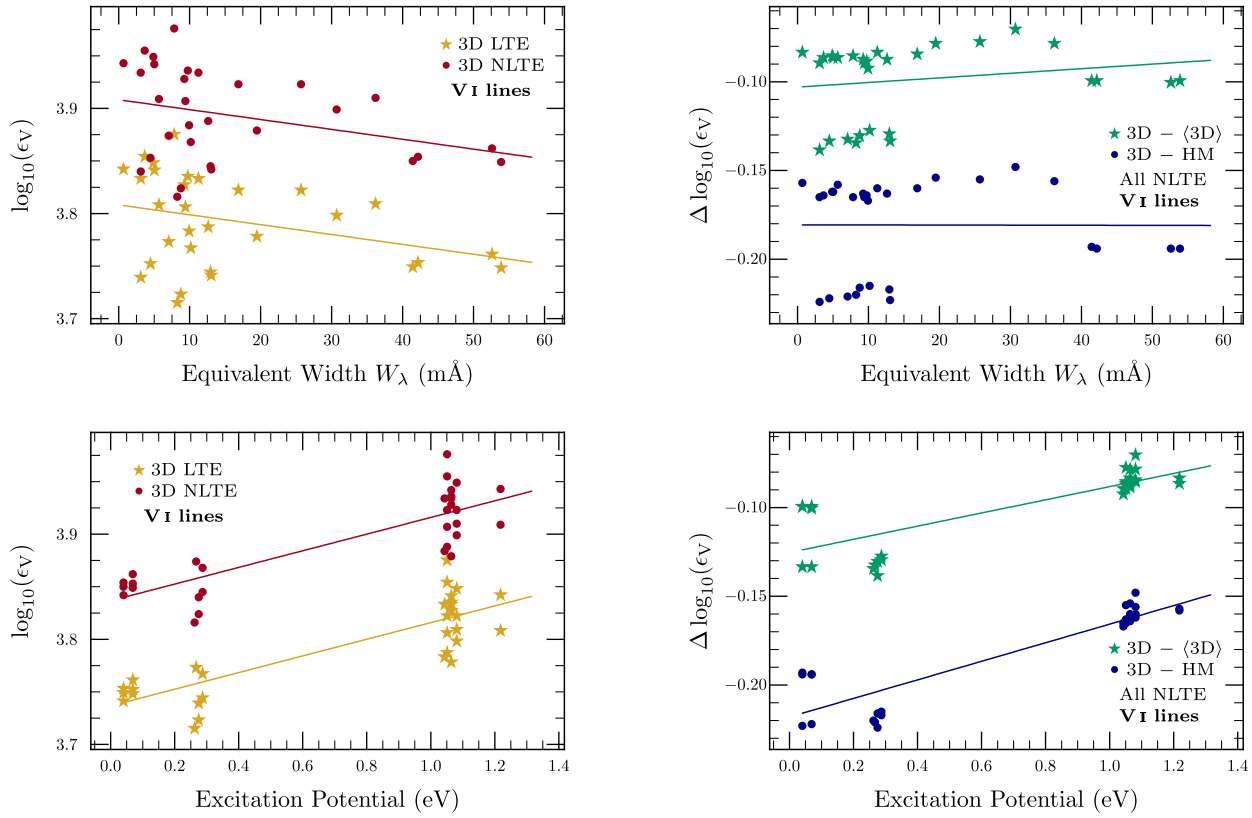

Fig. 5. *Left*: 3D V abundances from V I lines, as a function of equivalent width and lower excitation potential. *Right*: line-by-line differences between abundances obtained with the 3D and ⟨3D⟩ models, and between those obtained with the 3D and HM models.

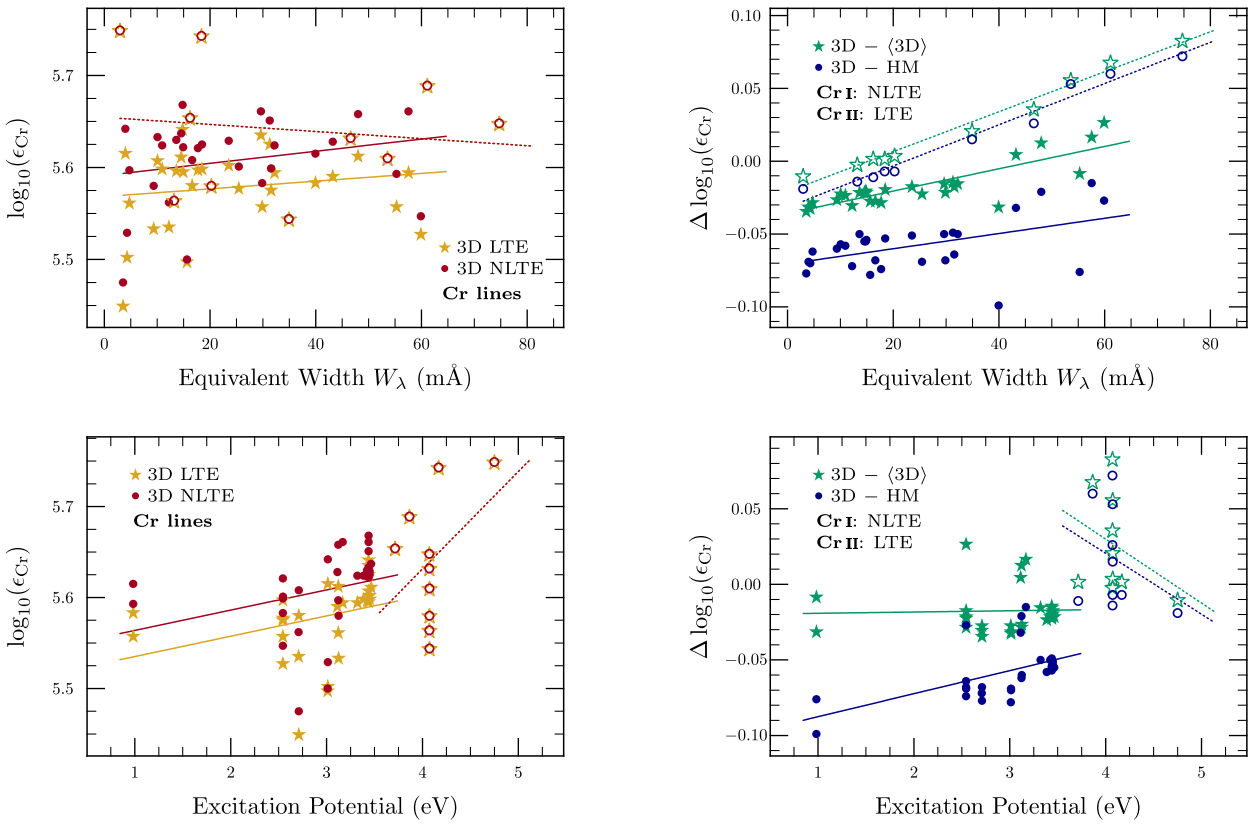

Fig. 6. *Left*: 3D Cr abundances from Cr I and Cr II lines, as a function of equivalent width and lower excitation potential. *Right*: line-by-line differences between abundances obtained with the 3D and ⟨3D⟩ models, and between those obtained with the 3D and HM models. Filled symbols and solid trendlines indicate neutral lines, open symbols and dotted lines indicate singly-ionised lines.

NLTE-corrected V I 3D result as our recommended value:

$\log \epsilon_V = 3.89 \pm 0.08$ (±0.01 stat, ±0.08 sys).

Our result is significantly lower than the stated HM-based abundances of Whaling et al. (1985, 3.99 ± 0.01) and Biémont et al. (1989, 4.02 ± 0.02); their quoted uncertainties only consider statistical errors, not systematic errors stemming from, for example, the gf-values, model atmospheres or LTE line formation. Our 3D result is also below the meteoritic value (3.96 ± 0.02; Lodders et al. 2009), but the mutual uncertainties overlap. Compared to AGSS09 ($\log \epsilon_V = 3.93 \pm 0.08$), here we have added laboratory HFS data for V II. We also discarded two V I lines (619.9 nm and 624.3 nm), because we are suspicious as to the accuracy of the experimental branching fractions measured from their shared upper level.

As noted in Sect. 6.3.1, Wood et al. (2014a) have recently measured new experimental transition probabilities for a large number of V II lines. Had we adopted their values for our five lines, the 3D-based V II abundance would be 0.02 dex lower, and thus in slightly better agreement with the V I results. Wood et al. also performed spectrum synthesis (using the HM model) rather than fitting equivalent widths as we do here, which further reduces the inferred V II abundance. Comparing the results obtained with the HM model by both Wood et al. and us, and taking into account the differences in the adopted gf-values, we estimate that employing spectrum synthesis with our 3D models would have reduced the abundance by a further 0.02 dex. Our final 3D V II abundance would then have become $\log \epsilon_V = 3.96$, in perfect agreement with the meteoritic value. We note that Wood et al. employed a larger set of 15 V II lines, resulting in a mean abundance of $\log \epsilon_V = 3.95 \pm 0.05$ (1σ), which should be contrasted with our HM-based value of $\log \epsilon_V = 4.01 \pm 0.05$ (1σ). Adopting the oscillator strengths of Wood et al. and taking into account the −0.02 dex impact of spectrum synthesis on our lines, our HM abundance would become $\log \epsilon_V = 3.97 \pm 0.04$, in perfect agreement with Wood et al. for the five lines in common. In other words, there is a real possibility that our 3D V II result should be decreased by about 0.04 dex, bringing it into better agreement with V I. However, we still argue that V I is a better indicator of the solar V abundance, in spite of the uncertainty in the NLTE effects.

7.4. Chromium

For Cr I, we have a large number of very good solar lines (Sect. 6.4.3) and very accurate gf-values (Sect. 6.4.1). Our derived NLTE abundance from Cr I lines is $\log \epsilon_{Cr} = 5.60 \pm 0.04$ (±0.01 stat, ±0.04 sys). Using the very few recent experimental gf-values for Cr II lines (Nilsson et al. 2006), we found a very large scatter in abundances. We therefore recommended (Sect. 6.4.1) the theoretical gf-values of Kurucz (2011) as the best currently available. With these data we find $\log \epsilon_{Cr} = 5.65 \pm 0.04$ (±0.02 stat, ±0.04 sys) from Cr II lines, in good agreement with both the Cr I result and the meteoritic abundance (5.64 ± 0.01; Lodders et al. 2009). We therefore adopt the mean result from all Cr lines

$\log \epsilon_{Cr} = 5.62 \pm 0.04$ (±0.01 stat, ±0.03 sys)

as our final recommended solar Cr abundance.

No significant trends are visible with line strength or excitation potential in the results with any model (Fig. 6, left panels).

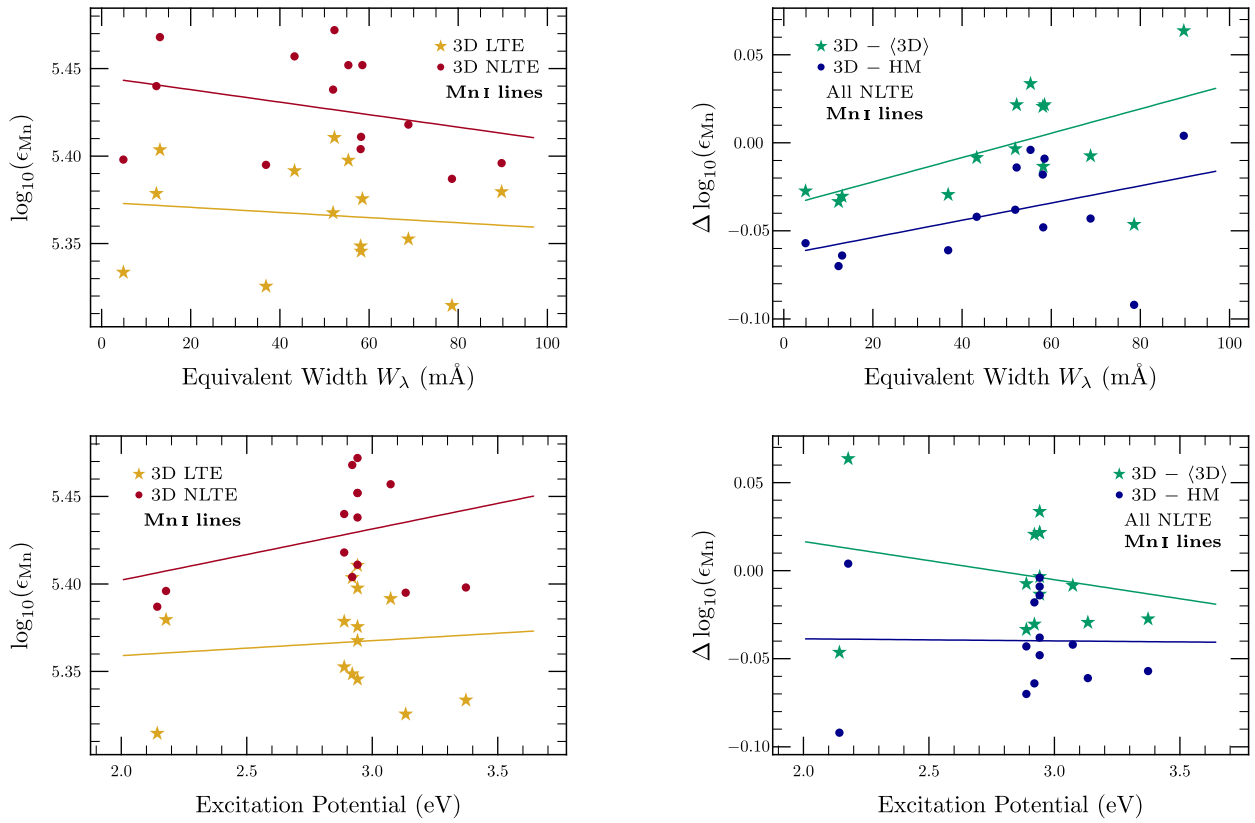

Fig. 7. *Left*: 3D Mn abundances from Mn I lines, as a function of equivalent width and lower excitation potential. *Right*: line-by-line differences between abundances obtained with the 3D and ⟨3D⟩ models, and between those obtained with the 3D and HM models.

Our NLTE results with the HM model agree very well with the LTE abundances derived from the Cr I lines by Biémont et al. (1978, $\log \epsilon_{\rm Cr} = 5.67$), Blackwell et al. (1987, $\log \epsilon_{\rm Cr} = 5.68$) and Sobeck et al. (2007, $\log \epsilon_{\rm Cr} = 5.64$), which however is somewhat of a coincidence given the significant NLTE corrections. The NLTE result of Bergemann (2011), obtained by choosing $S_{\rm H} = 0$ so as to impose ionisation balance with the MAFAGS-ODF model, is 0.12 dex higher: $\log \epsilon_{\rm Cr} = 5.74$.

For Cr II, our results are much smaller than those of Sobeck et al. (2007, $\log \epsilon_{\rm Cr} = 5.67 \pm 0.13$ with MARCS, $\log \epsilon_{\rm Cr} = 5.77 \pm 0.13$ with HM) or Bergemann & Cescutti (2010, $\log \epsilon_{\rm Cr} = 5.79 \pm 0.12$ with MAFAGS-ODF). Even using the theoretical gf-values of Kurucz, our dispersion is also much smaller ($\sigma = 0.06$) than either of these results. The substantially larger scatter seen with Nilsson et al. (2006) gf-values (as used by Sobeck et al. 2007; Bergemann & Cescutti 2010) than with semi-empirical Kurucz values is worrisome; it remains to be seen if the experimental measurements were affected by a systematic error of some kind.

The result we give here is slightly updated with respect to that in AGSS09 ($\log \epsilon_{\rm Cr} = 5.64 \pm 0.04$), as we now have dedicated NLTE intensity calculations for Cr I (Sect. 6.4.3) for our specific 1D models with $S_{\rm H} = 1$, based on the work of Bergemann & Cescutti (2010).

7.5. Manganese

Following our consideration of the most reliable lines and oscillator strengths for Mn I (Sect. 6.5.1), we find a final NLTE Mn abundance of

$$\log \epsilon_{\rm Mn} = 5.42 \pm 0.04 \ (\pm 0.01 \text{ stat}, \ \pm 0.04 \text{ sys}),$$

slightly smaller than the meteoritic value (5.48 ± 0.01; Lodders et al. 2009).

Our result is somewhat larger than the earlier LTE HM result of Booth et al. (1984b, $\log \epsilon_{\rm Mn} = 5.39$). This shift can mainly be attributed to the positive NLTE abundance corrections and our more accurate oscillator strengths. Our HM and MARCS abundances ($\log \epsilon_{\rm Mn} = 5.47$ and 5.37, respectively) are in good agreement with the corresponding results of Blackwell-Whitehead & Bergemann (2007, $\log \epsilon_{\rm Mn} = 5.46$ and 5.37, respectively). No significant trends with equivalent width or excitation potential are visible in Fig. 7.

Compared to the Mn abundance adopted in AGSS09 ($\log \epsilon_{\rm Mn} = 5.43 \pm 0.04$), we now have dedicated NLTE intensity calculations using the model atom of Bergemann & Gehren (2007) for the individual Mn lines and 1D models we employ (instead of relying on the MAFAGS-ODF model), and adopted $S_{\rm H} = 1$ (instead of $S_{\rm H} = 0.05$). We have also updated four oscillator strengths (Table 1) with the new data of Den Hartog et al. (2011).

7.6. Iron

Both Fe I and Fe II should be good indicators of the Fe abundance, as we have several clean solar lines, small NLTE corrections and accurate oscillator strengths. Our derived Fe abundance from Fe I lines ($\log \epsilon_{\rm Fe} = 7.45 \pm 0.04$; ± 0.01 stat, ± 0.04 sys) overlaps the Fe II result ($\log \epsilon_{\rm Fe} = 7.51 \pm 0.04$; ± 0.01 stat, ± 0.04 sys) to within the mutual uncertainties, but the agreement is not perfect. This may indicate a small error in the Fe II oscillator strengths (as they are at least partially based on theoretical results, which are not always accurate), or perhaps slightly too high an adopted value of $S_{\rm H}$ (resulting in slightly

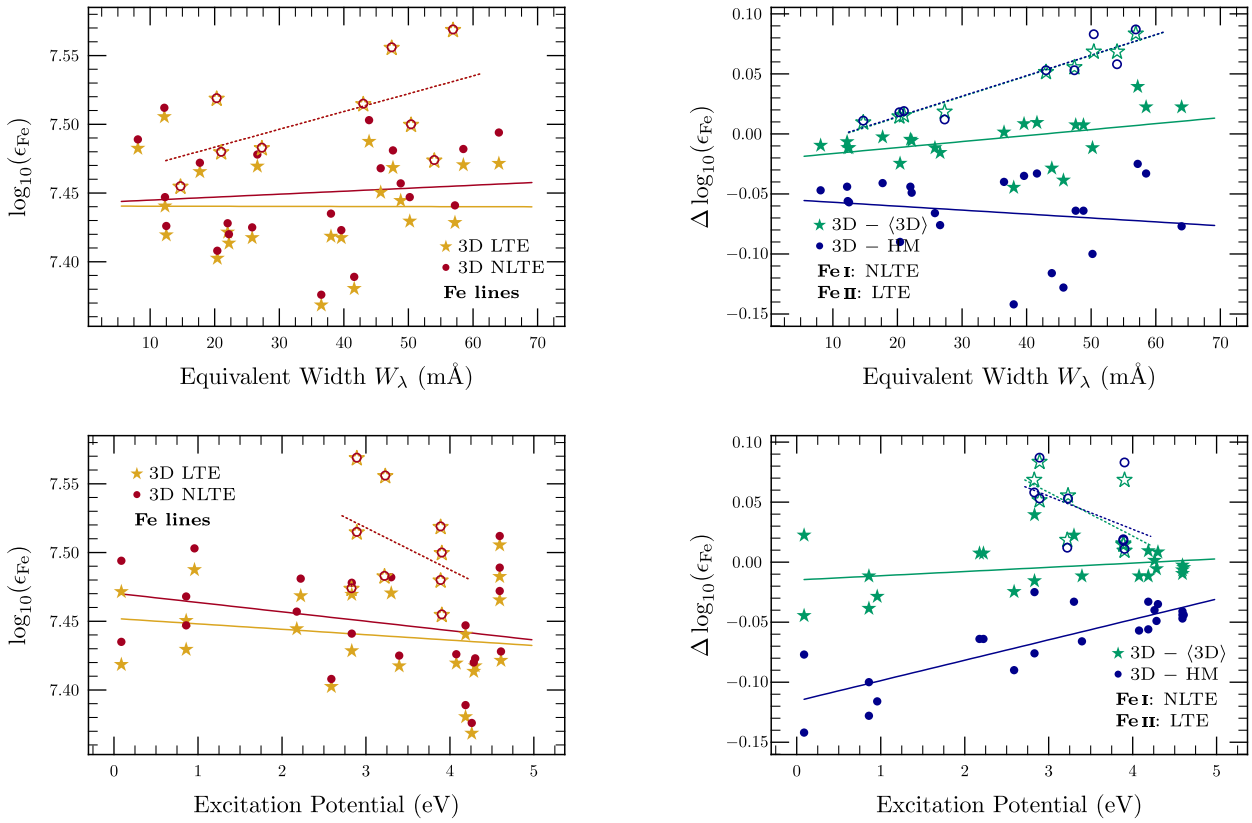

Fig. 8. *Left*: 3D Fe abundances from Fe I and Fe II lines, as a function of equivalent width and lower excitation potential. *Right*: line-by-line differences between abundances obtained with the 3D and ⟨3D⟩ models, and between those obtained with the 3D and HM models. Filled symbols and solid trendlines indicate neutral lines, open symbols and dotted lines indicate singly-ionised lines.

too low NLTE corrections). A similar size discrepancy exists in the HM results (Table 4), but reversed in sign: the neutral species returns an abundance 0.06 dex higher. The only significant trend visible in Fig. 8 is in the difference between the 3D and HM or ⟨3D⟩ results from Fe II as a function of line strength: stronger Fe II lines appear to show larger positive corrections due to 3D effects.

Considering all our adopted Fe I and Fe II lines, our final 3D+NLTE Fe abundance is

$$\log \epsilon_{\rm Fe} = 7.47 \pm 0.04 \ (\pm 0.01 \ \text{stat}, \ \pm 0.04 \ \text{sys}),$$

in very good agreement with the meteoritic value (7.45 ± 0.01; Lodders et al. 2009).

Our derived Fe abundance from Fe II lines is in perfect agreement with the 3D result of Caffau et al. (2011, $\log \epsilon_{\rm Fe} = 7.51$), although the standard deviation of our result is smaller (0.04 vs. 0.06 dex). For lines in common, the equivalent widths employed in the two studies agree to within a few percent, so the difference in scatter presumably reflects a difference in the quality of the line selection. Both our Fe I and Fe II abundances are consistent with those found in Asplund et al. (2000b, $\log \epsilon_{\rm Fe} = 7.44 \pm 0.05$ and 7.45 ± 0.10 respectively). The difference in the scatter of the Fe II result is in this case due to our use of the improved Meléndez & Barbuy (2009) oscillator strengths. The difference in the central value, whilst not statistically significant, probably reflects a slight difference in the temperature gradient between the two versions of the 3D model. Our results are also in full agreement with Bergemann et al. (2012, $\log \epsilon_{\rm Fe} = 7.46 \pm 0.02$), who investigated NLTE line formation of Fe with the same ⟨3D⟩ solar model atmosphere as we employ here.

Recently, Fabbian et al. (2010, 2012) revisited the issue of the solar Fe abundance in light of 3D magneto-hydrodynamic simulations of the solar atmosphere for different magnetic field strengths (B_z = 0–200 G). Their 3D models were calculated with the same STAGGER code as we employ, but with less up-to-date opacities and equation-of-state. They found quite substantial effects on the derived Fe abundance due to the presence of magnetic fields: in some cases up to +0.15 dex for the strongest magnetic fields. For typical Fe I lines employed here and elsewhere, with small or negligible Landé factors, the effects are much more sedate: ≈+0.04 dex for B_z = 200 G. Most of this is an indirect effect: it is not Zeeman broadening (which in any case would strengthen the line and thus lead to lower inferred Fe abundance), but the impact of magnetic fields on the atmospheric temperature structure that matters most. With magnetic dissipation included, the higher atmospheric layers are heated relative to the non-magnetic case, with the difference amounting to ≈130 K at $\log \tau_{500} = -2$ for the B_z = 200 G case (Fabbian et al. 2012). As a consequence, the number density of Fe I is decreased and a higher Fe abundance is required to reproduce the observed Fe I lines; although Fabbian et al. (2012) did not consider typical Fe II lines used for abundance purposes, the expectation is that those lines should be rather insensitive to the different temperature structures, as they are formed in significantly deeper layers. At face value, the agreement between the Fe I and Fe II results would be improved, especially since observations of the quiet Sun suggest the presence of a ubiquitous mixed-polarity magnetic field with an average strength of ≈100 G (Trujillo Bueno et al. 2004).

We intend to return to this important issue in the future, but in the meantime we note that the case for a significant upward revision of the solar Fe abundance (and by consequence many other elements) due to the presence of magnetic fields is not as

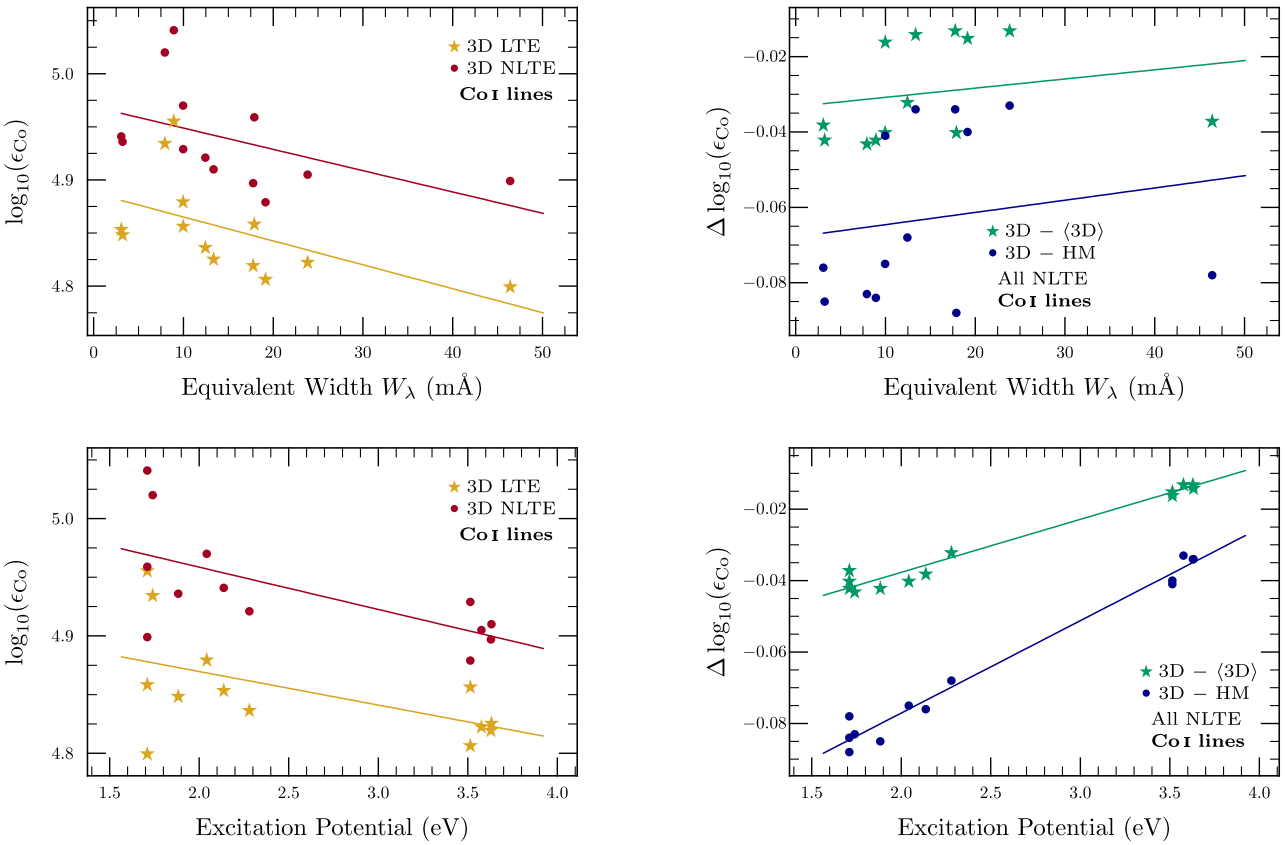

Fig. 9. *Left*: 3D Co abundances from Co I lines, as a function of equivalent width and lower excitation potential. *Right*: line-by-line differences between abundances obtained with the 3D and ⟨3D⟩ models, and between those obtained with the 3D and HM models.

unequivocal as argued by Fabbian et al. (2010, 2012). Firstly, at magnetic fields of 100 G, the effect is in fact rather minor: ≈0.02 dex for lines similar to those we use. Secondly, our recommended Fe abundance is based on both Fe I and Fe II lines. Thirdly, Pereira et al. (2013) found that 3D MHD models of the solar atmosphere perform worse than simulations without magnetic fields against a number of key observational diagnostics, including the continuum centre-to-limb variation; they thus conclude that current MHD solar models are in fact less realistic than the one employed by us. In view of these findings, we recommend our 3D+NLTE value based on a 3D hydrodynamic solar model, but caution that further studies into the importance of magnetic fields are needed.

In AGSS09, we adopted the result from Fe II ($\log \epsilon_{Fe} = 7.50 \pm 0.04$) as our reference abundance. Here we also utilise Fe I, because we now have dedicated NLTE calculations available for our lines with the ⟨3D⟩ model. Relative to the AGSS09 analysis, we have dropped two Fe I lines: 657.4 nm, because it sits in the wing of Hα, and 660.9 nm, because of its relatively large line strength.

7.7. Cobalt

From our selection of weak Co I lines, we find a mean NLTE Co abundance of

$$\log \epsilon_{Co} = 4.93 \pm 0.05 \ (\pm 0.01 \text{ stat}, \ \pm 0.05 \text{ sys}).$$

This is somewhat higher than the meteoritic value (4.87 ± 0.01; Lodders et al. 2009), but still marginally consistent to within the mutual errors. Our result agrees well with that of Bergemann (2011, 4.95 ± 0.04), although in that paper a different model atmosphere, flux spectra and $S_H = 0.05$ were used, resulting in larger NLTE corrections than we see here with $S_H = 1$ (+0.14 vs. +0.08 dex). Our mean LTE HM result ($\log \epsilon_{Co} = 4.94$) is also consistent with the HM-based abundance derived by Cardon et al. (1982, $\log \epsilon_{Co} = 4.92$). Our result exhibits a smaller dispersion however, reflecting the care we took in our line selection: $\sigma = 0.06$ in our HM results, $\sigma = 0.08$ in Cardon et al.'s. The dispersions of our 3D LTE and NLTE results were $\sigma = 0.05$ dex, similar to those of Bergemann et al. (2010), which is indicative of the intrinsic uncertainty of the oscillator strengths.

No substantial trend in abundances with line strength can be seen in Fig. 9. A weak trend with excitation potential is visible in the 3D results: lines with $\chi_{exc} > 3$ eV lead to an abundance of $\log \epsilon_{Co} = 4.90 \pm 0.02$ (1σ), whereas lower-excitation lines return an abundance of $\log \epsilon_{Co} = 4.97 \pm 0.05$ (1σ). This may be an effect of imperfect gf-values, NLTE corrections or the temperature structure of the model atmosphere. Inspection of the lower right panel of Fig. 9 reveals that the trend is more severe with the ⟨3D⟩ model than the full 3D model, and yet more severe again with the HM model. Using the HM model, the high-excitation lines give $\log \epsilon_{Co} = 4.92 \pm 0.02$ (1σ), whereas the low-excitation lines return $\log \epsilon_{Co} = 5.04 \pm 0.05$ (1σ); the switch to 3D atmospheric modelling is a clear improvement for solar analysis of Co.

Relative to AGSS09 ($\log \epsilon_{Co} = 4.99 \pm 0.07$), the main update to the Co abundance here is that we calculate NLTE intensity corrections (based on Bergemann et al. 2010) specifically for our different 1D models rather than the MAFAGS-ODF model, and use $S_H = 1$ instead of $S_H = 0.05$. This accounts for 0.03 dex of

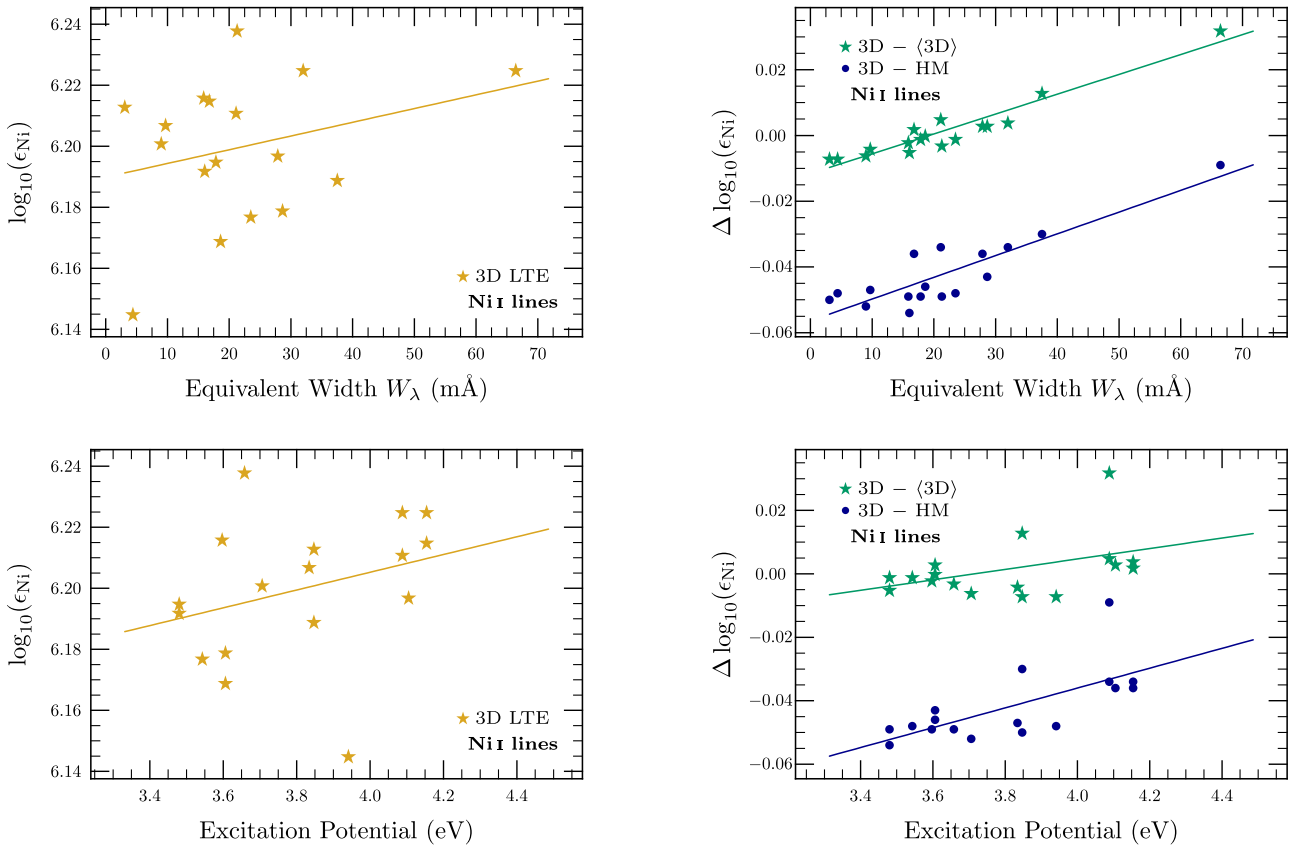

Fig. 10. *Left*: 3D Ni abundances from Ni I lines, as a function of equivalent width and lower excitation potential. *Right*: line-by-line differences between abundances obtained with the 3D and ⟨3D⟩ models, and between those obtained with the 3D and HM models.

the reduction; the remaining 0.03 dex comes from the updated opacities, equation of state, ionisation potentials and partition functions.

7.8. Nickel

The mean 3D nickel abundance from Ni I lines

$$\log \epsilon_{\rm Ni} = 6.20 \pm 0.04 \ (\pm < 0.01 \ \text{stat}, \ \pm 0.04 \ \text{sys})$$

is in excellent agreement with the meteoritic value (6.20 ± 0.01; Lodders et al. 2009). Ni II lines indicated widely varying abundances, though the mean values they return with each model are broadly consistent with Ni I results. Using the theoretical gf-values of Fritzsche et al. (2000) results in a far lower abundance scatter than any other gf-values, leading us to believe that these are currently the most accurate oscillator strengths available for optical Ni II lines. Given the uncertainty in the mean Ni II value, we adopt the 3D Ni I result as the most reliable estimate of the solar abundance. Ni II is the most model-sensitive of our ionised species.

No trends with line strength or excitation potential can be seen in the 3D results (Fig. 10). The abundance corrections due to 3D effects have a clear dependence upon line strength, and a smaller correlation with excitation potential. In contrast, the effect of the mean temperature structure is 0.04 dex regardless of line strength.

Our result is consistent with that presented in Scott et al. (2009, $\log \epsilon_{\rm Ni} = 6.17 \pm 0.05$), but slightly higher due to the improved temperature structure of the improved 3D model we use here. Compared to the result we reported in AGSS09 ($\log \epsilon_{\rm Ni} = 6.22 \pm 0.04$), our result here is slightly lower because we employed new gf-values and an expanded set of isotopic separations from Wood et al. (2014b) (in AGSS09 and Scott et al. 2009 we used gf-values from Wickliffe & Lawler 1997 and isotopic separations from Litzen et al. 1993). Improvements in the overall opacity, equation of state, ionisation potential and partition function also play a small role in the difference from AGSS09.

8. Comments and discussion

8.1. Sensitivity to temperature: 3D vs. ⟨3D⟩ vs. HM

Table 4 shows that the results for the once-ionised species are typically less model-dependent than those of the neutral species; this is to be expected for these dominant species. We notice that the model-dependence of the abundances of neutral species increases with decreasing ionisation potential, whereas the model-dependence of abundances from ionised lines increases with ionisation potential. This reflects the general rule that the more in majority a species is, the less sensitive its lines will be to the ionisation balance, and therefore less affected by the temperature structure of the model atmosphere.

From Table 4, we see that the differences 3D−⟨3D⟩ vary widely between different neutral species. From values of 0.06–0.10 dex for Sc I, Ti I and V I, they decrease to 0.00–0.03 dex for the rest of the neutrals, reflecting the lower ionisation energies and therefore more severe minority status of Sc I, Ti I and V I compared to the other neutrals.

When looking at the plots in Figs. 3–10, we clearly see that the 3D−⟨3D⟩ abundance difference is also related to the

Table 4. Average abundances implied by Sc I, Sc II, Ti I, Ti II, V I, V II, Cr I, Cr II, Mn I, Fe I, Fe II, Co I, Ni I and Ni II lines.

	Species	3D	⟨3D⟩	HM	MARCS	MISS	3D−HM	3D−⟨3D⟩	Recommended	Meteoritic
$\log \epsilon_{Sc}$	Sc I	3.14 ± 0.09	3.21	3.28	3.18	3.23	−0.14	−0.07	3.16 ± 0.04	3.05 ± 0.02
	Sc II	3.17 ± 0.04	3.16	3.19	3.14	3.19	−0.02	0.01		
	Sc all	3.16 ± 0.04	3.18	3.22	3.15	3.21	−0.07	−0.03		
$\log \epsilon_{Ti}$	Ti I	4.88 ± 0.05	4.94	4.99	4.90	4.93	−0.11	−0.06	4.93 ± 0.04	4.91 ± 0.03
	Ti II	4.97 ± 0.04	4.94	4.97	4.91	4.97	0.00	0.02		
	Ti all	4.90 ± 0.04	4.94	4.99	4.90	4.94	−0.08	−0.04		
$\log \epsilon_{V}$	V I	3.89 ± 0.08	3.99	4.07	3.96	4.00	−0.18	−0.10	3.89 ± 0.08	3.96 ± 0.02
	(V II)	4.00 ± 0.04	3.98	4.01	3.95	4.01	−0.01	0.02		
$\log \epsilon_{Cr}$	Cr I	5.60 ± 0.04	5.62	5.66	5.57	5.63	−0.06	−0.02	5.62 ± 0.04	5.64 ± 0.01
	Cr II	5.65 ± 0.04	5.62	5.63	5.56	5.65	+0.03	0.04		
	Cr all	5.62 ± 0.04	5.62	5.65	5.57	5.64	−0.04	−0.01		
$\log \epsilon_{Mn}$	Mn I	5.42 ± 0.04	5.43	5.47	5.37	5.42	−0.04	−0.00	5.42 ± 0.04	5.48 ± 0.01
$\log \epsilon_{Fe}$	Fe I	7.45 ± 0.04	7.46	7.52	7.41	7.46	−0.07	−0.00	7.47 ± 0.04	7.45 ± 0.01
	Fe II	7.51 ± 0.04	7.46	7.46	7.42	7.49	+0.05	0.05		
	Fe all	7.47 ± 0.04	7.46	7.50	7.41	7.47	−0.03	0.01		
$\log \epsilon_{Co}$	Co I	4.93 ± 0.05	4.96	4.99	4.92	4.96	−0.06	−0.03	4.93 ± 0.05	4.87 ± 0.01
$\log \epsilon_{Ni}$	Ni I	6.20 ± 0.04	6.20	6.24	6.15	6.23	−0.04	0.00	6.20 ± 0.04	6.20 ± 0.01
	(Ni II)	6.30 ± 0.10	6.23	6.24	6.19	6.26	+0.06	0.08		

Notes. Abundances are given as the weighted mean across all lines in the given list, taking into account NLTE corrections for Sc I, Sc II, Ti I, V I, Cr I, Mn I, Fe I and Co I. V II and Ni II are shown in brackets because we do not consider these results reliable enough to include in our final adopted abundances. We also give our final recommended solar photospheric abundance of each element, compared with the abundance in CI chondritic meteorites (Lodders et al. 2009, normalised to the silicon abundance determined in Paper I). Note that because all means were computed using abundances accurate to three decimal places, entries in Cols. 8 and 9 differ in some cases from the differences between the entries in Cols. 3–5.

excitation potentials of individual lines, or more precisely, the difference between the ionisation and excitation energies ($E_{ion} - E_{exc}$). This difference is the most important parameter for the temperature sensitivity of lines of minor species like the neutral iron group elements. Lines with lower excitation energies are typically more sensitive than higher-excitation lines to higher atmospheric layers and the presence of atmospheric inhomogeneities, as seen in our 3D−HM and 3D−⟨3D⟩ results, respectively. A similar argument holds also for line strengths: stronger lines are typically formed higher, so show larger sensitivity to both the mean structure and horizontal inhomogeneities.

8.2. Sensitivity to collisional broadening and HFS

Collisional broadening is now well determined for neutral species and Fe II (Anstee & O'Mara 1995; Barklem & O'Mara 1997; Barklem et al. 1998, 2000; Barklem & Aspelund-Johansson 2005). Even extreme collisional sensitivity should therefore not be a major source of error when using neutral lines and Fe II in the current analysis. For other ionic lines, the enhancement factor used with the classical Unsöld (1955) broadening recipe is a potential source of error. As Sc II, Ti II and V II lines were mostly insensitive to its variation though, even with ionic lines the broadening treatment should contribute very little to our uncertainties.

The sensitivity of derived abundances to hyperfine (and by implication, isotopic) structure varies greatly with different lines, species and abundance-determination techniques. Clearly, lines with large HFS (i.e. transitions between levels with large A, B, and/or J values, or in nuclei with large I) will be most affected. If one finds abundances using equivalent widths, the strongest lines are those most sensitive to the HFS treatment. This is because the spreading of a strong line into multiple components causes it to become either partially or wholly desaturated, whereas a single component would be more saturated. This means that completely neglecting HFS or isotopic structure often leads to overestimated abundances, a common concern in past 1D analyses (e.g. von der Heide 1968; Holweger & Oertel 1971; Kurucz 1993; Prochaska & McWilliam 2000). Broadening by HFS or isotopic structure modifies the depth of line formation in general for all lines (pushing them deeper into the photosphere), so it can play a role even for fainter lines, even when equivalent widths are used for fitting rather than profile fits. Furthermore, it is very important in combination with NLTE line formation, especially when NLTE abundance corrections are computed from differences between LTE and NLTE equivalent widths.

To ascertain the overall impact of HFS on our abundances, we also computed all ⟨3D⟩ abundances with HFS neglected, and calculated the mean HFS correction $\Delta_{HFS} \equiv \log \epsilon_{no\,HFS} - \log \epsilon_{HFS}$ for our sample of lines. We found that Mn I was by far the species most affected, with $\Delta_{HFS} = 0.16$ dex. Co I was the next most strongly affected ($\Delta_{HFS} = 0.05$ dex), followed by V II ($\Delta_{HFS} = 0.04$ dex), V I ($\Delta_{HFS} = 0.03$ dex) and Sc I/Sc II (both $\Delta_{HFS} = 0.01$ dex). HFS in Ti and Cr had virtually no effect.

9. Previous solar abundance compilations

Table 5 compares the values we recommend here with those adopted in some of the most commonly-used compilations: AG89, GS98, AGS05, AGSS09 and Lodders et al. (2009). We note however that with the exception of AGSS09, all of the others are in fact compilations of results from the literature, all with their own methodologies, spectrum synthesis codes, model atmospheres, and error estimation procedures, which makes the recommended solar values a rather inhomogeneous mixture. In particular, none of the previous studies have attempted to account for systematic errors in the quoted abundance uncertainties.

Not surprisingly, the solar abundances that we present here are quite similar to those of AGSS09. As outlined in

Table 5. The present-day solar photospheric abundances for the Fe-peak elements Sc to Ni that we recommend here, compared with oft-used solar abundance compilations: AG89, GS98, AGS05, AGSS09 and Lodders et al. (2009; LPG09).

Z	el.	This work	AG89	GS98	AGS05	AGSS09	LPG09
21	Sc	3.16 ± 0.04	3.10	3.17	3.05	3.15	3.10
22	Ti	4.93 ± 0.04	4.99	5.02	4.90	4.95	4.90
23	V	3.89 ± 0.08	4.00	4.00	4.00	3.93	4.00
24	Cr	5.62 ± 0.04	5.67	5.67	5.64	5.64	5.64
25	Mn	5.42 ± 0.04	5.39	5.39	5.39	5.43	5.37
26	Fe	7.47 ± 0.04	7.67	7.50	7.45	7.50	7.45
27	Co	4.93 ± 0.05	4.92	4.92	4.92	4.99	4.92
28	Ni	6.20 ± 0.04	6.25	6.25	6.23	6.22	6.23

detail in Sect. 7 however, we have updated them following a complete re-assessment of all analysis ingredients, including continuous opacities, equation-of-state, line selection, atomic data and NLTE abundance corrections. In most cases this has resulted in very minor changes. Cobalt (−0.06 dex, see Sect. 7.7) is the notable exception, explained mostly by improved NLTE calculations.

For the Fe-peak elements, AGS05 only included 1D-based analyses with the exception of Fe (Asplund et al. 2000b), although it still updated the recommended values for a few elements relative to GS98. GS98 was in turn primarily based on AG89. The main difference between the latter two is the adopted Fe value, where AG89 still preferred a high value (0.2 dex larger than derived here); see Grevesse & Sauval (1999) for a detailed description of the reasons for the long-standing debate on the solar Fe abundance. Since then the preferred Fe value has not changed drastically, in spite of the advent of 3D hydrodynamic model atmospheres, more complete NLTE calculations and improved gf-values – which is reassuring.

Compared with Lodders et al. (2009), our solar abundances for the Fe-peak elements are similar overall, but there are some rather large isolated differences. These include Sc (+0.06 dex), V (−0.11 dex) and Mn (+0.05 dex). As outlined in Sect. 7, we are confident that our analysis is the most reliable and accurate possible today.

10. Conclusions

We have determined the abundances of all the iron group elements in the Sun. For our analysis, we have carefully assessed all relevant atomic data, made very stringent line selections, employed a highly realistic 3D model for the solar atmosphere and accounted for departures from LTE. We have attempted to quantify the remaining systematic uncertainties stemming from possible errors in atmospheric and line-formation modelling, and to properly account for statistical errors.

Our final recommended abundances of Sc, Ti, V, Cr, Mn, Fe, Co and Ni are given in Table 4. The derived abundances generally show good agreement with the meteoritic values, and between different ionisation stages, but some discrepancies remain. Trends in abundances with excitation potential or line strength are largely absent in the 3D results, but are visible in a number of results from 1D models. The level of agreement between theoretical and observed line profiles with the 3D model is clearly satisfactory. Nonetheless, theoretical profiles computed in 3D systematically underestimate the line width by a small amount, suggesting that some additional work on improving the atmospheric velocity field or NLTE effects is still required before perfect agreement can be claimed. Nevertheless, we are confident that the solar photospheric abundances that we present here are the most accurate possible by today's standards.

Acknowledgements. We thank Dan Bayliss, Mike Bessell, Remo Collet, Peter Hannaford, Wolfgang Hayek, Lyudmila Mashonkina, Tiago Pereira, Chris Sneden and Regner Trampedach for helpful discussions, and the referee for constructive feedback. P.S., N.G. and M.A. variously thank the Max Planck Institut für Astrophysik, Garching, the Centre Spatial de Liège, the Department of Astrophysics, Geophysics and Oceanography, University of Liège and Mount Stromlo Observatory for support and hospitality during the production of this paper. We acknowledge further support from IAU Commission 46, the Lorne Trottier Chair in Astrophysics, the (Canadian) Institute for Particle Physics, the Banting Fellowship scheme as administered by the Natural Science and Engineering Research Council of Canada, the UK Science & Technology Facilities Council (P.S.), the Australian Research Council (M.A.) and the Royal Belgian Observatory (N.G.).

References

Aboussaïd, A., Carleer, M., Hurtmans, D., Biémont, E., & Godefroid, M. R. 1996, Phys. Scr., 53, 28
Adelman, S. J., Svatek, G. F., van Winkler, K., & Warren, Jr., W. H. 1989, A&AS, 80, 285
Allende Prieto, C., Barklem, P. S., Asplund, M., & Ruiz Cobo, B. 2001a, ApJ, 558, 830
Allende Prieto, C., Lambert, D. L., & Asplund, M. 2001b, ApJ, 556, L63
Allende Prieto, C., Lambert, D. L., & Asplund, M. 2002, ApJ, 573, L137
Anastassov, A., Gangrsky, Y. P., Marinova, K. P., Markov, B. N., & Zemlyanoi, S. G. 1994, Z. Phys. D, 30, 275
Anders, E., & Grevesse, N. 1989, Geochim. Cosmochim. Acta, 53, 197
Anstee, S. D., & O'Mara, B. J. 1995, MNRAS, 276, 859
Armstrong, N. M. R., Rosner, S. D., & Holt, R. A. 2011, Phys. Scr., 84, 055301
Arnesen, A., Hallin, R., Nordling, C., et al. 1982, A&A, 106, 327
Asplund, M. 2000, A&A, 359, 755
Asplund, M. 2004, A&A, 417, 769
Asplund, M., Gustafsson, B., Kiselman, D., & Eriksson, K. 1997, A&A, 318, 521
Asplund, M., Nordlund, Å., Trampedach, R., Allende Prieto, C., & Stein, R. F. 2000a, A&A, 359, 729
Asplund, M., Nordlund, Å., Trampedach, R., & Stein, R. F. 2000b, A&A, 359, 743
Asplund, M., Grevesse, N., Sauval, A. J., Allende Prieto, C., & Kiselman, D. 2004, A&A, 417, 751
Asplund, M., Grevesse, N., & Sauval, A. J. 2005a, in Cosmic Abundances as Records of Stellar Evolution and Nucleosynthesis, eds. T. G. Barnes III, & F. N. Bash (San Francisco: ASP), 336, 25
Asplund, M., Grevesse, N., Sauval, A. J., Allende Prieto, C., & Blomme, R. 2005b, A&A, 431, 693
Asplund, M., Grevesse, N., Sauval, A. J., & Scott, P. 2009, ARA&A, 47, 481
Atroshchenko, I. N., & Gadun, A. S. 1994, A&A, 291, 635
Aydin, R., Stachowska, E., Johann, U., et al. 1990, Z. Phys. D, 15, 281
Başar, G., Başar, G., Acar, G., Öztürk, İ. K., & Kröger, S. 2003, Phys. Scr., 67, 476
Başar, G., Başar, G. F., Öztürk, İ. K., & Kröger, S. 2004, Phys. Scr., 69, 189
Bard, A., & Kock, M. 1994, A&A, 282, 1014
Bard, A., Kock, A., & Kock, M. 1991, A&A, 248, 315
Barklem, P. S., & Aspelund-Johansson, J. 2005, A&A, 435, 373
Barklem, P. S., & O'Mara, B. J. 1997, MNRAS, 290, 102
Barklem, P. S., O'Mara, B. J., & Ross, J. E. 1998, MNRAS, 296, 1057
Barklem, P. S., Piskunov, N., & O'Mara, B. J. 2000, A&AS, 142, 467
Becker, U., Bucka, H., & Schmidt, A. 1977, A&A, 59, 145
Becker, U., Kwiatkowski, M., Teppner, U., & Zimmermann, P. 1980, J. Phys. B, 13, 2505
Bell, G. D., Kalman, L. B., & Tubbs, E. F. 1975, ApJ, 200, 520
Bergemann, M. 2011, MNRAS, 413, 2184
Bergemann, M., & Cescutti, G. 2010, A&A, 522, A9
Bergemann, M., & Gehren, T. 2007, A&A, 473, 291
Bergemann, M., Pickering, J. C., & Gehren, T. 2010, MNRAS, 401, 1334
Bergemann, M., Lind, K., Collet, R., Magic, Z., & Asplund, M. 2012, MNRAS, 427, 27
Bergeson, S. D., & Lawler, J. E. 1993a, ApJ, 408, 382
Bergeson, S. D., & Lawler, J. E. 1993b, J. Opt. Soc. Amer. B, 10, 794
Berrah-Mansour, N., Kurtz, C., Young, L., Beck, D. R., & Datta, D. 1992, Phys. Rev. A, 46, 5774
Biémont, E. 1974, Sol. Phys., 39, 305
Biémont, E. 1975, Sol. Phys., 44, 269

Biémont, E. 1978, Sol. Phys., 56, 79
Biémont, E., Grevesse, N., & Huber, M. C. E. 1978, A&A, 67, 87
Biémont, E., Grevesse, N., Huber, M. C. E., & Sandeman, R. J. 1980, A&A, 87, 242
Biémont, E., Grevesse, N., Faires, L. M., Marsden, G., & Lawler, J. E. 1989, A&A, 209, 391
Bieron, J., Froese Fischer, C., & Godefroid, M. 2002, J. Phys. B, 35, 3337
Bizzarri, A., Huber, M. C. E., Noels, A., et al. 1993, A&A, 273, 707
Blackwell, D. E., Collins, B. S., & Petford, A. D. 1972, Sol. Phys., 23, 292
Blackwell, D. E., Ibbetson, P. A., Petford, A. D., & Shallis, M. J. 1979a, MNRAS, 186, 633
Blackwell, D. E., Petford, A. D., & Shallis, M. J. 1979b, MNRAS, 186, 657
Blackwell, D. E., Menon, S. L. R., Petford, A. D., & Shallis, M. J. 1982a, MNRAS, 201, 611
Blackwell, D. E., Petford, A. D., Shallis, M. J., & Leggett, S. 1982b, MNRAS, 199, 21
Blackwell, D. E., Petford, A. D., Shallis, M. J., & Simmons, G. J. 1982c, MNRAS, 199, 43
Blackwell, D. E., Petford, A. D., & Simmons, G. J. 1982d, MNRAS, 201, 595
Blackwell, D. E., Menon, S. L. R., & Petford, A. D. 1983, MNRAS, 204, 883
Blackwell, D. E., Menon, S. L. R., & Petford, A. D. 1984, MNRAS, 207, 533
Blackwell, D. E., Booth, A. J., Haddock, D. J., Petford, A. D., & Leggett, S. K. 1986a, MNRAS, 220, 549
Blackwell, D. E., Booth, A. J., Menon, S. L. R., & Petford, A. D. 1986b, MNRAS, 220, 303
Blackwell, D. E., Booth, A. J., Menon, S. L. R., & Petford, A. D. 1986c, MNRAS, 220, 289
Blackwell, D. E., Booth, A. J., Menon, S. L. R., & Petford, A. D. 1987, A&A, 180, 229
Blackwell, D. E., Booth, A. J., Petford, A. D., & Laming, J. M. 1989, MNRAS, 236, 235
Blackwell, D. E., Lynas-Gray, A. E., & Smith, G. 1995, A&A, 296, 217
Blackwell-Whitehead, R., & Bergemann, M. 2007, A&A, 472, L43
Blackwell-Whitehead, R. J., Pickering, J. C., Pearse, O., & Nave, G. 2005a, ApJS, 157, 402
Blackwell-Whitehead, R. J., Xu, H. L., Pickering, J. C., Nave, G., & Lundberg, H. 2005b, MNRAS, 361, 1281
Blackwell-Whitehead, R. J., Lundberg, H., Nave, G., et al. 2006, MNRAS, 373, 1603
Booth, A. J., Blackwell, D. E., Petford, A. D., & Shallis, M. J. 1984a, MNRAS, 208, 147
Booth, A. J., Blackwell, D. E., & Shallis, M. J. 1984b, MNRAS, 209, 77
Brault, J., & Neckel, H. 1987, Spectral atlas of solar absolute disc-averaged and disc-centre intensity from 3290 to 12 510 Å (ftp://ftp.hs.uni-hamburg.de/pub/outgoing/FTS-Atlas)
Brault, J. W., & Holweger, H. 1981, ApJ, 249, L43
Brodzinski, T., Kronfeldt, H.-D., Kropp, J.-R., & Winkler, R. 1987, Z. Phys. D, 7, 161
Bruls, J. H. M. J. 1993, A&A, 269, 509
Butler, K., & Giddings, J. R. 1985, Newsletter on Analysis of Astronomical Spectra, 9 (University of London)
Caffau, E., Ludwig, H.-G., Steffen, M., Freytag, B., & Bonifacio, P. 2011, Sol. Phys., 268, 255
Cardon, B. L., Smith, P. L., Scalo, J. M., & Testerman, L. 1982, ApJ, 260, 395
Channappa, K. H., & Pendlebury, J. M. 1965, Proc. Phys. Soc., 86, 1145
Childs, W. J. 1971, Phys. Rev. A, 4, 1767
Childs, W. J., & Goodman, L. S. 1967, Phys. Rev., 156, 64
Childs, W. J., & Goodman, L. S. 1968, Phys. Rev., 170, 50
Childs, W. J., Poulsen, O., Goodman, L. S., & Crosswhite, H. 1979, Phys. Rev. A, 19, 168
Cochrane, E. C. A., Benton, D. M., Forest, D. H., & Griffith, J. A. R. 1998, J. Phys. B, 31, 2203
Cooper, J. C., Gibson, N. D., & Lawler, J. E. 1997, J. Quant. Spectr. Rad. Transf., 58, 85
Corliss, C., & Sugar, J. 1977, J. Phys. Chem. Ref. Data, 6, 1253
Corliss, C. H., & Bozman, W. R. 1962, Experimental transition probabilities for spectral lines of seventy elements; derived from the NBS Tables of spectral-line intensities (Washington: NBS Monograph 53, National Bureau of Standards, US Government Printing Office)
Cruz, F. C., Mirage, A., Gomide, J. V. B., Scalabrin, A., & Pereira, D. 1994, Opti. Comm., 106, 59
Davis, D. S., & Andrew, K. L. 1978, J. Opt. Soc. Amer. (1917–1983), 68, 206
Davis, S. J., Wright, J. J., & Balling, L. C. 1971, Phys. Rev. A, 3, 1220
Delbouille, L., Neven, L., & Roland, G. 1973, Atlas photométrique du spectre solaire de λ3000 a λ10 000 (Institut d'Astrophysique, Université de Liège, Liège)
Dembczyński, J., Ertmer, W., Johann, U., Penselin, S., & Stinner, P. 1979, Z. Phys. A, 291, 207
Den Hartog, E. A., Lawler, J. E., Sobeck, J. S., Sneden, C., & Cowan, J. J. 2011, ApJS, 194, 35
Doerr, A., Kock, M., Kwiatkowski, M., & Werner, K. 1985, J. Quant. Spectr. Rad. Transf., 33, 55
Doidge, P. S. 1995, Spectrochim. Acta B, 50, 209
Drawin, H. W. 1969, Z. Phys., 225, 483
El-Kashef, H., & Ludwig, N. 1992, Phys. B Condensed Matter, 179, 103
Ertmer, W., & Hofer, B. 1976, Z. Phys. A, 276, 9
Fabbian, D., Khomenko, E., Moreno-Insertis, F., & Nordlund, Å. 2010, ApJ, 724, 1536
Fabbian, D., Moreno-Insertis, F., Khomenko, E., & Nordlund, Å. 2012, A&A, 548, A35
Figger, H., Siomos, K., Walther, H., & Heldt, J. 1975, A&A, 43, 389
Forsberg, P. 1991, Phys. Scr., 44, 446
Freytag, B., Steffen, M., & Dorch, B. 2002, Astron. Nachr., 323, 213
Fritzsche, S., Dong, C. Z., & Gaigalas, G. 2000, Atom. Data Nuc. Data Tables, 76, 155
Fuhr, J. R., Martin, G. A., & Wiese, W. L. 1988, J. Phys. Chem. Ref. Data, 17, Supp. 4
Fuhr, J. R., Kramida, A. E., Felrice, H. R., Olsen, K., & Kotochigova, S. 2007, NIST Atomic Transition Probability Bibliographical Database (National Institute of Standards and Technology, http://www.physics.nist.gov/cgi-bin/ASBib1/TransProbBib.cgi)
Fuhrmann, K., Pfeiffer, M., Frank, C., Reetz, J., & Gehren, T. 1997, A&A, 323, 909
Furmann, B., Jarosz, A., Stefańska, D., Dembczyński, J., & Stachowska, E. 2005, Spectrochim. Acta B, 60, 33
Gangrsky, Y. P., Marinova, K. P., & Zemlyanoi, S. G. 1995, J. Phys. B, 28, 957
Giddings, J. 1981, Ph.D. Thesis, University of London, UK
Gough, D. S., Hannaford, P., Lowe, R. M., & Willis, A. P. 1985, J. Phys. B, 18, 3895
Greenlee, T. R., & Whaling, W. 1979, J. Quant. Spectr. Rad. Transf., 21, 55 (GW)
Grevesse, N., & Sauval, A. J. 1998, Space Sci. Rev., 85, 161
Grevesse, N., & Sauval, A. J. 1999, A&A, 347, 348
Grevesse, N., Blackwell, D. E., & Petford, A. D. 1989, A&A, 208, 157
Grevesse, N., Asplund, M., & Sauval, A. J. 2007, Space Sci. Rev., 130, 105
Grevesse, N., Scott, P., Asplund, M., & Sauval, A. J. 2014, A&A, 573, A27 (Paper III)
Guern, Y., & Lotrian, J. 1982, J. Phys. B, 15, 713
Gurell, J., Nilsson, H., Engström, L., et al. 2010, A&A, 511, A68
Gustafsson, B., Bell, R. A., Eriksson, K., & Nordlund, Å. 1975, A&A, 42, 407
Gustafsson, B., Edvardsson, B., Eriksson, K., et al. 2008, A&A, 486, 951
Guthöhrlein, G. H., & Keller, H. P. 1990, Z. Phys. D, 17, 181
Handrich, E., Steudel, A., & Walther, H. 1969, Phys. Lett. A, 29, 486
Hannaford, P., & Lowe, R. M. 1981, J. Phys. B, 14, L5
Hannaford, P., Lowe, R. M., Grevesse, N., & Noels, A. 1992, A&A, 259, 301
Heilig, K., & Wendlandt, D. 1967, Phys. Lett. A, 25, 277
Heise, C., & Kock, M. 1990, A&A, 230, 244
Holweger, H., & Müller, E. A. 1974, Sol. Phys., 39, 19 (HM)
Holweger, H., & Oertel, K. B. 1971, A&A, 10, 434
Huber, M. C. E., & Sandeman, R. J. 1977, Proc. R. Soc. London Ser. A, 357, 355
Huldt, S., Johansson, S., Litzén, U., & Wyart, J.-F. 1982, Phys. Scr., 25, 401
Jarosz, A., Stefańska, D., Elantkowska, M., et al. 2007, J. Phys. B, 40, 2785
Jin, W.-G., Nemoto, Y., & Minowa, T. 2009, J. Phys. Soc. Japan, 78, 094301
Johann, U., Dembczyński, J., & Ertmer, W. 1981, Z. Phys. A, 303, 7
Johansson, S., & Litzén, U. 1980, Phys. Scr., 22, 49
Johansson, S., Litzén, U., Lundberg, H., & Zhang, Z. 2003, ApJ, 584, L107
Karamatskos, N., Michalak, R., Zimmermann, P., Kroll, S., & Kock, M. 1986, Z. Phys. D, 3, 391
Kaufman, V., & Sugar, J. 1988, J. Phys. Chem. Ref. Data, 17, 1679
Kerola, D. X., & Aller, L. H. 1976, PASP, 88, 122
Kroll, S., & Kock, M. 1987, A&AS, 67, 225
Kronfeldt, H. D., Kropp, J. R., Subaric, A., & Winkler, R. 1985, Z. Phys. A, 322, 349
Kupka, F., Piskunov, N., Ryabchikova, T. A., Stempels, H. C., & Weiss, W. W. 1999, A&AS, 138, 119
Kurucz, R. L. 1993, Phys. Scr., T47, 110
Kurucz, R. M. 2011, http://kurucz.harvard.edu/
Kwiatkowski, M., Micali, G., Werner, K., & Zimmermann, P. 1981, A&A, 103, 108
Kwong, H. S., & Measures, R. M. 1980, Appl. Opt., 19, 1025
Lawler, J. E. 1991, A&A, 252, 853
Lawler, J. E., & Dakin, J. T. 1989, J. Opt. Soc. Amer. B, 6, 1457
Lawler, J. E., Guzman, A., Wood, M. P., Sneden, C., & Cowan, J. J. 2013, ApJS, 205, 11
Lefèbvre, P.-H., Garnir, H.-P., & Biémont, E. 2002, Phys. Scr., 66, 363
Lefèbvre, P.-H., Garnir, H.-P., & Biémont, E. 2003, A&A, 404, 1153

Lind, K., Meléndez, J., Asplund, M., Collet, R., & Magic, Z. 2013, A&A, 554, A96
Litzen, U., Brault, J. W., & Thorne, A. P. 1993, Phys. Scr., 47, 628
Lodders, K., Palme, H., & Gail, H.-P. 2009, Landolt Börnstein, New Series, Vol. VI/4B, Chap. 4.4, Abundances of the Elements in the Solar System, ed. J. E. Trümper (Berlin: Springer-Verlag), 560
Luc, P., & Gerstenkorn, S. 1972, A&A, 18, 209
Mansour, N. B., Dinneen, T., Young, L., & Cheng, K. T. 1989, Phys. Rev. A, 39, 5762
Marek, J. 1975, A&A, 44, 69
Marek, J., & Richter, J. 1973, A&A, 26, 155
Marek, J., & Vogt, K. 1977, Z. Phys. A, 280, 235
Marsden, G. C., den Hartog, E. A., Lawler, J. E., Dakin, J. T., & Roberts, V. D. 1988, J. Opt. Soc. Amer. B, 5, 606
Martin, G. A., Fuhr, J. R., & Wiese, W. L. 1988, J. Phys. Chem. Ref. Data, 17, Supp. 3
Mashonkina, L., Gehren, T., Shi, J.-R., Korn, A. J., & Grupp, F. 2011, A&A, 528, A87
McWilliam, A., & Rich, R. M. 1994, ApJS, 91, 749
McWilliam, A., Preston, G. W., Sneden, C., & Searle, L. 1995, AJ, 109, 2757
Measures, R. M., Drewell, N., & Kwong, H. S. 1977, Phys. Rev. A, 16, 1093
Meléndez, J., & Asplund, M. 2008, A&A, 490, 817
Meléndez, J., & Barbuy, B. 1999, ApJS, 124, 527
Meléndez, J., & Barbuy, B. 2009, A&A, 497, 611
Moore, C. E., Minnaert, M. G. J., & Houtgast, J. 1966, The solar spectrum 2935 Å to 8770 Å (Washington: NBS Monograph 61, National Bureau of Standards, US Government Printing Office)
Morton, D. C. 2003, ApJS, 149, 205
Nave, G., & Johansson, S. 2013, ApJS, 204, 1
Nave, G., Johansson, S., Learner, R. C. M., Thorne, A. P., & Brault, J. W. 1994, ApJS, 94, 221
Neckel, H. 1999, Sol. Phys., 184, 421
Neuforge, C. 1993, in Origin and evolution of the elements: Proc. of a symposium in honour of H. Reeves (held in Paris, June 22–25, 1992), eds. N. Prantzos, E. Vangioni-Flam, & M. Casse (Cambridge University Press), 63
Nilsson, H., Ljung, G., Lundberg, H., & Nielsen, K. E. 2006, A&A, 445, 1165
Nitz, D. E., Bergeson, S. D., & Lawler, J. E. 1995, J. Opt. Soc. Amer. B, 12, 377
Nitz, D. E., Wickliffe, M. E., & Lawler, J. E. 1998, ApJS, 117, 313
Nitz, D. E., Kunau, A. E., Wilson, K. L., & Lentz, L. R. 1999, ApJS, 122, 557
Nouri, Z., Rosner, S. D., Li, R., Scholl, T. J., & Holt, R. A. 2010, Phys. Scr., 81, 065301
O'Brian, T. R., Wickliffe, M. E., Lawler, J. E., Whaling, W., & Brault, J. W. 1991, J. Opt. Soc. Amer. B, 8, 1185
Pagel, B. E. J. 1997, Nucleosynthesis and Chemical Evolution of Galaxies (Cambridge University Press)
Palmeri, P., Biémont, E., Aboussaid, A., & Godefroid, M. 1995, J. Phys. B, 28, 3741
Palmeri, P., Biémont, E., Quinet, P., et al. 1997, Phys. Scr., 55, 586
Pereira, T. M. D., Asplund, M., & Kiselman, D. 2009, A&A, 508, 1403
Pereira, T. M. D., Asplund, M., Collet, R., et al. 2013, A&A, 554, A118
Pickering, J. C. 1996, ApJS, 107, 811
Pickering, J. C., & Thorne, A. P. 1996, ApJS, 107, 761
Pickering, J. C., Thorne, A. P., & Perez, R. 2001, ApJS, 132, 403
Pickering, J. C., Thorne, A. P., & Perez, R. 2002, ApJS, 138, 247
Prochaska, J. X., & McWilliam, A. 2000, ApJ, 537, L57
Reddy, B. E., Tomkin, J., Lambert, D. L., & Allende Prieto, C. 2003, MNRAS, 340, 304
Roberts, J. R., Andersen, T., & Sørensen, G. 1973, ApJ, 181, 567
Rosman, K. J. R., & Taylor, P. D. P. 1998, Pure & Appl. Chem., 70, 217
Rudolph, J., & Helbig, V. 1982, J. Phys. B, 15, L1
Rutten, R. J., & Kostik, R. I. 1982, A&A, 115, 104
Salih, S., & Lawler, J. E. 1990, A&A, 239, 407
Schade, W., Langhans, G., & Helbig, V. 1987, Phys. Scr., 36, 890
Schade, W., Mundt, B., & Helbig, V. 1990, Phys. Rev. A, 42, 1454
Schnabel, R., Bard, A., & Kock, M. 1995, Z. Phys. D, 34, 223
Schnabel, R., Kock, M., & Holweger, H. 1999, A&A, 342, 610
Schnabel, R., Schultz-Johanning, M., & Kock, M. 2004, A&A, 414, 1169
Scott, P., Asplund, M., Grevesse, N., & Sauval, A. J. 2006, A&A, 456, 675
Scott, P., Asplund, M., Grevesse, N., & Sauval, A. J. 2009, ApJ, 691, L119
Scott, P., Grevesse, N., Asplund, M., et al. 2014, A&A, 573, A25 (Paper I)
Singh, R., Rao, G. N., & Thareja, R. K. 1991, J. Opt. Soc. Amer. B, 8, 12
Sobeck, J. S., Lawler, J. E., & Sneden, C. 2007, ApJ, 667, 1267
Stachowska, E., Fabiszisky, M., & Dembczyński, J. 1994, Z. Phys. D, 32, 27
Sugar, J., & Corliss, C. 1985, Atomic energy levels of the iron-period elements: Potassium through Nickel (Washington: American Chemical Society)
Tozzi, G. P., Brunner, A. J., & Huber, M. C. E. 1985, MNRAS, 217, 423
Trujillo Bueno, J., Shchukina, N., & Asensio Ramos, A. 2004, Nature, 430, 326
Unkel, P., Buch, P., Dembczyński, J., Ertmer, W., & Johann, U. 1989, Z. Phys. D, 11, 259
Unsöld, A. 1955, Physik der Sternatmospharen, MIT besonderer Berucksichtigung der Sonne., 2nd edn. (Berlin: Springer)
Vernazza, J. E., Avrett, E. H., & Loeser, R. 1976, ApJS, 30, 1
Vieytes, M. C., & Fontenla, J. M. 2013, ApJ, 769, 103
Villemoes, P., van Leeuwen, R., Arnesen, A., et al. 1992, Phys. Rev. A, 45, 6241
Vogel, O., Ward, L., Arnesen, A., et al. 1985, Phys. Scr., 31, 166
von der Heide, K. 1968, ZAp, 69, 220
Walther, H. 1962, Z. Phys., 170, 507
Whaling, W., Hannaford, P., Lowe, R. M., Biémont, E., & Grevesse, N. 1985, A&A, 153, 109
Wickliffe, M. E., & Lawler, J. E. 1997, ApJS, 110, 163
Wood, M. P., Lawler, J. E., Sneden, C., & Cowan, J. J. 2013, ApJS, 208, 27
Wood, M. P., Lawler, J. E., Den Hartog, E. A., Sneden, C., & Cowan, J. J. 2014a, ApJS, accepted, [arXiv:1408.4175]
Wood, M. P., Lawler, J. E., Sneden, C., & Cowan, J. J. 2014b, ApJS, 211, 20
Yalchenko, Y., Kramida, A. E., Reader, J., et al. 2007, NIST Atomic Spectra Database (National Institute of Standards and Technology) http://physics.nist.gov/PhysRefData/ASD/)
Young, L., Childs, W. J., Dinneen, T., et al. 1988, Phys. Rev. A, 37, 4213
Youssef, N. H., & Amer, M. A. 1989, A&A, 220, 281
Zhang, H. W., Gehren, T., & Zhao, G. 2008, A&A, 481, 489

Pages 25 to 33 are available in the electronic edition of the journal at http://www.aanda.org

Table 1. Lines retained in this analysis: atomic and solar data, line weightings, LTE abundance results for the 5 models used in this analysis, NLTE corrections to the LTE result (when available), and the corresponding 3D+NLTE abundance result.

λ	Atomic levels		E_{exc}	log gf	gf	W_λ	Wt.	LTE Abundances					Δ_{NLTE}	3D
(nm)	Lower	Upper	(eV)		ref.	(pm)		3D	⟨3D⟩	HM	MARCS	MISS	(3D)	NLTE
						Sc I								
474.3821	$(^3F)4s\ ^4F_{\frac{9}{2}}$	$(^3F)4p\ ^4D_{\frac{7}{2}}$	1.448	0.422	1	0.82	1	2.974	3.039	3.104	3.006	3.065	+0.15	3.124
508.1561	$(^3F)4s\ ^4F_{\frac{9}{2}}$	$(^3F)4p\ ^4F_{\frac{9}{2}}$	1.448	0.469	1	1.00	2	2.989	3.056	3.121	3.022	3.080	+0.16	3.149
535.6097	$(^3F)4s\ ^2F_{\frac{7}{2}}$	$(^3F)4p\ ^2D_{\frac{5}{2}}$	1.865	0.168	1	0.20	3	2.974	3.030	3.089	2.994	3.056	+0.15	3.124
567.1828	$(^3F)4s\ ^4F_{\frac{9}{2}}$	$(^3F)4p\ ^4G_{\frac{11}{2}}$	1.448	0.495	1	1.24	2	3.024	3.092	3.159	3.058	3.114	+0.15	3.174
623.9800	$4s^2\ ^2D_{\frac{3}{2}}$	$(^3D)4sp\ ^4D_{\frac{3}{2}}$	0.000	−1.780	1	0.22	1	2.985	3.133	3.224	3.108	3.146	+0.15	3.135
						Sc II								
442.0661	$3d^2\ ^3F_4$	$4p\ ^3F_3$	0.618	−2.273	1	1.51	2	3.109	3.109	3.140	3.093	3.143	−0.01	3.099
443.1362	$3d^2\ ^3F_3$	$4p\ ^3F_2$	0.605	−1.969	1	2.92	1	3.165	3.162	3.193	3.142	3.195	−0.01	3.155
535.7202	$3d^2\ ^3P_2$	$4p\ ^1P_1$	1.507	−2.111	1	0.43	2	3.131	3.130	3.153	3.110	3.164	0.00	3.131
564.1000	$3d^2\ ^3P_1$	$4p\ ^3P_2$	1.500	−1.131	1	3.65	1	3.246	3.236	3.255	3.205	3.264	−0.02	3.226
565.8362	$3d^2\ ^3P_0$	$4p\ ^3P_1$	1.497	−1.208	1	3.14	1	3.221	3.212	3.232	3.183	3.241	−0.01	3.211
566.7164	$3d^2\ ^3P_1$	$4p\ ^3P_1$	1.500	−1.309	1	2.81	1	3.245	3.238	3.258	3.212	3.268	−0.01	3.235
566.9055	$3d^2\ ^3P_1$	$4p\ ^3P_0$	1.500	−1.200	1	3.26	1	3.256	3.243	3.263	3.214	3.272	−0.01	3.246
568.4214	$3d^2\ ^3P_2$	$4p\ ^3P_1$	1.507	−1.074	1	3.56	2	3.174	3.164	3.183	3.133	3.193	−0.02	3.154
660.4578	$3d^2\ ^1D_2$	$4p\ ^1D_2$	1.357	−1.309	1	3.54	1*	3.214	3.202	3.219	3.173	3.227	−0.01	3.204
						Ti I								
428.1363	$(^4F)4s\ ^5F_1$	$(^4F)4p\ ^5D_2$	0.813	−1.260	2	2.40	1	4.787	4.856	4.938	4.825	4.878	+0.056	4.843
446.5805	$(^4P)4s\ ^5P_2$	$(^4P)4p\ ^5P_3$	1.739	−0.130	2	3.56	2	4.829	4.862	4.933	4.822	4.886	+0.050	4.879
475.8118	$(^2H)4s\ ^3H_5$	$(^2H)4p\ ^3H_5$	2.249	0.510	2	4.18	3	4.792	4.809	4.876	4.763	4.832	+0.053	4.845
475.9269	$(^2H)4s\ ^3H_6$	$(^2H)4p\ ^3H_6$	2.256	0.590	2	4.60	2	4.810	4.821	4.889	4.772	4.842	+0.053	4.863
496.4715	$(^3F)4sp\ ^5G_2$	$4s(^4F)5s\ ^5F_2$	1.969	−0.820	3	0.77	2	4.826	4.880	4.942	4.845	4.905	+0.060	4.886
502.2866	$(^4F)4s\ ^5F_3$	$(^4F)4p\ ^5G_3$	0.826	−0.330	2	6.99	1	4.817	4.804	4.896	4.753	4.808	+0.065	4.882
511.3439	$(^4F)4s\ ^3F_3$	$(^3P)4sp\ ^3D_2$	1.443	−0.700	2	2.45	2	4.782	4.838	4.912	4.802	4.860	+0.049	4.831
514.5459	$(^4F)4s\ ^3F_4$	$(^3P)4sp\ ^3D_3$	1.460	−0.540	2	3.31	1	4.838	4.884	4.959	4.845	4.904	+0.048	4.886
514.7477	$4s^2\ ^3F_2$	$(^3F)4sp\ ^3F_3$	0.000	−1.940	2	3.46	1	4.781	4.871	4.968	4.840	4.882	+0.086	4.867
515.2184	$4s^2\ ^3F_3$	$(^3F)4sp\ ^3F_4$	0.021	−1.950	2	3.32	2	4.782	4.873	4.970	4.843	4.885	+0.084	4.866
521.9699	$4s^2\ ^3F_3$	$(^3F)4sp\ ^3F_2$	0.021	−2.220	2	2.24	2	4.783	4.896	4.991	4.868	4.909	+0.081	4.864
522.3620	$(^3F)4sp\ ^5F_2$	$4s(^4F)5s\ ^5F_2$	2.092	−0.490	2	1.22	1	4.824	4.874	4.935	4.836	4.899	+0.054	4.878
524.7288	$(^3F)4sp\ ^5F_3$	$4s(^4F)5s\ ^5F_2$	2.103	−0.640	3	0.85	1	4.802	4.853	4.914	4.817	4.879	+0.057	4.859
525.2098	$4s^2\ ^3F_4$	$(^3F)4sp\ ^3F_3$	0.048	−2.360	4	1.64	1	4.768	4.890	4.984	4.863	4.905	+0.079	4.847
529.5774	$4s^2\ ^3P_2$	$(^1D)4sp\ ^3D_3$	1.067	−1.590	2	1.06	2	4.824	4.907	4.984	4.875	4.927	+0.065	4.889
549.0147	$(^4F)4s\ ^3F_4$	$(^4F)4p\ ^5D_3$	1.460	−0.840	2	2.03	1	4.795	4.857	4.929	4.821	4.878	+0.051	4.846
566.2147	$(^3F)4sp\ ^5D_4$	$4s(^4F)5s\ ^5F_5$	2.318	0.010	3	2.12	1	4.802	4.843	4.903	4.802	4.866	+0.057	4.859
568.9459	$(^3F)4sp\ ^5D_2$	$4s(^4F)5s\ ^5F_3$	2.297	−0.360	3	1.13	1	4.824	4.871	4.930	4.833	4.896	+0.058	4.882
570.2658	$(^3F)4sp\ ^5D_1$	$4s(^4F)5s\ ^5F_2$	2.292	−0.590	3	0.70	1	4.815	4.864	4.922	4.827	4.889	+0.059	4.874
571.6441	$(^3F)4sp\ ^5D_2$	$4s(^4F)5s\ ^5F_2$	2.297	−0.720	3	0.54	1	4.828	4.878	4.935	4.841	4.903	+0.058	4.886
586.6429[a]	$4s^2\ ^3P_2$	$(^4F)4p\ ^3D_3$	1.067	−0.790	2	4.46	2	4.833	4.887	4.971	4.849	4.899	+0.042	4.875
592.2088[a]	$4s^2\ ^3P_0$	$(^4F)4p\ ^3D_1$	1.046	−1.380	2	1.79	2	4.802	4.886	4.964	4.853	4.903	+0.048	4.850
609.2789	$(^2G)4s\ ^3G_5$	$(^4F)4p\ ^3G_5$	1.887	−1.380	2	0.36	2	4.881	4.942	5.008	4.909	4.964	+0.057	4.938
625.8099	$(^4F)4s\ ^3F_3$	$(^3F)4sp\ ^3G_4$	1.443	−0.390	2	5.05	3	4.912	4.943	5.023	4.901	4.952	+0.045	4.957
630.3753	$(^4F)4s\ ^3F_3$	$(^3F)4sp\ ^3G_3$	1.443	−1.580	2	0.68	1	4.912	4.986	5.061	4.955	5.004	+0.056	4.968
631.2234	$(^4F)4s\ ^3F_4$	$(^3F)4sp\ ^3G_4$	1.460	−1.550	2	0.68	2	4.892	4.966	5.040	4.935	4.985	+0.055	4.947
659.9104	$4s^2\ ^1D_2$	$(^3F)4sp\ ^1F_3$	0.900	−2.029	5	0.80	2	4.857	4.955	5.038	4.927	4.970	+0.083	4.940
735.7726	$(^4F)4s\ ^3F_3$	$(^3F)4sp\ ^3F_3$	1.443	−1.020	2	1.99	2	4.814	4.886	4.960	4.854	4.901	+0.054	4.868
842.6504	$(^4F)4s\ ^5F_3$	$(^3F)4sp\ ^5D_2$	0.826	−1.197	6	4.66	2	4.832	4.903	4.992	4.871	4.904	+0.071	4.903
843.5648	$(^4F)4s\ ^5F_4$	$(^3F)4sp\ ^5D_3$	0.836	−0.967	6	5.76	1	4.805	4.859	4.951	4.825	4.855	+0.073	4.878
867.5371	$4s^2\ ^3P_2$	$(^3F)4sp\ ^3D_3$	1.067	−1.500	2	1.85	2	4.774	4.869	4.948	4.838	4.880	+0.075	4.849
868.2979	$4s^2\ ^3P_1$	$(^3F)4sp\ ^3D_2$	1.053	−1.790	2	1.07	2	4.773	4.876	4.954	4.846	4.888	+0.075	4.848
869.2328	$4s^2\ ^3P_0$	$(^3F)4sp\ ^3D_1$	1.046	−2.130	2	0.52	2	4.765	4.874	4.951	4.845	4.887	+0.074	4.839
873.4711	$4s^2\ ^3P_1$	$(^3F)4sp\ ^3D_1$	1.053	−2.240	2	0.41	1	4.771	4.880	4.957	4.851	4.894	+0.075	4.846

Notes. Asterisks (*) indicate lines for which the weighting has been reduced by 1 due to a large uncertainty in the gf value. [(a)] Isotopic splitting included (see Table 2); wavelength corresponds to ^{50}Ti component.

References. 1) Lawler & Dakin (1989); 2) Lawler et al. (2013); 3) Nitz et al. (1998); 4) Blackwell et al. (1982b), as corrected by Grevesse et al. (1989); 5) Blackwell et al. (1983), as corrected by Grevesse et al. (1989); 6) Blackwell et al. (1982a), as corrected by Grevesse et al. (1989).

Table 1. continued.

λ (nm)	Atomic levels Lower	Upper	E_{exc} (eV)	log gf	gf ref.	W_λ (pm)	Wt.	LTE Abundances 3D	⟨3D⟩	HM	MARCS	MISS	Δ_{NLTE} (3D)	3D NLTE
						Ti II								
440.9520	$(^3P)4s\ ^4P_{\frac{3}{2}}$	$(^3F)4p\ ^4D_{\frac{3}{2}}$	1.231	−2.530	7	3.81	2	4.938	4.923	4.951	4.894	4.956		
444.4524[a]	$3d^3\ ^2G_{\frac{7}{2}}$	$(^3F)4p\ ^2F_{\frac{7}{2}}$	1.116	−2.200	7	5.99	1	4.960	4.923	4.952	4.881	4.951		
449.3525[a]	$(^1D)4s\ ^2D_{\frac{3}{2}}$	$(^3F)4p\ ^4F_{\frac{5}{2}}$	1.080	−2.780	7	3.18	1	4.897	4.887	4.916	4.862	4.920		
458.3396[a]	$3d^3\ ^4P_{\frac{3}{2}}$	$(^3F)4p\ ^2F_{\frac{5}{2}}$	1.165	−2.840	7	3.02	2	4.985	4.977	5.005	4.953	5.010		
460.9253[a]	$3d^3\ ^4P_{\frac{5}{2}}$	$(^3F)4p\ ^2F_{\frac{5}{2}}$	1.180	−3.320	7	1.16	1	4.933	4.932	4.959	4.914	4.966		
465.7212	$(^3P)4s\ ^4P_{\frac{5}{2}}$	$(^3F)4p\ ^2F_{\frac{7}{2}}$	1.243	−2.290	7	5.18	1	4.988	4.956	4.983	4.917	4.986		
470.8656[a]	$3d^3\ ^2P_{\frac{3}{2}}$	$(^3F)4p\ ^2F_{\frac{5}{2}}$	1.237	−2.350	7	5.06	1	4.951	4.923	4.949	4.885	4.953		
471.9533	$(^3P)4s\ ^4P_{\frac{5}{2}}$	$(^3F)4p\ ^2F_{\frac{5}{2}}$	1.243	−3.320	7	1.22	1	5.013	5.011	5.038	4.993	5.043		
476.4518[a]	$3d^3\ ^2P_{\frac{3}{2}}$	$(^3F)4p\ ^4F_{\frac{5}{2}}$	1.237	−2.690	7	3.35	1	4.968	4.956	4.982	4.928	4.989		
479.8535[a]	$(^1D)4s\ ^2D_{\frac{3}{2}}$	$(^3F)4p\ ^4G_{\frac{5}{2}}$	1.080	−2.660	7	4.29	1	4.990	4.970	4.997	4.937	5.001		
486.5597[a]	$3d^3\ ^2G_{\frac{7}{2}}$	$(^3F)4p\ ^4G_{\frac{5}{2}}$	1.116	−2.700	7	3.50	1	4.877	4.866	4.893	4.838	4.898		
533.6770[a]	$3d^3\ ^2D2_{\frac{5}{2}}$	$(^3F)4p\ ^2F_{\frac{7}{2}}$	1.582	−1.600	7	7.20	2	4.991	4.922	4.944	4.870	4.942		
538.1013[a]	$3d^3\ ^2D2_{\frac{3}{2}}$	$(^3F)4p\ ^2F_{\frac{5}{2}}$	1.566	−1.970	7	5.66	1	5.004	4.963	4.983	4.918	4.988		
541.8760[a]	$3d^3\ ^2D2_{\frac{5}{2}}$	$(^3F)4p\ ^2F_{\frac{5}{2}}$	1.582	−2.130	7	4.81	3	4.999	4.970	4.990	4.930	4.997		
						V I								
458.6370	$4s^2\ ^4F_{\frac{7}{2}}$	$(^4F)4sp\ ^4G_{\frac{9}{2}}$	0.040	−0.793	8	4.14	2	3.750	3.849	3.943	3.820	3.865	+0.1	3.850
459.4119	$4s^2\ ^4F_{\frac{9}{2}}$	$(^4F)4sp\ ^4G_{\frac{11}{2}}$	0.069	−0.672	8	5.26	2	3.762	3.862	3.956	3.833	3.878	+0.1	3.862
463.5172	$4s^2\ ^4F_{\frac{9}{2}}$	$(^4F)4sp\ ^4G_{\frac{9}{2}}$	0.069	−1.924	8	0.45	1	3.753	3.886	3.975	3.861	3.905	+0.1	3.853
482.7452	$4s^2\ ^4F_{\frac{7}{2}}$	$(^4F)4sp\ ^4D_{\frac{7}{2}}$	0.040	−1.478	8	1.30	1	3.742	3.875	3.965	3.849	3.892	+0.1	3.842
487.5486	$4s^2\ ^4F_{\frac{7}{2}}$	$(^4D)4sp\ ^4G_{\frac{5}{2}}$	0.040	−0.806	8	4.22	1	3.754	3.853	3.948	3.822	3.866	+0.1	3.854
488.1555	$4s^2\ ^4F_{\frac{9}{2}}$	$(^4F)4sp\ ^4D_{\frac{7}{2}}$	0.069	−0.657	8	5.39	1	3.749	3.848	3.943	3.818	3.861	+0.1	3.849
562.6019	$(^5D)4s\ ^4D_{\frac{1}{2}}$	$(^5D)4p\ ^4D_{\frac{1}{2}}$	1.043	−1.252	8	0.31	1	3.834	3.923	3.999	3.894	3.943	+0.1	3.934
564.6108	$(^5D)4s\ ^4D_{\frac{3}{2}}$	$(^5D)4p\ ^4D_{\frac{1}{2}}$	1.051	−1.187	8	0.37	2	3.855	3.941	4.019	3.912	3.961	+0.1	3.955
565.7438	$(^5D)4s\ ^4D_{\frac{5}{2}}$	$(^5D)4p\ ^4D_{\frac{3}{2}}$	1.064	−1.018	8	0.50	3	3.842	3.928	4.004	3.898	3.947	+0.1	3.942
566.8361	$(^5D)4s\ ^4D_{\frac{7}{2}}$	$(^5D)4p\ ^4D_{\frac{5}{2}}$	1.081	−1.021	8	0.49	1	3.849	3.934	4.011	3.905	3.954	+0.1	3.949
567.0847	$(^5D)4s\ ^4D_{\frac{7}{2}}$	$(^4F)4sp\ ^2G_{\frac{9}{2}}$	1.081	−0.425	8	1.69	3	3.823	3.907	3.983	3.876	3.926	+0.1	3.923
570.3586	$(^5D)4s\ ^4D_{\frac{3}{2}}$	$(^5D)4p\ ^4F_{\frac{5}{2}}$	1.051	−0.212	8	2.57	2	3.823	3.900	3.978	3.867	3.917	+0.1	3.923
572.7046	$(^5D)4s\ ^4D_{\frac{7}{2}}$	$(^5D)4p\ ^4F_{\frac{9}{2}}$	1.081	−0.012	8	3.62	3	3.810	3.888	3.966	3.855	3.905	+0.1	3.910
572.7655	$(^5D)4s\ ^4D_{\frac{3}{2}}$	$(^5D)4p\ ^4F_{\frac{3}{2}}$	1.051	−0.875	8	0.78	2	3.876	3.961	4.041	3.933	3.980	+0.1	3.976
573.1249	$(^5D)4s\ ^4D_{\frac{5}{2}}$	$(^4F)4sp\ ^2G_{\frac{7}{2}}$	1.064	−0.732	8	0.97	2	3.836	3.924	4.000	3.894	3.943	+0.1	3.936
573.7065	$(^5D)4s\ ^4D_{\frac{5}{2}}$	$(^5D)4p\ ^4F_{\frac{5}{2}}$	1.064	−0.736	8	0.92	2	3.828	3.915	3.991	3.885	3.934	+0.1	3.928
600.2294	$4s^2\ ^4P_{\frac{5}{2}}$	$(^5D)4p\ ^4D_{\frac{7}{2}}$	1.218	−1.773	8	0.07	1	3.843	3.926	4.000	3.897	3.946	+0.1	3.943
603.9728	$(^5D)4s\ ^4D_{\frac{5}{2}}$	$(^5D)4p\ ^4P_{\frac{5}{2}}$	1.064	−0.652	8	1.12	3	3.834	3.917	3.994	3.886	3.934	+0.1	3.934
608.1441	$(^5D)4s\ ^4D_{\frac{3}{2}}$	$(^5D)4p\ ^4P_{\frac{3}{2}}$	1.051	−0.579	8	1.26	3	3.788	3.875	3.951	3.844	3.893	+0.1	3.888
609.0208	$(^5D)4s\ ^4D_{\frac{7}{2}}$	$(^5D)4p\ ^4P_{\frac{5}{2}}$	1.081	−0.062	8	3.07	3	3.799	3.869	3.947	3.835	3.884	+0.1	3.899
611.1650	$(^5D)4s\ ^4D_{\frac{1}{2}}$	$(^5D)4p\ ^4P_{\frac{1}{2}}$	1.043	−0.714	8	0.99	3	3.784	3.876	3.951	3.846	3.895	+0.1	3.884
611.9528	$(^5D)4s\ ^4D_{\frac{5}{2}}$	$(^5D)4p\ ^4P_{\frac{3}{2}}$	1.064	−0.320	8	1.95	2	3.779	3.857	3.933	3.824	3.874	+0.1	3.879
613.5363	$(^5D)4s\ ^4D_{\frac{3}{2}}$	$(^5D)4p\ ^4P_{\frac{1}{2}}$	1.051	−0.746	8	0.94	1	3.807	3.896	3.972	3.866	3.914	+0.1	3.907
624.2828	$(^5D)4s\ ^6D_{\frac{1}{2}}$	$(^4F)4sp\ ^6D_{\frac{3}{2}}$	0.262	−1.552	8	0.83	3	3.716	3.850	3.936	3.823	3.863	+0.1	3.816
625.1823	$(^5D)4s\ ^6D_{\frac{7}{2}}$	$(^4F)4sp\ ^6D_{\frac{7}{2}}$	0.287	−1.342	8	1.29	3	3.745	3.874	3.962	3.847	3.887	+0.1	3.845
625.6903	$(^5D)4s\ ^6D_{\frac{5}{2}}$	$(^4F)4sp\ ^6D_{\frac{5}{2}}$	0.275	−2.006	8	0.31	2	3.740	3.878	3.964	3.851	3.892	+0.1	3.840
627.4653	$(^5D)4s\ ^6D_{\frac{3}{2}}$	$(^4F)4sp\ ^6D_{\frac{1}{2}}$	0.267	−1.673	8	0.71	1	3.774	3.906	3.995	3.880	3.919	+0.1	3.874
628.5160	$(^5D)4s\ ^6D_{\frac{5}{2}}$	$(^4F)4sp\ ^6D_{\frac{3}{2}}$	0.275	−1.512	8	0.88	3	3.724	3.854	3.940	3.826	3.867	+0.1	3.824
629.2824	$(^5D)4s\ ^6D_{\frac{7}{2}}$	$(^4F)4sp\ ^6D_{\frac{5}{2}}$	0.287	−1.471	8	1.02	1	3.768	3.895	3.983	3.869	3.908	+0.1	3.868
653.1401	$4s^2\ ^4P_{\frac{5}{2}}$	$(^5D)4p\ ^4P_{\frac{5}{2}}$	1.218	−0.836	8	0.57	2	3.809	3.895	3.967	3.864	3.913	+0.1	3.909
						V II								
376.0222	$3d^4\ ^3F_4$	$(^4F)4p\ ^3F_3$	1.687	−1.153	9	3.64	1	3.958	3.942	3.970	3.917	3.975		
386.6740	$3d^4\ ^3P_1$	$(^4F)4p\ ^5D_2$	1.428	−1.550	9	3.29	1	4.015	4.000	4.030	3.978	4.034		
395.1960	$3d^4\ ^3P_2$	$(^4F)4p\ ^3D_3$	1.476	−0.740	10	6.47	1	3.950	3.904	3.933	3.861	3.932		

Notes. [(a)] Isotopic splitting included (see Table 2); wavelength corresponds to ^{50}Ti component.

References. 7) Wood et al. (2013); 8) Whaling et al. (1985), with 572.77 nm corrected for arithmetic error in converting from BFs to A values as per Martin et al. (1988); 9) Biémont et al. (1989); 10) Karamatskos et al. (1986).

Table 1. continued.

λ (nm)	Atomic levels Lower	Upper	E_{exc} (eV)	log gf	gf ref.	W_λ (pm)	Wt.	LTE Abundances 3D	⟨3D⟩	HM	MARCS	MISS	Δ_{NLTE} (3D)	3D NLTE
399.7117	$3d^4\ ^3P_2$	$(^4F)4p\ ^5F_3$	1.476	−1.230	9	5.01	1	4.062	4.041	4.069	4.008	4.073		
403.6777	$3d^4\ ^3P_2$	$(^4F)4p\ ^5F_2$	1.476	−1.594	9	3.17	1	4.015	4.006	4.036	3.986	4.041		
						Cr I								
437.3259	$4s^2\ ^5D_2$	$(^5D)4sp\ ^5F_1$	0.983	−2.323	11	3.76	1	5.584	5.615	5.698	5.578	5.636	+0.031	5.615
452.9838[b]	$(^4G)4s\ ^5G_6$	$(^4G)4p\ ^5G_5$	2.544	−1.380	12	1.77	1	5.598	5.626	5.685	5.589	5.653	+0.023	5.621
453.5127	$(^4G)4s\ ^5G_3$	$(^4G)4p\ ^5G_4$	2.544	−0.993	13	3.15	2	5.576	5.593	5.653	5.550	5.619	+0.023	5.599
454.1060	$(^4G)4s\ ^5G_4$	$(^4G)4p\ ^5G_3$	2.545	−1.143	13	2.50	1	5.578	5.600	5.660	5.560	5.627	+0.023	5.601
463.3259	$(^5D)4sp\ ^7F_3$	$4s5s\ ^7D_4$	3.125	−1.110	14	0.93	2	5.534	5.560	5.610	5.522	5.589	+0.046	5.580
470.0599	$(^4P)4s\ ^5P_1$	$(^3P2)4sp\ ^5S_2$	2.710	−1.255	15	1.51	2	5.581	5.608	5.665	5.570	5.636	+0.027	5.608
470.8017	$(^5D)4sp\ ^7F_5$	$4s5s\ ^7D_4$	3.168	0.090	16	5.67	1	5.595	5.578	5.633	5.516	5.599	+0.066	5.661
474.5270	$(^4P)4s\ ^5P_3$	$(^3P2)4sp\ ^5D_4$	2.708	−1.380	14	1.22	2	5.536	5.566	5.622	5.528	5.595	+0.026	5.562
478.9340	$(^4G)4s\ ^5G_6$	$(^5D)4sp\ ^5F_5$	2.544	−0.348	16	5.99	2	5.528	5.501	5.567	5.443	5.519	+0.019	5.547
480.1048	$4s^2\ ^3F_4$	$(^4G)4p\ ^3F_3$	3.122	−0.131	15	4.79	2	5.613	5.600	5.657	5.544	5.623	+0.045	5.658
488.5733	$(^4G)4s\ ^5G_3$	$(^5D)4sp\ ^5P_2$	2.544	−1.055	15	2.82	2	5.558	5.579	5.639	5.536	5.604	+0.025	5.583
493.6336	$4s^2\ ^3F_4$	$(^4G)4p\ ^3H_4$	3.113	−0.237	16	4.27	1	5.591	5.586	5.642	5.533	5.610	+0.037	5.628
495.3714	$4s^2\ ^3F_4$	$(^4G)4p\ ^3H_4$	3.122	−1.480	14	0.47	1	5.562	5.590	5.639	5.551	5.619	+0.035	5.597
522.0913	$(^5D)4sp\ ^7D_1$	$4s5s\ ^7D_1$	3.385	−0.890	14	1.09	2	5.599	5.622	5.669	5.581	5.650	+0.025	5.624
524.1454	$(^4P)4s\ ^5P_1$	$(^5D)4sp\ ^5P_1$	2.710	−1.920	14	0.35	3	5.450	5.484	5.540	5.449	5.512	+0.025	5.475
527.2008	$(^5D)4sp\ ^7P_3$	$4s5s\ ^7D_4$	3.449	−0.421	16	2.29	1	5.603	5.620	5.667	5.573	5.646	+0.026	5.629
528.7201	$(^5D)4sp\ ^7P_2$	$4s5s\ ^7D_3$	3.438	−0.888	16	1.00	2	5.608	5.630	5.677	5.589	5.657	+0.025	5.633
530.0743	$4s^2\ ^5D_2$	$(^6S)4p\ ^5P_3$	0.983	−2.083	17	5.48	2	5.558	5.566	5.652	5.522	5.575	+0.035	5.593
530.4184	$(^5D)4sp\ ^7P_4$	$4s5s\ ^7D_4$	3.464	−0.681	16	1.45	2	5.612	5.633	5.679	5.590	5.659	+0.025	5.637
531.2871	$(^5D)4sp\ ^7P_3$	$4s5s\ ^7D_3$	3.449	−0.556	16	1.85	1	5.599	5.618	5.665	5.573	5.644	+0.026	5.625
531.8810	$(^5D)4sp\ ^7P_2$	$4s5s\ ^7D_2$	3.438	−0.679	16	1.49	3	5.596	5.617	5.663	5.573	5.643	+0.026	5.622
534.0474	$(^5D)4sp\ ^7P_2$	$4s5s\ ^7D_1$	3.438	−0.730	16	1.48	1	5.642	5.662	5.710	5.620	5.688	+0.026	5.668
562.8621	$4s^2\ ^3G_3$	$(^4G)4p\ ^3H_4$	3.422	−0.756	16	1.36	2	5.597	5.618	5.665	5.575	5.644	+0.033	5.630
571.9809	$(^4D)4s\ ^5D_3$	$(^5D)4sp\ ^5D_4$	3.013	−1.620	16	0.43	1	5.503	5.535	5.586	5.496	5.562	+0.026	5.529
578.1163	$(^4D)4s\ ^5D_4$	$(^5D)4sp\ ^5D_3$	3.011	−1.000	14	1.56	1	5.498	5.525	5.577	5.483	5.551	+0.002	5.500
578.5024	$(^6S)4p\ ^5P_3$	$(^6S)4d\ ^5D_3$	3.321	−0.380	15	3.13	1	5.595	5.610	5.659	5.560	5.633	+0.029	5.624
584.4592	$(^4D)4s\ ^5D_3$	$(^5D)4sp\ ^5D_2$	3.013	−1.770	14	0.40	2	5.616	5.647	5.698	5.609	5.673	+0.026	5.642
688.2477	$(^5D)4sp\ ^7P_2$	$(^6S)4d\ ^7D_2$	3.438	−0.375	15	3.13	1	5.626	5.640	5.687	5.592	5.659	+0.025	5.651
688.2997	$(^5D)4sp\ ^7P_2$	$(^6S)4d\ ^7D_1$	3.438	−0.420	15	2.96	3	5.636	5.651	5.698	5.604	5.671	+0.025	5.661
						Cr II								
455.4990	$d^5\ ^4F_{\frac{7}{2}}$	$(^5D)4p\ ^4D_{\frac{7}{2}}$	4.071	−1.249	18	4.66	1	5.632	5.596	5.606	5.538	5.627		
458.8200	$d^5\ ^4F_{\frac{7}{2}}$	$(^5D)4p\ ^4D_{\frac{5}{2}}$	4.071	−0.594	18	7.47	2	5.648	5.565	5.576	5.492	5.588		
484.8237	$(^3F)4s\ ^4F_{\frac{7}{2}}$	$(^5D)4p\ ^4F_{\frac{7}{2}}$	3.864	−1.160	18	6.11	3	5.689	5.621	5.629	5.555	5.648		
523.7328	$d^5\ ^4F_{\frac{9}{2}}$	$(^5D)4p\ ^4F_{\frac{9}{2}}$	4.073	−1.087	18	5.36	2	5.610	5.554	5.557	5.490	5.581		
524.6768	$(^3F)4s\ ^4P_{\frac{1}{2}}$	$(^5D)4p\ ^4P_{\frac{3}{2}}$	3.714	−2.436	18	1.62	1	5.654	5.652	5.665	5.620	5.684		
527.9877	$d^5\ ^4F_{\frac{9}{2}}$	$(^5D)4p\ ^4F_{\frac{7}{2}}$	4.073	−1.909	18	2.02	1	5.580	5.576	5.587	5.539	5.608		
531.0686	$d^5\ ^4F_{\frac{3}{2}}$	$(^5D)4p\ ^4F_{\frac{5}{2}}$	4.072	−2.144	18	1.32	1	5.564	5.566	5.578	5.534	5.597		
531.3561	$d^5\ ^4F_{\frac{5}{2}}$	$(^5D)4p\ ^4F_{\frac{5}{2}}$	4.073	−1.473	18	3.49	1	5.544	5.523	5.529	5.473	5.553		
550.2068	$(^3G)4s\ ^4G_{\frac{9}{2}}$	$(^5D)4p\ ^4F_{\frac{7}{2}}$	4.168	−2.049	18	1.84	2	5.743	5.741	5.750	5.704	5.770		
612.9226	$(^3G)4s\ ^4D_{\frac{5}{2}}$	$(^5D)4p\ ^4D_{\frac{5}{2}}$	4.750	−2.478	18	0.29	1	5.749	5.759	5.768	5.731	5.785		
						Mn I								
408.2945	$(^5D)4s\ ^6D_{\frac{3}{2}}$	$(^5D)4p\ ^6D_{\frac{5}{2}}$	2.178	−0.365	19	8.97	2	5.380	5.316	5.392	5.256	5.329	+0.016	5.396
426.5928	$(^5D)4s\ ^4D_{\frac{3}{2}}$	$(^5D)4p\ ^4P_{\frac{3}{2}}$	2.941	−0.400	20	5.85	1*	5.376	5.354	5.420	5.301	5.376	+0.076	5.452
445.3013	$(^5D)4s\ ^4D_{\frac{3}{2}}$	$(^5D)4p\ ^4D_{\frac{1}{2}}$	2.941	−0.620	21	5.19	2	5.368	5.371	5.436	5.322	5.395	+0.070	5.438
445.7041	$(^6S)4sp\ ^6P_{\frac{5}{2}}$	$(^7S)4sd\ ^6D_{\frac{3}{2}}$	3.073	−0.685	20	4.33	1*	5.392	5.400	5.460	5.353	5.426	+0.065	5.457
447.0142	$(^5D)4s\ ^4D_{\frac{3}{2}}$	$(^5D)4p\ ^4D_{\frac{3}{2}}$	2.941	−0.560	21	5.22	2	5.411	5.389	5.454	5.336	5.411	+0.061	5.472
449.8897	$(^5D)4s\ ^4D_{\frac{3}{2}}$	$(^5D)4p\ ^4D_{\frac{5}{2}}$	2.941	−0.460	21	5.54	1	5.398	5.364	5.430	5.309	5.385	+0.054	5.452

Notes. Asterisks (*) indicate lines for which the weighting has been reduced by 1 due to a large uncertainty in the gf value. [(b)] Isotopic splitting included (see Table 2); wavelength corresponds to ^{50}Cr component.

References. 9) Biémont et al. (1989); 10) Karamatskos et al. (1986); 11) mean of Sobeck et al. (2007) and Blackwell et al. (1984); 12) mean of Sobeck et al. (2007) and Tozzi et al. (1985); 13) mean of Sobeck et al. (2007), Tozzi et al. (1985) and Blackwell et al. (1986b); 14) Sobeck et al. (2007); 15) Blackwell et al. (1986b); 16) mean of Sobeck et al. (2007) and Blackwell et al. (1986b); 17) mean of Sobeck et al. (2007), Tozzi et al. (1985) and Blackwell et al. (1984); 18) Kurucz (2011); 19) Den Hartog et al. (2011); 20) Booth et al. (1984a), renormalised to the absolute scale of Blackwell-Whitehead & Bergemann (2007) (lines with excitation potential ≈ 3 eV; see Sect. 6.5.1); 21) Blackwell-Whitehead & Bergemann (2007).

Table 1. continued.

λ (nm)	Atomic levels Lower	Upper	E_{exc} (eV)	log gf	gf ref.	W_λ (pm)	Wt.	LTE Abundances 3D	⟨3D⟩	HM	MARCS	MISS	Δ_{NLTE} (3D)	3D NLTE
450.2223	$(^5D)4s\ ^4D_{\frac{5}{2}}$	$(^5D)4p\ ^4D_{\frac{7}{2}}$	2.920	−0.430	21	5.81	2	5.349	5.328	5.393	5.273	5.348	+0.055	5.404
467.1688	$(^5D)4s\ ^4D_{\frac{7}{2}}$	$(^5D)4p\ ^4F_{\frac{5}{2}}$	2.888	−1.660	21	1.23	1	5.379	5.412	5.472	5.377	5.440	+0.061	5.440
470.9710	$(^5D)4s\ ^4D_{\frac{7}{2}}$	$(^5D)4p\ ^4F_{\frac{7}{2}}$	2.888	−0.487	19	6.88	2	5.353	5.360	5.427	5.306	5.379	+0.065	5.418
473.9110	$(^5D)4s\ ^4D_{\frac{3}{2}}$	$(^5D)4p\ ^4F_{\frac{3}{2}}$	2.941	−0.604	19	5.82	3	5.346	5.359	5.424	5.310	5.382	+0.065	5.411
500.4891	$(^5D)4s\ ^4D_{\frac{5}{2}}$	$(^5D)4p\ ^6F_{\frac{7}{2}}$	2.920	−1.636	22	1.31	2	5.404	5.434	5.493	5.398	5.461	+0.064	5.468
525.5330	$4s^2\ ^4G_{\frac{11}{2}}$	$(^5D)4p\ ^4F_{\frac{9}{2}}$	3.133	−0.858	19	3.69	2	5.326	5.355	5.413	5.313	5.381	+0.069	5.395
538.8538	$4s^2\ ^4P_{\frac{5}{2}}$	$(^5D)4p\ ^4D_{\frac{7}{2}}$	3.373	−1.620	21	0.49	1	5.334	5.361	5.416	5.322	5.389	+0.064	5.398
542.0368	$(^5D)4s\ ^6D_{\frac{7}{2}}$	$(^6S)4sp\ ^6P_{\frac{5}{2}}$	2.143	−1.462	23	7.86	3	5.315	5.361	5.434	5.323	5.382	+0.072	5.387
					Fe I									
444.5472	$4s^2\ ^5D_2$	$4s4p(^3P)\ ^7F_2$	0.087	−5.412	24	3.80	2	7.419	7.463	7.568	7.436	7.474	+0.016	7.435
524.7050	$4s^2\ ^5D_2$	$4s4p(^3P)\ ^7D_3$	0.087	−4.961	24	6.40	3	7.472	7.449	7.559	7.412	7.440	+0.022	7.494
549.1832	$3d^8\ ^3F_2$	$(^2P)4p\ ^3D_3$	4.186	−2.188	25	1.23	1	7.441	7.452	7.500	7.411	7.481	+0.006	7.447
560.0224	$4s4p(^3P)\ ^3P_1$	$4s(^4D)5s\ ^5D_1$	4.260	−1.420	25	3.65	1	7.369	7.367	7.412	7.316	7.390	+0.007	7.376
566.1346	$4s4p(^3P)\ ^3P_0$	$4s(^4D)5s\ ^5D_1$	4.284	−1.756	25	2.22	2	7.414	7.419	7.465	7.374	7.445	+0.006	7.420
570.5465	$(^4F)4p\ ^5F_1$	$4s(^4D)5s\ ^5D_1$	4.301	−1.355	25	3.96	2	7.418	7.409	7.455	7.356	7.431	+0.005	7.423
577.8453	$4s^2\ ^3F2_3$	$(^4F)4p\ ^3D_3$	2.588	−3.440	25	2.04	2	7.403	7.427	7.495	7.391	7.450	+0.005	7.408
578.4658	$4s4p(^3P)\ ^5F_3$	$4s(^6D)5s\ ^5D_4$	3.396	−2.532	25	2.58	2	7.418	7.429	7.486	7.387	7.453	+0.007	7.425
585.5077	$(^4F)4p\ ^3F_3$	$(^4F)4d\ ^5H_4$	4.608	−1.478	25	2.20	1	7.422	7.426	7.468	7.379	7.452	+0.006	7.428
595.6694	$(^4F)4s\ ^5F_5$	$4s4p(^3P)\ ^7P_4$	0.859	−4.552	24	5.02	3	7.430	7.441	7.538	7.408	7.443	+0.017	7.447
615.1618	$(^4P)4s\ ^5P_3$	$(^4F)4p\ ^5D_2$	2.176	−3.282	26	4.88	3	7.445	7.437	7.514	7.397	7.447	+0.012	7.457
624.0646	$(^4P)4s\ ^5P_1$	$4s4p(^3P)\ ^3P_2$	2.223	−3.287	27	4.76	3	7.469	7.461	7.538	7.421	7.472	+0.012	7.481
631.1500	$(^4P)4s\ ^3P_2$	$(^4F)4p\ ^3D_2$	2.831	−3.141	25	2.66	1	7.470	7.485	7.549	7.447	7.505	+0.008	7.478
649.8939	$(^4F)4s\ ^5F_3$	$4s4p(^3P)\ ^7F_3$	0.958	−4.695	24	4.39	3	7.488	7.516	7.610	7.486	7.519	+0.015	7.503
651.8367	$(^4P)4s\ ^3P_2$	$(^4F)4p\ ^3D_3$	2.831	−2.448	27	5.72	2	7.429	7.389	7.459	7.343	7.396	+0.012	7.441
669.9142	$(^2F)4s\ ^3F_4$	$(^2P)4p\ ^3D_3$	4.593	−2.101	25	0.81	2	7.515	7.469	7.543	7.422	7.471	+0.006	7.489
679.3259	$3d^8\ ^3F_4$	$4s4p(^3P)\ ^5G_4$	4.076	−2.326	25	1.25	1	7.420	7.431	7.479	7.390	7.455	+0.006	7.426
683.7006	$(^2F)4s\ ^3F_4$	$(^2H)4p\ ^3G_4$	4.593	−1.687	25	1.77	1	7.466	7.468	7.509	7.422	7.492	+0.006	7.472
685.4823	$(^2F)4s\ ^3F_4$	$4s4p(^3P)\ ^1H_5$	4.593	−1.926	25	1.22	1	7.506	7.512	7.553	7.469	7.536	+0.006	7.512
740.1685	$3d^8\ ^3F_2$	$(^4P)4p\ ^3D_1$	4.186	−1.500	25	4.16	3	7.381	7.371	7.417	7.323	7.387	+0.008	7.389
791.2867	$(^4F)4s\ ^5F_5$	$4s4p(^3P)\ ^7D_4$	0.859	−4.848	28	4.57	2	7.451	7.489	7.586	7.462	7.486	+0.017	7.468
829.3515	$(^2D)4s\ ^3D_2$	$(^4F)4p\ ^3D_2$	3.301	−2.203	29	5.85	1*	7.471	7.448	7.509	7.401	7.453	+0.011	7.482
					Fe II									
462.0513	$4s\ ^4F_{\frac{7}{2}}$	$4p\ ^4D_{\frac{7}{2}}$	2.828	−3.210	30	5.40	1	7.474	7.405	7.416	7.350	7.436		
526.4804	$4s\ ^4G_{\frac{5}{2}}$	$4p\ ^4D_{\frac{3}{2}}$	3.230	−3.130	30	4.74	3	7.556	7.500	7.503	7.445	7.530		
541.4072	$4s\ ^4G_{\frac{7}{2}}$	$4p\ ^4D_{\frac{7}{2}}$	3.221	−3.580	30	2.73	2	7.483	7.464	7.471	7.424	7.496		
643.2676	$4s^2\ ^6S_{\frac{5}{2}}$	$4p\ ^6D_{\frac{5}{2}}$	2.891	−3.570	30	4.30	3	7.515	7.463	7.462	7.416	7.488		
651.6077	$4s^2\ ^6S_{\frac{5}{2}}$	$4p\ ^6D_{\frac{7}{2}}$	2.891	−3.310	30	5.69	3	7.569	7.485	7.482	7.432	7.504		
722.2392	$4s\ ^4D_{\frac{3}{2}}$	$4p\ ^4D_{\frac{1}{2}}$	3.889	−3.260	30	2.03	1	7.519	7.504	7.501	7.466	7.530		
722.4479	$4s\ ^4D_{\frac{1}{2}}$	$4p\ ^4D_{\frac{1}{2}}$	3.889	−3.200	30	2.10	1	7.480	7.464	7.461	7.425	7.490		
751.5831	$4s\ ^4D_{\frac{7}{2}}$	$4p\ ^4D_{\frac{5}{2}}$	3.903	−3.390	30	1.47	2	7.455	7.445	7.444	7.411	7.472		
771.1721	$4s\ ^4D_{\frac{7}{2}}$	$4p\ ^4D_{\frac{7}{2}}$	3.903	−2.500	30	5.04	3	7.500	7.431	7.417	7.378	7.448		
					Co I									
521.2688	$(^4F)4sp\ ^4F_{\frac{9}{2}}$	$4s(^5F)5s\ ^4F_{\frac{9}{2}}$	3.514	−0.110	31	1.91	3	4.807	4.822	4.873	4.785	4.851	+0.072	4.879
528.0627	$(^4F)4sp\ ^4G_{\frac{9}{2}}$	$4s(^5F)5s\ ^4F_{\frac{7}{2}}$	3.629	−0.030	31	1.78	2	4.820	4.833	4.883	4.795	4.862	+0.077	4.897
530.1044	$4s^2\ ^4P_{\frac{5}{2}}$	$(^3F)4p\ ^4D_{\frac{5}{2}}$	1.710	−1.940	32	1.79	1	4.859	4.899	4.973	4.869	4.922	+0.100	4.959
535.2041	$(^4F)4sp\ ^4G_{\frac{11}{2}}$	$4s(^5F)5s\ ^4F_{\frac{9}{2}}$	3.576	0.060	31	2.38	2	4.823	4.836	4.886	4.796	4.864	+0.082	4.905
548.3353	$4s^2\ ^4P_{\frac{5}{2}}$	$(^3F)4p\ ^4D_{\frac{7}{2}}$	1.710	−1.410	32	4.64	3	4.800	4.837	4.913	4.804	4.857	+0.099	4.899
564.7233	$(^3P)4s\ ^2P_{\frac{3}{2}}$	$(^3F)4p\ ^2D_{\frac{5}{2}}$	2.280	−1.560	31	1.24	2*	4.837	4.869	4.936	4.836	4.894	+0.084	4.921

References. 19) Den Hartog et al. (2011); 20) Booth et al. (1984a), renormalised to the absolute scale of Blackwell-Whitehead & Bergemann (2007) (lines with excitation potential ≈ 3 eV; see Sect. 6.5.1); 21) Blackwell-Whitehead & Bergemann (2007); 22) derived from BFs of Greenlee & Whaling (1979) and lifetimes of Schnabel et al. (1995); 23) Booth et al. (1984a); 24) mean of Oxford data (Blackwell et al. 1979a,b, 1982c,d, 1986a, 1995) and O'Brian et al. (1991); 25) Hannover data (Bard et al. 1991; Bard & Kock 1994); 26) mean of Oxford (see Ref. 24) and Hannover data (see Ref. 25); 27) mean of Hannover data (see Ref. 25) and O'Brian et al. (1991), with double weight to Hannover; 28) Oxford data (see Ref. 24); 29) mean of Hannover data (see Ref. 25) and O'Brian et al. (1991); 30) Meléndez & Barbuy (2009); 31) Cardon et al. (1982); 32) Nitz et al. (1999); 33) Wood et al. (2014b).

Table 1. continued.

λ	Atomic levels		E_{exc}	log gf	gf	W_λ	Wt.	LTE Abundances					Δ_{NLTE}	3D
(nm)	Lower	Upper	(eV)		ref.	(pm)		3D	⟨3D⟩	HM	MARCS	MISS	(3D)	NLTE
593.5390	$(^3P)4s\ ^4P_{\frac{5}{2}}$	$(^3F)4p\ ^4D_{\frac{7}{2}}$	1.883	−2.610	32	0.32	1	4.849	4.891	4.963	4.861	4.914	+0.087	4.936
608.2423	$(^4F)4sp\ ^4F_{\frac{9}{2}}$	$(^3F)5s\ ^4F_{\frac{9}{2}}$	3.514	−0.520	31	1.00	3	4.857	4.873	4.924	4.836	4.901	+0.072	4.929
609.3141	$4s^2\ ^4P_{\frac{3}{2}}$	$(^4F)4sp\ ^4D_{\frac{3}{2}}$	1.740	−2.440	31	0.79	2*	4.935	4.978	5.050	4.950	4.998	+0.085	5.020
618.9005	$4s^2\ ^4P_{\frac{5}{2}}$	$(^4F)4sp\ ^4D_{\frac{5}{2}}$	1.710	−2.450	31	0.89	2*	4.956	4.998	5.071	4.971	5.018	+0.085	5.041
642.9913	$4s^2\ ^2G_{\frac{7}{2}}$	$(^4F)4sp\ ^2F_{\frac{5}{2}}$	2.137	−2.410	31	0.31	2*	4.854	4.892	4.960	4.861	4.914	+0.087	4.941
645.4995	$(^4F)4sp\ ^4D_{\frac{7}{2}}$	$(^3F)5s\ ^4F_{\frac{9}{2}}$	3.632	−0.250	31	1.34	2	4.826	4.840	4.889	4.803	4.867	+0.084	4.910
741.7386	$(^1D)4s\ ^2D_{\frac{3}{2}}$	$(^4F)4sp\ ^4D_{\frac{5}{2}}$	2.042	−2.070	31	1.00	2*	4.880	4.920	4.989	4.892	4.939	+0.090	4.970
						Ni I								
474.0166[c]	$(^3F)4sp\ ^5G_4$	$(^2D)4d\ ^3G_5$	3.480	−1.720	33	1.60	1	6.192	6.197	6.246	6.160	6.228		
481.1977[c]	$(^2D)4p\ ^3P_1$	$(^2D)4d\ ^3P_0$	3.658	−1.450	34	2.13	1	6.238	6.241	6.287	6.201	6.271		
481.4598	$(^3F)4sp\ ^5G_2$	$4s(^4F)5s\ ^5F_3$	3.597	−1.630	33	1.59	1	6.216	6.218	6.265	6.179	6.248		
487.4793	$(^3F)4sp\ ^5G_3$	$4s(^4F)5s\ ^5F_4$	3.543	−1.440	33	2.35	1	6.177	6.178	6.225	6.137	6.207		
488.6711	$(^2D)4p\ ^3D_2$	$4s(^4F)5s\ ^5F_2$	3.706	−1.810	33	0.90	1	6.201	6.207	6.253	6.170	6.238		
490.0971	$(^3F)4sp\ ^5G_4$	$4s(^4F)5s\ ^5F_5$	3.480	−1.660	33	1.79	1	6.195	6.196	6.244	6.156	6.226		
497.6135[c]	$(^3F)4sp\ ^5F_4$	$(^2D)4d\ ^3G_4$	3.606	−1.260	33	2.86	2	6.179	6.176	6.222	6.132	6.204		
515.7981	$(^3F)4sp\ ^5F_4$	$4s(^4F)5s\ ^5F_5$	3.606	−1.510	33	1.86	3	6.169	6.169	6.215	6.128	6.198		
550.4095	$(^3F)4sp\ ^3G_5$	$4s(^4F)5s\ ^5F_4$	3.834	−1.690	33	0.97	1	6.207	6.211	6.254	6.170	6.240		
551.0009[c]	$(^2D)4p\ ^1F_3$	$(^2D)4d\ ^3G_4$	3.847	−0.880	33	3.75	2	6.189	6.176	6.219	6.125	6.201		
553.7105	$(^2D)4p\ ^1F_3$	$4s(^4F)5s\ ^5F_4$	3.847	−2.220	33	0.31	3	6.213	6.220	6.263	6.182	6.250		
574.9280[c]	$(^3F)4sp\ ^3G_3$	$(^2D)4d\ ^3G_4$	3.941	−1.920	33	0.44	2	6.145	6.152	6.193	6.113	6.181		
617.6820[c]	$(^3F)4sp\ ^3F_4$	$(^2D)4d\ ^3G_5$	4.088	−0.260	33	6.64	2	6.225	6.193	6.234	6.130	6.208		
620.4605	$(^3F)4sp\ ^3F_4$	$4s(^4F)5s\ ^5F_4$	4.088	−1.080	33	2.11	3	6.211	6.206	6.245	6.161	6.232		
622.3991[c]	$(^3F)4sp\ ^3F_3$	$(^2D)4d\ ^3G_4$	4.105	−0.910	33	2.79	3	6.197	6.194	6.233	6.148	6.220		
637.8258[c]	$(^3F)4sp\ ^3D_3$	$(^2D)4d\ ^3G_4$	4.154	−0.820	33	3.20	3	6.225	6.221	6.259	6.173	6.245		
641.4588	$(^3F)4sp\ ^3D_3$	$4s(^4F)5s\ ^5F_4$	4.154	−1.160	33	1.68	2	6.215	6.213	6.251	6.169	6.239		

Notes. [(c)] Isotopic splitting included (see Table 2); wavelength corresponds to ^{58}Ni component.

References. 31) Cardon et al. (1982); 32) Nitz et al. (1999); 33) Wood et al. (2014b); 34) Johansson et al. (2003).

Table 2. HFS and isotopic splitting data for the lines retained in this analysis.

		Lower level				Upper level			
λ (nm)	Iso.	J	A (MHz)	B (MHz)	HFS ref.	J	A (MHz)	B (MHz)	HFS ref.
				Sc I: 100% ^{45}Sc ($I = \frac{7}{2}$)					
474.3821	^{45}Sc	9/2	285.967	−15.460	1	7/2			
508.1561	^{45}Sc	9/2	285.967	−15.460	1	9/2			
535.6097	^{45}Sc	7/2	−25.000		2	5/2			
567.1828	^{45}Sc	9/2	285.967	−15.460	1	11/2	55.000	25.000	3
623.9800	^{45}Sc	3/2	269.556	−26.346	4	3/2	348.320		5
				Sc II					
442.0661	^{45}Sc	4	38.357	−16.456	6	3	205.400	−70.000	7
443.1362	^{45}Sc	3	113.674	−12.615	6	2	366.800	−40.000	7
535.7202	^{45}Sc	2	−27.732	22.127	8	1			
564.1000	^{45}Sc	1	−107.501	−12.300	8	2	106.117	−20.200	8
565.8362	^{45}Sc	0	0.000	0.000	N	1	255.155	11.753	8
566.7164	^{45}Sc	1	−107.501	−12.300	8	1	255.155	11.753	8
566.9055	^{45}Sc	1	−107.501	−12.300	8	0	0.000	0.000	N
568.4214	^{45}Sc	2	−27.732	22.127	8	1	255.155	11.753	8
624.5641	^{45}Sc	2	−27.732	22.127	8	3	99.730	21.495	8
630.0746	^{45}Sc	2	−27.732	22.127	8	2	125.423	8.769	8
632.0843	^{45}Sc	1	−107.501	−12.300	8	1	304.788	3.824	8
660.4578	^{45}Sc	2	149.361	7.818	6	2	215.700	18.000	9
				Ti I: 8.25% ^{46}Ti ($I = 0$), 7.44% ^{47}Ti ($I = \frac{5}{2}$), 73.72% ^{48}Ti ($I = 0$), 5.41% ^{49}Ti ($I = \frac{7}{2}$), 5.18% ^{50}Ti ($I = 0$) Isotopic separations from Gangrsky et al. (1995)				
586.6429	^{50}Ti	2	0.000	0.000	N	3	0.000	0.000	N
586.6439	^{49}Ti	2	−25.216	−39.202	10	3			
586.6448	^{48}Ti	2	0.000	0.000	N	3	0.000	0.000	N
586.6458	^{47}Ti	2	−25.216	−47.826	10	3			
586.6468	^{46}Ti	2	0.000	0.000	N	3	0.000	0.000	N
592.2088	^{50}Ti	0	0.000	0.000	N	1	0.000	0.000	N
592.2097	^{49}Ti	0	0.000	0.000	N	1	−140.600	0.000	11
592.2107	^{48}Ti	0	0.000	0.000	N	1	0.000	0.000	N
592.2117	^{47}Ti	0	0.000	0.000	N	1	−140.700	0.000	11
592.2128	^{46}Ti	0	0.000	0.000	N	1	0.000	0.000	N
				Ti II: Isotopic separations from Nouri et al. (2010)					
4444.524	^{50}Ti	7/2	0.000	0.000	N	7/2	0.000	0.000	N
4444.530	^{49}Ti	7/2	−54.374	26.422	12	7/2	−31.500	−14.000	12
4444.536	^{48}Ti	7/2	0.000	0.000	N	7/2	0.000	0.000	N
4444.542	^{47}Ti	7/2	−54.374	32.235	12	7/2	−31.500	−17.080	12
4444.547	^{46}Ti	7/2	0.000	0.000	N	7/2	0.000	0.000	N
4493.520	^{46}Ti	3/2	0.000	0.000	N	5/2	0.000	0.000	N
4493.521	^{47}Ti	3/2	97.013	−19.453	12	5/2			
4493.523	^{48}Ti	3/2	0.000	0.000	N	5/2	0.000	0.000	N
4493.524	^{49}Ti	3/2	97.013	−23.733	12	5/2			
4493.525	^{50}Ti	3/2	0.000	0.000	N	5/2	0.000	0.000	N
4583.396	^{50}Ti	3/2	0.000	0.000	N	5/2	0.000	0.000	N
4583.403	^{49}Ti	3/2	−6.630	−24.100	13	5/2	−84.210	−44.000	12
4583.409	^{48}Ti	3/2	0.000	0.000	N	5/2	0.000	0.000	N
4583.415	^{47}Ti	3/2	−6.630	−29.402	13	5/2	−84.210	−53.680	12
4583.421	^{46}Ti	3/2	0.000	0.000	N	5/2	0.000	0.000	N

References. 1) Ertmer & Hofer (1976, ABMR); 2) Başar et al. (2004, theoretical calculations); 3) Singh et al. (1991); 4) Childs (1971); 5) Aboussaïd et al. (1996); 6) Mansour et al. (1989); 7) Young et al. (1988); 8) statistically-weighted average of Mansour et al. (1989) and Villemoes et al. (1992); 9) Arnesen et al. (1982); 10) Aydin et al. (1990); 11) Gangrsky et al. (1995); 12) Berrah-Mansour et al. (1992); 13) Nouri et al. (2010).

Table 2. continued.

		Lower level				Upper level			
λ (nm)	Iso.	J	A (MHz)	B (MHz)	HFS ref.	J	A (MHz)	B (MHz)	HFS ref.
4609.253	^{50}Ti	5/2	0.000	0.000	N	5/2	0.000	0.000	N
4609.259	^{49}Ti	5/2	11.520	38.400	13	5/2	−84.210	−44.000	12
4609.265	^{48}Ti	5/2	0.000	0.000	N	5/2	0.000	0.000	N
4609.271	^{47}Ti	5/2	11.520	46.848	13	5/2	−84.210	−53.680	12
4609.277	^{46}Ti	5/2	0.000	0.000	N	5/2	0.000	0.000	N
4708.656	^{50}Ti	3/2	0.000	0.000	N	5/2	0.000	0.000	N
4708.659	^{49}Ti	3/2	53.334	−23.471	12	5/2	−84.210	−44.000	12
4708.662	^{48}Ti	3/2	0.000	0.000	N	5/2	0.000	0.000	N
4708.665	^{47}Ti	3/2	53.334	−28.635	12	5/2	−84.210	−53.680	12
4708.668	^{46}Ti	3/2	0.000	0.000	N	5/2	0.000	0.000	N
4764.518	^{50}Ti	3/2	0.000	0.000	N	5/2	0.000	0.000	N
4764.521	^{49}Ti	3/2	53.334	−23.471	12	5/2			
4764.524	^{48}Ti	3/2	0.000	0.000	N	5/2	0.000	0.000	N
4764.527	^{47}Ti	3/2	53.334	−28.635	12	5/2			
4764.530	^{46}Ti	3/2	0.000	0.000	N	5/2	0.000	0.000	N
4798.529	^{46}Ti	3/2	0.000	0.000	N	5/2	0.000	0.000	N
4798.530	^{47}Ti	3/2	97.013	−19.453	12	5/2			
4798.532	^{48}Ti	3/2	0.000	0.000	N	5/2	0.000	0.000	N
4798.533	^{49}Ti	3/2	97.013	−23.733	12	5/2			
4798.535	^{50}Ti	3/2	0.000	0.000	N	5/2	0.000	0.000	N
4865.597	^{50}Ti	7/2	0.000	0.000	N	5/2	0.000	0.000	N
4865.605	^{49}Ti	7/2	−54.374	26.422	12	5/2			
4865.611	^{48}Ti	7/2	0.000	0.000	N	5/2	0.000	0.000	N
4865.618	^{47}Ti	7/2	−54.374	32.235	12	5/2			
4865.625	^{46}Ti	7/2	0.000	0.000	N	5/2	0.000	0.000	N
5336.770	^{50}Ti	5/2	0.000	0.000	N	7/2	0.000	0.000	N
5336.774	^{49}Ti	5/2				7/2	−31.500	−14.000	12
5336.778	^{48}Ti	5/2	0.000	0.000	N	7/2	0.000	0.000	N
5336.782	^{47}Ti	5/2				7/2	−31.500	−17.080	12
5336.786	^{46}Ti	5/2	0.000	0.000	N	7/2	0.000	0.000	N
5381.013	^{50}Ti	3/2	0.000	0.000	N	5/2	0.000	0.000	N
5381.017	^{49}Ti	3/2				5/2	−84.210	−44.000	12
5381.021	^{48}Ti	3/2	0.000	0.000	N	5/2	0.000	0.000	N
5381.025	^{47}Ti	3/2				5/2	−84.210	−53.680	12
5381.029	^{46}Ti	3/2	0.000	0.000	N	5/2	0.000	0.000	N
5418.760	^{50}Ti	5/2	0.000	0.000	N	5/2	0.000	0.000	N
5418.764	^{49}Ti	5/2				5/2	−84.210	−44.000	12
5418.768	^{48}Ti	5/2	0.000	0.000	N	5/2	0.000	0.000	N
5418.771	^{47}Ti	5/2				5/2	−84.210	−53.680	12
5418.775	^{46}Ti	5/2	0.000	0.000	N	5/2	0.000	0.000	N
		V I : 99.75% ^{51}V ($I = \frac{7}{2}$)							
458.6370	^{51}V	7/2	249.739	5.081	14	9/2	408.197		15
459.4119	^{51}V	9/2	227.132	7.822	14	11/2	448.669		15
463.5172	^{51}V	9/2	227.132	7.822	14	9/2	408.197		15
482.7452	^{51}V	7/2	249.739	5.081	14	7/2	606.150		15
487.5486	^{51}V	7/2	249.739	5.081	14	5/2	611.067		15
488.1555	^{51}V	9/2	227.132	7.822	14	7/2	606.150		15
562.6019	^{51}V	1/2	1276.000		16	1/2	1100.238		15
564.6108	^{51}V	3/2	6.966	−10.854	16	1/2	1100.238		15
565.7438	^{51}V	5/2	−143.432	−1.196	16	3/2	141.202		15
566.8361	^{51}V	7/2	−160.219	10.229	16	5/2	15.289		15
567.0847	^{51}V	7/2	−160.219	10.229	16	9/2	94.644		15
570.3586	^{51}V	3/2	6.966	−10.854	16	5/2	215.851		17
572.7046	^{51}V	7/2	−160.219	10.229	16	9/2	89.038		15
572.7655	^{51}V	3/2	6.966	−10.854	16	3/2	634.361		15
573.1249	^{51}V	5/2	−143.432	−1.196	16	7/2	431.551		15
573.7065	^{51}V	5/2	−143.432	−1.196	16	5/2	215.851		17
600.2294	^{51}V	5/2	112.835		18	7/2	−17.088		15

References. 12) Berrah-Mansour et al. (1992); 13) Nouri et al. (2010); 14) Childs & Goodman (1967); 15) Palmeri et al. (1995); 16) Childs et al. (1979); 17) Lefèbvre et al. (2002); 18) Johann et al. (1981).

Table 2. continued.

		Lower level				Upper level			
λ (nm)	Iso.	J	A (MHz)	B (MHz)	HFS ref.	J	A (MHz)	B (MHz)	HFS ref.
603.9728	^{51}V	5/2	−143.432	−1.196	16	5/2	−89.800	8.000	16
608.1441	^{51}V	3/2	6.966	−10.854	16	3/2	−286.400	−6.000	16
609.0208	^{51}V	7/2	−160.219	10.229	16	5/2	−89.800	8.000	16
611.1650	^{51}V	1/2	1276.000		16	1/2	−795.200		16
611.9528	^{51}V	5/2	−143.432	−1.196	16	3/2	−286.400	−6.000	16
613.5363	^{51}V	3/2	6.966	−10.854	16	1/2	−795.200		16
619.9191	^{51}V	7/2	382.367	2.268	14	9/2	503.460	3.300	19
624.2828	^{51}V	1/2	751.478	3.337	14	3/2	594.690	−4.400	19
624.3110	^{51}V	9/2	406.851	14.324	14	9/2	503.460	3.300	19
625.1823	^{51}V	7/2	382.367	2.268	14	7/2	514.350	−1.200	19
625.6903	^{51}V	5/2	373.518	−5.459	14	5/2	537.440	−4.000	19
627.4653	^{51}V	3/2	405.604	−8.107	14	1/2	939.940	0.000	19
628.5160	^{51}V	5/2	373.518	−5.459	14	3/2	594.690	−4.400	19
629.2824	^{51}V	7/2	382.367	2.268	14	5/2	537.440	−4.000	19
653.1401	^{51}V	5/2	112.835		18	5/2	−89.800	8.000	17
				V II					
371.8152	^{51}V	3	250.910		20	4	178.223		20
376.0222	^{51}V	4	171.400		20	3	301.130		20
386.6740	^{51}V	1	−73.330		20	2			
395.1960	^{51}V	2	0.000		20	3	160.220		20
399.7117	^{51}V	2	50.000		21	3	200.000		21
403.6777	^{51}V	2	0.000		20	2	239.500		20
				Cr I: 4.35% ^{50}Cr (I = 0), 83.79% ^{52}Cr (I = 0), 9.50% ^{53}Cr ($I = \frac{3}{2}$), 2.37% ^{54}Cr (I = 0) Isotopic separations from Furmann et al. (2005)				
452.98384	^{50}Cr	6	0.000	0.000	N	5	0.000	0.000	N
452.98396	^{52}Cr	6	0.000	0.000	N	5	0.000	0.000	N
452.98404	^{53}Cr	6	112.000	8.300	22	5	0.000	0.000	N
452.98412	^{54}Cr	6	0.000	0.000	N	5	0.000	0.000	N
				Mn I: 100% ^{55}Mn ($I = \frac{5}{2}$)					
408.2945	^{55}Mn	3/2	469.391	−65.091	23	5/2	−26.981		24
426.5928	^{55}Mn	3/2	50.965		24	3/2	−293.797		24
445.3013	^{55}Mn	3/2	50.965		24	1/2	1067.261		24
445.7041	^{55}Mn	5/2	467.410	−73.460	25	3/2	683.527	224.844	26
447.0142	^{55}Mn	3/2	50.965		24	3/2	191.867		24
449.8897	^{55}Mn	3/2	50.965		24	5/2	92.936		24
450.2223	^{55}Mn	5/2	−137.905		24	7/2	44.969		24
467.1688	^{55}Mn	7/2	−161.888		24	5/2	284.803		24
470.9710	^{55}Mn	7/2	−161.888		24	7/2	170.882		24
473.9110	^{55}Mn	3/2	50.965		24	3/2	668.537		24
500.4891	^{55}Mn	5/2	−137.905		24	7/2	137.905		27
525.5330	^{55}Mn	11/2	405.265		28	9/2	131.909		24
538.8538	^{55}Mn	5/2	89.938		24	7/2	44.969		24
542.0368	^{55}Mn	7/2	458.930	21.701	23	5/2	−549.000		23
				Co I: 100% ^{59}Co ($I = \frac{7}{2}$)					
521.2688	^{59}Co	9/2	810.039	−59.958	29	9/2	1076.855	149.896	29
528.0627	^{59}Co	9/2	517.142	179.875	29	7/2	846.914	89.938	29

References. 16) Childs et al. (1979); 17) Lefèbvre et al. (2002); 18) Johann et al. (1981); 19) Cochrane et al. (1998); 20) Armstrong et al. (2011); 21) estimated from solar profiles by trial and error with a single snapshot of an earlier version of the 3D model (Asplund et al. 2000a); 22) Jarosz et al. (2007); 23) Dembczyński et al. (1979); 24) Blackwell-Whitehead et al. (2005a); 25) Handrich et al. (1969); 26) Luc & Gerstenkorn (1972); 27) Lefèbvre et al. (2003); 28) Johann et al. (1981); 29) Pickering (1996).

Table 2. continued.

		Lower level				Upper level			
λ (nm)	Iso.	J	A (MHz)	B (MHz)	HFS ref.	J	A (MHz)	B (MHz)	HFS ref.
530.1044	^{59}Co	5/2	178.900	−170.000	30	5/2	464.678		29
535.2041	^{59}Co	11/2	771.966	209.855	29	9/2	1076.855	149.896	29
548.3353	^{59}Co	5/2	178.900	−170.000	30	7/2	478.169	149.896	29
564.7233	^{59}Co	3/2	332.000	101.000	30	5/2	491.660	0.000	29
593.5390	^{59}Co	5/2	1124.800	144.000	30	7/2	478.169	149.896	29
608.2423	^{59}Co	9/2	810.039	−59.958	29	9/2	401.722		29
609.3141	^{59}Co	3/2	317.780	119.917	29	3/2	702.400	−15.000	31
618.9005	^{59}Co	5/2	178.900	−170.000	30	5/2	696.118	29.979	29
642.9913	^{59}Co	7/2	839.400	−97.000	30	5/2	1046.276		29
645.4995	^{59}Co	7/2	751.500	31.000	30	9/2	401.722		29
741.7386	^{59}Co	3/2	389.730		29	5/2	696.118	29.979	29
Ni I: 68.08% ^{58}Ni (I = 0), 26.22% ^{60}Ni (I = 0), 5.7% ^{61,62,64}Ni Isotopic separations from Johansson et al. (2003; 481.2 nm) and Wood et al. (2014b; all except 481.2 nm)									
474.0134	^{61,62,64}Ni	4	0.000	0.000	N	5	0.000	0.000	N
474.0150	^{60}Ni	4	0.000	0.000	N	5	0.000	0.000	N
474.0166	^{58}Ni	4	0.000	0.000	N	5	0.000	0.000	N
481.1977	^{58}Ni	1	0.000	0.000	N	0	0.000	0.000	N
481.1993	^{60}Ni	1	0.000	0.000	N	0	0.000	0.000	N
481.1993	^{61,62,64}Ni	1	0.000	0.000	N	0	0.000	0.000	N
497.6114	^{61,62,64}Ni	4	0.000	0.000	N	4	0.000	0.000	N
497.6125	^{60}Ni	4	0.000	0.000	N	4	0.000	0.000	N
497.6135	^{58}Ni	4	0.000	0.000	N	4	0.000	0.000	N
550.9994	^{61,62,64}Ni	3	0.000	0.000	N	4	0.000	0.000	N
551.0002	^{60}Ni	3	0.000	0.000	N	4	0.000	0.000	N
551.0009	^{58}Ni	3	0.000	0.000	N	4	0.000	0.000	N
574.9257	^{61,62,64}Ni	3	0.000	0.000	N	4	0.000	0.000	N
574.9280	^{60}Ni	3	0.000	0.000	N	4	0.000	0.000	N
574.9304	^{58}Ni	3	0.000	0.000	N	4	0.000	0.000	N
617.6777	^{61,62,64}Ni	4	0.000	0.000	N	5	0.000	0.000	N
617.6798	^{60}Ni	4	0.000	0.000	N	5	0.000	0.000	N
617.6820	^{58}Ni	4	0.000	0.000	N	5	0.000	0.000	N
622.3949	^{61,62,64}Ni	3	0.000	0.000	N	4	0.000	0.000	N
622.3971	^{60}Ni	3	0.000	0.000	N	4	0.000	0.000	N
622.3991	^{58}Ni	3	0.000	0.000	N	4	0.000	0.000	N
637.8206	^{61,62,60}Ni	3	0.000	0.000	N	4	0.000	0.000	N
637.8233	^{60}Ni	3	0.000	0.000	N	4	0.000	0.000	N
637.8258	^{58}Ni	3	0.000	0.000	N	4	0.000	0.000	N

References. 29) Pickering (1996); 30) Guthöhrlein & Keller (1990); 31) unpublished work of R. Wenzel, reproduced in Guthöhrlein & Keller (1990); 32) N) no HFS because J = 0 or I = 0.

Table 3. Our adopted ionisation energies $E_{\rm ion}$ and partition functions $U(T)$ for relevant ionisation stages of the iron group elements.

Species	$E_{\rm ion}$ (eV)	$U(T)$			
		3000 K	5000 K	8000 K	12 000 K
Sc I	6.562	9.65	11.95	21.54	49.08
Sc II	12.800	17.80	22.74	29.45	37.65
Ti I	6.828	20.88	29.61	54.83	114.24
Ti II	13.580	44.03	55.45	72.24	95.29
V I	6.746	34.67	47.50	79.09	152.62
V II	14.660	31.77	43.36	64.24	98.87
Cr I	6.766	7.61	10.26	20.20	52.33
Cr II	16.500	6.03	7.09	12.15	27.16
Mn I	7.434	5.99	6.34	9.95	24.10
Fe I	7.902	22.01	27.78	43.05	81.05
Fe II	16.190	34.20	43.21	56.33	78.50
Co I	7.881	24.44	33.43	48.16	76.50
Ni I	7.640	26.34	30.76	36.35	48.84
Ni II	18.170	8.30	10.83	15.73	23.21